

PAN

Concrete Structures Section
Committee on Civil Engineering and Hydroengineering
Polish Academy of Sciences



Faculty of Civil Engineering
and Environmental Sciences
BIALYSTOK UNIVERSITY OF TECHNOLOGY



11TH INTERNATIONAL CONFERENCE AMCM 2025 ANALYTICAL MODELS AND NEW CONCEPTS IN CONCRETE AND MASONRY STRUCTURES

Bialystok, 3-5 December, 2025

Bialystok University of Technology



11TH INTERNATIONAL CONFERENCE AMCM 2025

**ANALYTICAL MODELS AND NEW CONCEPTS
IN CONCRETE AND MASONRY STRUCTURES
DECEMBER 3-5, 2025, BIALYSTOK POLAND**

CONFERENCE PROCEEDINGS

Editors

Mirosław Broniewicz, Marcin Gryniewicz

Copy editors:
Aniela Staszewska, Katarzyna Duniewska

DTP:
Marcin Dominów

ISBN 978-83-68673-07-4 (e-Book)
DOI: 10.24427/978-83-68673-07-4

2025 Faculty of Civil Engineering and Environmental Sciences,
Białystok University of Technology, Białystok University of Technology, Poland

Białystok, 2025



11TH INTERNATIONAL CONFERENCE AMCM 2025

ANALYTICAL MODELS AND NEW CONCEPTS IN CONCRETE AND MASONRY STRUCTURES

The Conference is organised by:

- Faculty of Civil Engineering and Environmental Sciences, Bialystok University of Technology
- Concrete Structures Section at the Committee on Civil Engineering and Hydroengineering of the Polish Academy of Sciences
- Polish Group of the Fédération Internationale du Béton – *fib*
- Polish Association of Civil Engineers and Technicians, Department Podlaski in Bialystok

Under the auspices of:

- Rector of the Bialystok University of Technology
- Dean of the Faculty of Civil Engineering and Environmental Sciences
- Chairperson of the Polish Association of Civil Engineers and Technicians

Supported by:

- The Minister of Infrastructure
- Marshal of the Podlaskie Voivodeship
- President of Białystok

Polish Patronage

- Rector of Bialystok University of Technology
- The Polish Academy of Sciences
- The Governor of Podlaskie Voivodeship
- Polish Association of Civil Engineers and Technicians
- Polish Chamber of Civil Engineers

International Patronage

- RILEM International Union of Laboratories and Experts in Construction Materials, Systems and Structures
- FIB The International Federation for Structural Concrete
- ACI American Concrete Institute



AMCM2025 Secretariat

Department of Building Structures

Bialystok University of Technology

45E Wiejska St.

15-351 Bialystok, Poland

Phone: 48 85 746 96 00, e-mail: amcm2025@pb.edu.pl

website: <https://pb.edu.pl/amcm2025/>

Scientific Committee

Chairwoman of the Scientific Committee

Marta Kosior-Kazberuk – Rector of the Bialystok University of Technology

Vice-chairman of the Scientific Committee

Michał Bołtryk – Dean of the Faculty of Civil Engineering and Environmental Sciences

Vice-chairman of the Scientific Committee

Wit Derkowski – Chairman of the Concrete Structures Section of the Polish Academy of Sciences

Scientific Secretary

Marcin Gryniewicz

International Advisory Committee

- Hakim Abdelgader, University of Tripoli (Libya)
- Erkan Akpinar, Kocaeli University (Turkey)
- Riadh Al-Mahaidi, Swinburne University of Technology (Australia)
- Gyorgy Balazs, Budapest University of Technology and Economics (Hungary)
- Joaquim Barros, University of Minho (Portugal)
- Abdeldjelil Belarbi, University of Huston (USA)
- Agnieszka Bigaj-van, Vliet Netherlands Organization for Applied Scientific Research (The Netherlands)
- Billy Boshoff, University of Pretoria (South Africa)
- Vladimir Cervenka, CEO at Cervenka Consulting (Czech Republic)
- Frank Dehn, The Karlsruhe Institute of Technology (Germany)
- Vincenzo Di Naso, University of Florence (Italia)
- Christopher Eamon, Wayne State University (USA)
- Raafat El-Hacha, University of Calgary (Canada)
- Jose Maria Fernandez, Rodriguez University of Cordoba (Spain)
- M.A. Flórez de la Colina, Technical University of Madrid (Spain)
- Alper Ilki Istanbul, Technical University (Turkey)
- José Ramón Jiménez Romero, University of Cordoba (Spain)
- Lujien Mohammed, Hama University (Syria)
- G. Murali, Graphic Era Deemed to be University (India)



- Antonio Nanni, University of Miami (USA)
- Piotr Noakowski, Dortmund University of Technology (Germany)
- Andrzej S. Nowak, Auburn University (USA)
- Ioan Pepenar, Research Institute for Construction and Technology – ICECON S.A (Romania)
- Anton Schindler, Auburn University (USA)
- Tsuyoshi Takada, University of Tokyo (Japan)
- Tamon Ueda, Shenzhen University and Hokkaido University (Japan)
- Leonas Ustinovičius, Vilnius Gediminas Technical University (Lithuania)
- Joost C. Walraven, Delft University of Technology (The Netherlands)
- George Wardeh, CY Cergy Paris University (France)

Polish Scientific Committee

- Adam Baryłka, Warsaw University of Life Sciences
- Danuta Barnat-Hunek, Lublin University of Technology
- Jan Biliszczyk, Wrocław University of Science and Technology
- Elżbieta Broniewicz, Białystok University of Technology
- Tadeusz Chyży, Białystok University of Technology
- Jacek Domski, Koszalin University of Technology
- Łukasz Drobiec, Silesian University of Technology
- Kazimierz Flaga, Cracow University of Technology
- Wojciech Franus, Lublin University of Technology
- Kazimierz Furtak, Cracow University of Technology
- Andrzej Garbacz, Warsaw University of Technology
- Wiesława Głodkowska, Koszalin University of Technology
- Barbara Goszczyńska, Kielce University of Technology
- Krzysztof Gromysz, Kielce University of Technology
- Anna Halicka, Lublin University of Technology
- Jerzy Hoła, Wrocław University of Science and Technology
- Jacek Hulimka, Silesian University of Technology
- Maria Kaszyńska, West Pomeranian University of Technology
- Jacek Korentz, University of Zielona Góra
- Renata Kotynia, Łódź University of Technology
- Robert Kowalski, Warsaw University of Technology
- Janusz Krentowski, Białystok University of Technology
- Jan Kubica, Silesian University of Technology
- Cezary Madryas, Wrocław University of Science and Technology
- Czesław Miedziałowski, Białystok University of Technology
- Krystyna Nagrodzka-Godycka, Gdańsk University of Technology
- Beata Nowogońska, University of Zielona Góra
- Edyta Pawluczuk, Białystok University of Technology
- Wojciech Radomski, Warsaw University of Technology
- Barbara Sadowska-Buraczewska, Białystok University of Technology



- Łukasz Sadowski, Wrocław University of Science and Technology
- Jacek Szafran, Łódź University of Technology
- Elżbieta Szmigiera, Warsaw University of Technology
- Anna Szymczak-Graczyk, Poznań University of Life Sciences
- Jacek Śliwiński, Cracow University of Technology
- Piotr Woyciechowski, Warsaw University of Technology

Local Organising Committee

Chairman of the OC

Mirosław Broniewicz

Vice-chairperson of the OC for Scientific Affairs

Elżbieta Broniewicz

Vice-chairperson of the OC for organisational matters

Katarzyna Kalinowska-Wichrowska

Vice-chairperson of the OC for Contact with Companies

Nina Szklennik

**Vice-chairman of the OC for the organisation of the Conference in Vilnius
(Lithuania)**

Leonas Ustinovičius

- Filip Broniewicz, Department of Building Structures and Structural Mechanics
- Krzysztof Czech, Department of Building Structures and Structural Mechanics
- Michał Dzun, Department of Building Structures and Structural Mechanics
- Robert Grygo, Department of Building Structures and Structural Mechanics
- Marcin Gryniewicz, Department of Building Structures and Structural Mechanics
- Agnieszka Jabłońska-Krysiewicz, Department of Building Structures and Structural Mechanics
- Jan Klimasara, Department of Building Structures and Structural Mechanics
- Julita Krassowska, Department of Building Structures and Structural Mechanics
- Monika Mackiewicz, Department of Building Structures and Structural Mechanics
- Dorota Maleszewska, Department of Building Structures and Structural Mechanics
- Sandra Mlonek, Department of Building Structures and Structural Mechanics
- Ewa Ołdakowska, Department of Geotechnics, Roads and Geodesy
- Marcin Orłowski, Department of Construction and Landscaping
- Edyta Pawluczuk, Department of Construction and Landscaping
- Jolanta Anna Prusiel, Department of Building Structures and Structural Mechanics
- Beata Sadowska, Department of Sustainable Construction and Building Systems
- Barbara Sadowska-Buraczewska, Department of Building Structures and Structural Mechanics
- Natalia Stankiewicz, Department of Construction and Landscaping

Promotion coordinator:

Agnieszka Sakowicz-Stasiulewicz Promotion Department

IT coordinator:

Tomasz Huścio Department of Industrial Process Automation

Office:

Dorota Maleszewska
amcm2025 [at] pb.edu.pl

Financial matters:

Agnieszka Szmidt



Content

Foreword	
<i>Marta Kosior-Kazberuk</i>	12
Prediction of the service life of brick walls using the coefficient method for national conditions	
<i>Beata Nowogońska</i>	14
Optimizing calcination conditions of coffee-ground biochar for use in portland cement mortars	
<i>Adrieli Oliveira Soares, Kárita Christina Soares, Kanaïama Alves, Arthur Aviz Palma e Silva</i>	17
Possibilities of using waste from the processing of steel components to reinforce cement mortars	
<i>Paulina Zajdel, Krzysztof Ostrowski, Piotr Kuraś</i>	20
Influence of resin type, concrete grade and anchorage depth on the pull-out load-bearing capacity of anchors	
<i>Agnieszka Jabłońska-Krysiewicz, Dariusz Tomaszewicz</i>	23
Response of the masonry wall to horizontal prestressing	
<i>Dominik Pernecký, Ladislav Klusáček</i>	26
Characterisation of the interfacial transition zone	
<i>Shivani Sharma, Sudhanshu Sharma, Dhiman Basu</i>	30
Design of reinforced concrete cylindrical tanks using numerical and analytical methods	
<i>Jan Klimasara, Jolanta A. Prusiel</i>	33
Low carbon recycled binder from concrete waste as a more ecoefficient alternative in earth stabilisation	
<i>José A. Bogas, Ricardo Cruz, Maria Gomes</i>	36
Development of sustainable cement-based materials using recycled concrete aggregate and expansive agent	
<i>Benoit Bissonnette, Luc Courard, Andrzej Garbacz</i>	39
From obligation to opportunity US Buy Clean policies to decarbonize concrete	
<i>Tien Y. Peng</i>	42



Analysis of the potential use of waste in the form of powders and fine aggregates in cement composites <i>Teresa Rucińska, Olga Borziak</i>	45
Mechanical and economic evaluation of recycled aggregate self-compacting concrete in the context of large panel buildings deconstruction <i>Seweryn Malazdrewicz</i>	48
Durability, deterioration patterns and life cycle costs of hollow concrete blocks partitions: A comparative study <i>Igal M. Shohet Monica Paciuk, Alon Uralainis, Gili Lifshitz Sherzer</i>	51
Underwater structural investigation Scour monitoring around bridge piers <i>Łukasz Topczewski, Paweł Mikołajewski</i>	54
Simulations of wire ropes used in prestressed concrete. Model validation based on archival complex experiment <i>Marcin Gryniiewicz, Michał Dzun, Julita Krassowska, Zhihua Chen, Dai Wang</i>	57
Effect of fresh and spent FCC catalyst (ECAT) on the mechanical and microstructural properties of eco-friendly ultra-high-performance concrete <i>Hassan Abdolpour, Jennifer Udebunu, Benedykt Mrosek, Michał Pachnicz</i>	60
Advanced engineering of eco-efficient UHPFRC using recycled steel fibres and pozzolanic petrochemical waste <i>Hassan Abdolpour</i>	63
Probabilistic maintenance optimization of concrete culverts: Integrating corrosion-driven deterioration and structural simulation <i>Gili Lifshitz Sherzer, Igal M. Shohet</i>	65
Static analysis of the post-tensioned SPP truss girder <i>Petr Moštěk, Ladislav Klusáček</i>	68
Influence of casting method on bond performance and self-compacting concrete properties <i>Milena Kucharska, Piotr Dybeł</i>	72
Experimental assessment of crushed prefabricated fibre-reinforced concrete rings <i>Agnieszka Głuszek, Lidia Buda-Ożóg</i>	75
Assessment of second-generation Eurocode 2 in predicting shear resistance of FRP-reinforced lightweight concrete members <i>Agnieszka Wiater, Tomasz Wojciech Siwowski</i>	78
Effect of perforation in CFRP tubes on load-bearing capacity of short concrete columns <i>Oliwia Sikora, Krzysztof Adam Ostrowski</i>	81



Experimental verification of rigid plastic bond model in the design of composite steel concrete columns <i>Bartosz Grzeszykowski, Magdalena Szadkowska, Maciej Lewandowski-Szewczyk, Elżbieta Szmigiera</i>	84
Torsional strength and stiffness of concrete elements: An experimental approach <i>Magdalena Lewandowska, Michał Demby, Szymon Wojciechowski, Robert Studziński</i>	87
Limitations of simplified methods for determining second-order effects in high-slenderness rc cantilever columns <i>Dawid M. Zmyślony, Czesław Bywalski, Roman J. Wróblewski</i>	90
Flexural moment distribution in hollow core floors. Code provisions in light of new experimental data <i>Miłosz Jeziorski, Wit Derkowski</i>	93
Comparative Finite element analysis of sunk wells lowering in varying soil <i>Anna Szymczak-Graczyk, Tomasz Garbowski</i>	98
Two-variable individual-layer nonlocal model of static bending of asymmetric sandwich plate with laminate facings <i>Stanisław Karczmarczyk</i>	101
Stirrup-deficient post-tensioned concrete girders – shear failure mode and shear performance analysis <i>Rafał Walczak, Wit Derkowski</i>	104
Diagnostics of cable post-tensioned concrete grinders – the effect of temperature <i>Tadeusz Chyży, Czesław Miedziałowski, Krzysztof Czech, Marcin Orłowski, Dai Wang, Hai Zhang, Jacek Karpiesiuk</i>	108
Longitudinal forces in concrete structures. An ignored phenomenon which severely changes the structure behavior <i>Piotr Noakowski</i>	111
Numerical and experimental study on fiber content. Optimization of high-strength steel fiber-reinforced concrete cylinders <i>Gili Lifshitz Sherzer, Yuri Ribakov</i>	114
Impact of basalt minibars on the structural performance of BFRP bar reinforced concrete beams <i>Abel A. Belay, Marta Kosior-Kazberuk, Julita Krassowska</i>	117
Accelerated CO ₂ curing of alkali-activated pervious paving blocks with seashell aggregates <i>Ágata González-Caro, Antonio Manuel Merino-Lechuga, José Ramón Jiménez, José María Fernández-Rodríguez</i>	120



Influence of pore structure on mechanical and thermal performance of cementitious composites <i>Marzena Kurpińska</i>	123
Accelerated carbonation curing of alkali-activated pervious paving blocks <i>Antonio Manuel Merino-Lechuga, Ágata González Caro, José María Fernández-Rodríguez, José Ramón Jiménez</i>	127
Effect of calcium nitrate and fly ash on the mechanical properties of grout for two-stage concrete <i>Farzam Omid Moaf, Marzena Kurpinska, Hakim S. Abdelgader, Mikolaj Miskiewicz, Barbara Sadowska-Buraczewska</i>	130
Innovative formulation and evaluation of bio-based self-healing capsules (biocach) for enhanced concretes sustainability and durability. Capsule formulation, stability (pH-value of 7.77), and preliminary compressive strength of capsule-modified concrete <i>Isaac O. Agbamu, Marcin Wysokowski, Teofil Jesionowski, Mieczyslaw Kuczma</i> ...	133
Finite element analysis of steel-concrete composite beams with web openings <i>Bilal Ahmed, Jan Kubica, Mohamad Ahmad</i>	137
Development of an elastic and waterproof cement mortar incorporating polymeric aggregate: An innovative and sustainable solution for screed application <i>Carolina Piña Ramírez, Alejandra Vidales Barriguete, Sonia Navarrete Ocaña</i>	141
Bond-slip behavior between concrete with pozzolanic additives and BFRP and GFRP bars <i>Julita Krassowska, Filip Chyliński, Marta Kosior-Kazberuk, Dai Wang, Dawei Shu</i>	144
Investigation of concrete beams reinforced with GFRP or steel bars: An experimental approach <i>Janusz Rogowski, Damian Szczech, Jakub Zajac, Renata Kotynia</i>	147
Predicting pre-failure behaviour of GFRP lighting poles <i>Filip Broniewicz</i>	150
Shear and bending capacities of concrete beams with composite reinforcement <i>Rafał Kostro, Marta Kosior-Kazberuk, Julita Krassowska</i>	153
Investigation of concrete beams reinforced with GFRP bars: finite element modelling <i>Jakub Zajac, Damian Szczech, Janusz Rogowski, Renata Kotynia</i>	156
Experimental investigation of the bond behaviour of GFRP reinforcing bars in low-clinker concrete <i>Paul Heber, Oliver Sikorski, Alexander Schumann, Paul-Martin Großkopff, Birgit Beckmann, Steffen Marx</i>	159



Foreword

The conference “Analytical Models and New Concepts in Concrete and Masonry Structures”, held in Białystok on December 3–5, 2025, represents the eleventh edition of the international event series organised triennially in Poland.

After ten editions held in various cities—including Łódź (1996, 2008), Wrocław (1999, 2014), Kraków (2002, 2011), Gliwice (2005, 2017), and Lublin (2020)—the Conference, which originated in Białystok in 1993, will return there in 2025.

The primary objective of the Conferences is to showcase recent research advances in the modelling and analysis of concrete and masonry structures, as well as to highlight new ideas and noteworthy engineering projects. As in previous years, the event has been promoted through international networks and journals, including “Structural Concrete” and “fib-news”.

The 11th Conference was jointly organised by:

- Faculty of Civil Engineering and Environmental Sciences, Białystok University of Technology.
- Concrete Structures Section of the Committee on Civil and Hydroengineering of the Polish Academy of Sciences.
- Polish National Group of the Fédération Internationale du Béton (fib).
- Podlaski Branch of the Polish Association of Civil Engineers and Technicians (PZITB) in Białystok.

As in earlier editions of the Conference, participants were invited to organise their submissions according to the key thematic areas, which included Concrete and Innovative Materials, Structural Performance and Design, Construction Techniques and Management, Outstanding Structures, Masonry Structures, Composite Structures and Innovative Composite Materials, Structural Dynamic Diagnostics, Prefabricated Structures and Materials, and Sustainable Development.

With contributions from distinguished academics, researchers, designers, and practitioners representing numerous countries, we aim to create an outstanding platform for sharing ideas and advancing research in concrete and masonry structures. The three-day Conference will feature a diverse program of sessions, including plenary and keynote lectures, as well as presentations of peer-reviewed papers.

A two-page abstract will appear in the electronic Conference Proceedings. Authors of conference submissions may have the opportunity to publish extended versions of their work as full papers—subject to journal-specific guidelines and selection



by the AMCM 2025 Scientific Committee—following an additional review process. The eligible journals are: Archives of Civil Engineering, Materiały Budowlane, Environment and Economics, Builder.

Within the limited duration of the Conference, it became necessary to schedule presentations in two parallel sessions to accommodate oral contributions and foster direct discussions. We trust that every participant will gain valuable insights, both scientifically and through opportunities for establishing or renewing professional contacts.

We extend our sincere appreciation to the invited sponsors for their valuable contributions and financial support. The organisers sincerely hope that the Conference proves engaging for all participants and that the tradition of these meetings will be continued in the coming years.

Marta Kosior-Kazberuk
Chairperson of the Scientific Committee
Białystok, December 2025



Prediction of the service life of brick walls using the coefficient method for national conditions

Beata Nowogońska

University of Zielona Gora, Poland, b.nowogonska@ib.uz.zgora.pl

Keywords: brick walls, service life, prediction

1. Introduction

Understanding the aging process of a building is crucial for maintaining its technical condition throughout its lifetime [1–4]. Service Life Planning (SLP) is closely linked to predicting the service life of a building's components [5–7]. The standard [7] outlines a ratio method for predicting service life, which determines the Estimated Service Life (ESL) of a building component.

2. Forecasting the service life of walls using the coefficient method

To predict the service life of brick masonry walls ESL, it is necessary to apply a modification of the Reference Service Life (RSL) using a set of coefficients that account for actual service conditions, as outlined in the standard. The formula is as follows:

$$ESL = RSL \times A \times B \times C \times D \times E \times F \times G \quad (1)$$

where: A, B, C, D, E, F, G – coefficients describing the differences between the conditions include: coefficient A, which represents the quality of the building components; coefficient B, which indicates the design level; coefficient C, which reflects the execution level of the construction work; coefficient D, which pertains to the internal environment; coefficient E, which addresses the external environment; coefficient F, which corresponds to the actual conditions; and coefficient G, which denotes the maintenance level.

The values of the coefficients typically range from 0.8 to 1.2. A value smaller than 1.0 reduces the estimated useful life, while a value larger than 1.0 increases it.

The A-factor refers to the brick-and-mortar class. The higher the strength class and resistance to external agents, the better.



The B-factor considers the quality of the technical documentation. Well-designed details (e.g., eaves, caps, damp proofing) protect the masonry from degradation, while design errors can lead to dampness, heaving, and cracking.

The C-factor pertains to the level of workmanship. The quality of the masonry work, execution of joints, and compliance with standards are assessed. Workmanship errors (e.g., bricklaying in poor weather conditions) shorten the useful life of the walls, while adherence to good building practices extends it.

The D-factor takes into account the conditions of the building's internal environment, such as humidity and temperature levels. Ventilation and heating influence the stability of the microclimate. In wet rooms (bathrooms, kitchens), degradation can be accelerated.

The E-factor determines the conditions of the external environment. Walls exposed to rain, frost, wind, and air pollution age more quickly. Additionally, high humidity and fluctuating temperatures promote the formation of cracks and defects.

The F-value pertains to the conditions of use. Walls in industrial buildings bear heavier loads than those in single-family homes. The intensity of use – such as impacts, vibrations, and dynamic loads – can shorten their service life.

The G-factor considers the level of maintenance. Regular inspection, maintenance, and repair of minor defects enhance durability, while neglecting maintenance results in the accumulation of issues, such as dampness and cracks.

3. Life cycle analysis of brick walls

In Zielona Góra, as in other Polish cities, tenement houses from the late 19th century have been preserved. Since then, most building components, such as roof tiles, gutters, downpipes, plaster, and installations, have been replaced with new materials, while the brick walls have remained unchanged. The typical lifespan of solid brick walls is reported to be 130 to 150 years. The buildings analysed were constructed approximately 140 years ago, indicating that the useful life of the structural walls in these buildings is also 140 years. During periodic inspections, the walls' technical condition was assessed as average, with an estimated degree of technical deterioration around 50%.

In theory, brick masonry walls should be in poor condition after 140 years of use. However, due to the quality of the materials, good workmanship and design, proper environmental conditions, and adequate maintenance, the lifespan of the walls can be extended.

According to standard [7], the coefficient method should be employed. The Reference Service Life (RSL) of the walls is stated as 140 years, but this service life can be extended by applying specific coefficients. The reference RSL is adjusted based on a set of coefficients that reflect actual service conditions.

A well-maintained brick wall can last significantly longer than 140 years. Under optimal conditions, with each coefficient set at 1.2, it could even last up to 600 years.



4. Conclusion

The coefficient method enables the estimation of the actual lifetime of building components. The results from the ratio method analysis of all building components can assist in decision-making regarding whether to invest in more expensive materials, superior workmanship, or more intensive maintenance.

References

1. Bourke, K., Silva, A. L., & Gaspar, P. (2023). Application of service life planning to existing buildings – Perspectives on condition appraisal, performance and cost. In *16th International Conference on Durability of Building Materials and Components* (pp. 1–8).
2. Lacasse, M. A., & Sjoström, C. (2004). Recent advances in methods for service life prediction at building materials and components – an overview. In *Proceedings of the CIB World Building Congress 2004, Conference on Research and Innovation* (Toronto, Ontario, 5/2/2004) (pp. 1–9).
3. Nowogońska, B. (2016). The life cycle of a building as a technical object. *Periodica Polytechnica Civil Engineering*, 60(3).
4. Silva, A., & Brito, J. (2021). Service life of building envelopes: A critical literature review. *Journal of Building Engineering*, 44, 102646.
5. ISO 15686-1:2012 *Buildings and constructed assets – Service life planning – Part 1: General principles*.
6. ISO 15686-2:2012 *Buildings and constructed assets – Service life planning – Part 2: Service life prediction procedures*.
7. ISO 15686-7:2012 *Buildings and constructed assets – Service life planning – Part 7: Assessment of performance based on service life data from practice*.



Optimizing calcination conditions of coffee-ground biochar for use in portland cement mortars

*Adrieli Oliveira Soares¹, Kárita Christina Soares Kanaïama Alves¹
Arthur Aviz Palma e Silva²*

¹Federal Institute Tocantins, Brazil, adrieli.soares@estudante.ifto.edu.br, karita.alves@ifto.edu.br

²Estácio de Sá University Center, Brazil, eng.aviz@gmail.com

Keywords: coffee-ground biochar, pozzolanic activity, calcination temperature, supplementary cementitious materials

1. Introduction

The construction sector is a major consumer of natural resources and a key source of CO₂ emissions, with cement production accounting for about 2.3% of Brazil's industrial output. Reusing agro-industrial residues such as spent coffee grounds (SCG) through pyrolysis to produce biochar offers a sustainable alternative, promoting circular economy practices. This carbon-rich, porous material can enhance cement hydration and matrix densification [1–3], improving strength and pore refinement when properly calcined. This study investigates the effect of coffee-ground biochar produced at 350°C and 500°C, replacing 10% and 20% of sand, on the compressive strength of Portland cement mortars.

2. Methodology

Spent coffee grounds from local producers in Gurupi (Brazil) were washed, oven-dried at 60°C, and pyrolyzed at 350°C and 500°C for 2 h to produce biochars (BCP350 and BCP500) with densities of 0.365 and 0.39 g/cm³, respectively. Portland cement mortars (1:2:0.35) were prepared with 10% and 20% sand replacement by biochar, using reference and modified mixes ranging from 1000 g cement and 2000–1600 g sand. Nine 50 × 100 mm specimens per mix were tested for compressive strength at 7, 14, and 28 days. SEM–EDS analyses examined morphological and compositional changes between unburned residue and biochars to assess calcination effects.

3. Results and discussions

Compressive strength results (Figure 1) revealed that incorporating coffee-ground biochar significantly affected mortar performance, depending on both calcination temperature and replacement level. At 7 days, mortars with BCP350 achieved slightly higher strength (16 MPa) than the reference (13 MPa), due to residual oxygenated groups enhancing hydration.

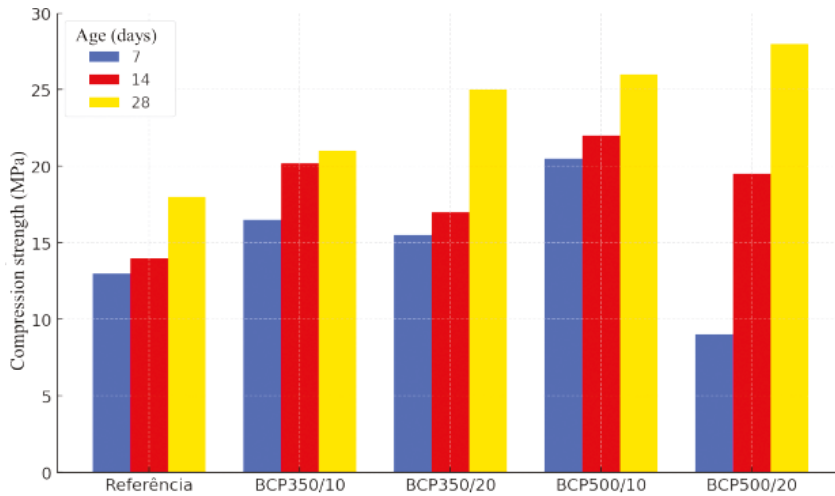


FIG. 1. Compressive strength of biochar mortars

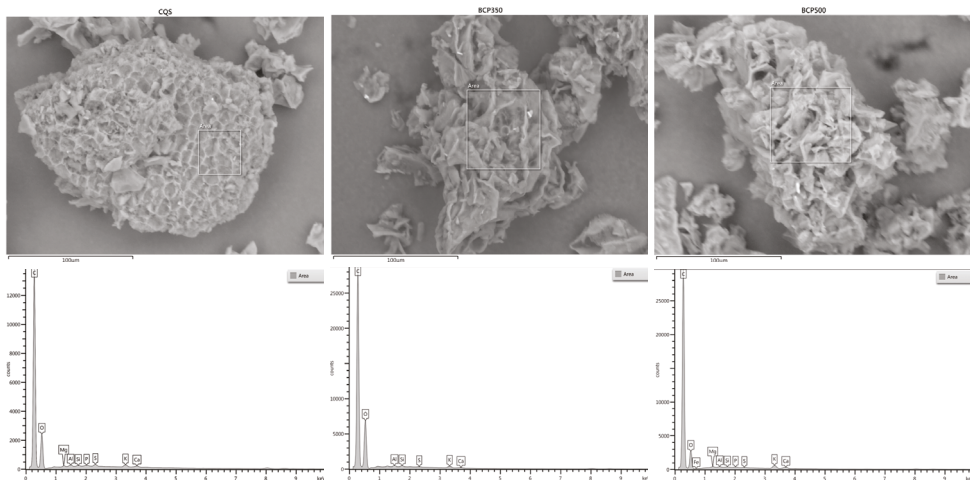


FIG. 2. Scanning Electron Microscopy (SEM) images of coffee-ground biochar sample



BCP500/20 showed lower early strength (9 MPa) due to reduced surface polarity but reached 28 MPa at 28 days – a 55% increase over the control – indicating that higher calcination temperature and 20% replacement enhanced long-term hydration and matrix densification. SEM revealed that increasing temperature from 350°C to 500°C produced a more porous, stable carbon matrix, while EDS confirmed carbon enrichment, oxygen loss, and exposure of Si, K, and Ca minerals that improve interfacial bonding and pozzolanic reactivity.

4. Conclusions

Coffee-ground biochar is an effective and sustainable partial replacement for sand in cement mortars, with 20% calcined at 500°C showing the best performance. Its use enhances strength through matrix densification and interfacial bonding while promoting coffee waste valorization.

Acknowledgments

The authors acknowledge the financial support of CAPES, CNPq, the Fundação de Amparo à Pesquisa do Distrito Federal (FAPDF), and the Fundação de Amparo à Pesquisa do Tocantins (FAPT), as well as the institutional support of the Instituto Federal do Tocantins (IFTO) and the Centro Universitário Estácio de Brasília.

References

1. Stylianou, M., Christou, A., Dalias, P., & Polycarpou, P. (2020). Physicochemical and structural characterization of biochar derived from the pyrolysis of biosolids, cattle manure, and spent coffee grounds. *Journal of Energy Institute*, 93, 2063–2073. <https://doi.org/10.1016/j.joei.2020.05.002>
2. Ma, W., Fan, J., Cui, X., Wang, Y., Yan, Y., Meng, Z., Gao, H., Lu, R., & Zhou, W. (2023). Pyrolyzing spent coffee ground to biochar treated with H_3PO_4 for efficient removal of 2,4-D herbicide: Adsorptive behaviors and mechanism. *Journal of Environmental Chemical Engineering*, 11, 109165. <https://doi.org/10.1016/j.jece.2022.109165>
3. Dixit, A., Gupta, S., Dai, S., & Wei, H. (2019). Waste valorisation using biochar for cement replacement and internal curing in ultra-high performance concrete. *Journal of Cleaner Production*, 238, 117876. <https://doi.org/10.1016/j.jclepro.2019.117876>



Possibilities of using waste from the processing of steel components to reinforce cement mortars

Paulina Zajdel, Krzysztof Ostrowski, Piotr Kuraś

*Cracow University of Technology, Poland,
paulina.zajdel@pk.edu.pl, krzysztof.ostrowski.1@pk.edu.pl, piotr.kuras@student.pk.edu.pl*

Keywords: cement mortar, steel shavings, strength properties, waste

1. Introduction

Modern technologies for the production of materials for construction are striving not only to increase material efficiency, but also to reduce negative environmental impacts. One innovative approach is the use of waste materials as secondary raw materials in the production of cement mortars. The use of waste materials can contribute to reducing CO₂ emissions, lowering production costs and modifying mortar properties. Various types of industrial wastes, glass, plastics, steel shavings and organic materials can improve the properties of cement mortars and concretes, while reducing the negative impact on the environment [1–4]. However, the use of waste materials that have not been popularly used so far as an additive for the innovative self-compacting cement mortars being designed under the LIDER14/0270/2023 project, requires experimental studies.

2. Experimental research

The aim of the study was to consider the effect of using waste steel shavings for high-strength cement mortars with suitable rheological properties. The designed mortars were characterized by varying amounts of steel shavings in the mortar volume, the content of which was 1%, 2% and 3%. For comparison, reference mixtures without steel waste were also made. The mortars used CEM I 52.5 R cement, Sika ViscoCrete-98 RS plasticizer, SikaFume HR/TU microsilica-containing additive and sand with a grain size of 0–2 mm. Steel shavings obtained as waste from the machining processes of steel components were used for the study with a 0.5–4 mm fraction. Composition of the analysed mixtures was designed experimentally, based on pilot studies.

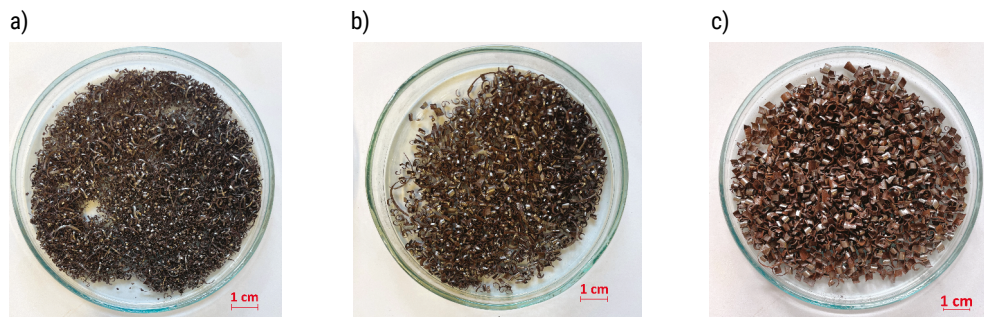


FIG. 1. Steel shavings used in the research of relevant fractions: a) 0.5–1 mm, b) 1–2 mm, c) 2–4 mm

For all analysed mortars, bending and compression tests were performed on 4 x 4 x 16 cm beams according to [5] after curing period of 7 and 28 days in water. The research proved a positive effect of the addition of steel shavings on the mechanical properties of the mortar, as well as on the consistency of the mixtures. In general, for most mixes, a significant increase in tensile strength and compressive strength was observed after 7 and also after 28 days compared to reference samples. In some cases, the addition of steel shavings resulted in increases in compressive strength as high as 20%.

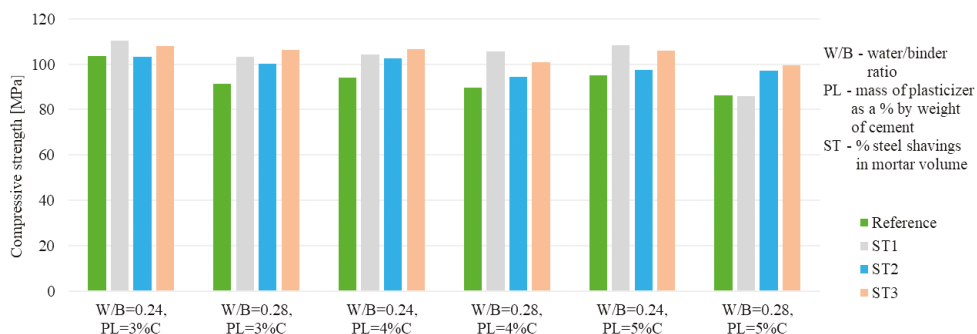


FIG. 2. Compressive strength of selected mixtures without the addition of shavings (green colour) and with the addition of 1%, 2% and 3% steel shavings, respectively, after curing period of 28 days in water

3. Conclusion

The addition of steel shavings can have a positive effect on the compressive strength and tensile strength of cement mortars, especially when high mixture strength together with fluidity and stability is required. However, inferring the qualitative and quantitative impact of this type of waste requires detailed analysis and further research. If the mortar will be used as a sealant dedicated to steel or composite anchors



to be installed, the adhesion of the anchor to the mortar and the pull-off strength should be verified in addition to the compressive and tensile strength. What is more, the addition of steel shavings may adversely impact the mortar's freeze-thaw resistance, which may require the use of additional materials to seal and protect the mortar mix from the effects of water.

Acknowledgments

This research was funded from a project supported by the National Center for Research and Development, Poland (Grant no. LIDER14/0270/2023 "Non-conductive Composite Chain with an Anchoring System"). We would like to thank the companies supporting the implementation of this research of self-compacting mortars with the addition of steel shavings: WIŚNIOWSKI Sp. z o.o. S.K.A., SIKA Poland Sp. z o.o., GÓRAŹDŹE CEMENT S.A.

References

1. Głuszko, A. (2024). Przegląd wad i zalet wybranego zbrojenia rozproszonego pochodzącego z recyklingu. *Przegląd Budowlany*, 7(224), 92–95.
2. Seo-Eun, O., Sang-Yeop, C., Kyuwon, K., & Soo-Ho, H. (2024). Comparative analysis of the effects of waste shell aggregates on the material properties of cement mortars. *Construction and Building Materials*, 412, 134887.
3. Pengfei, D., Qifeng, L., Meirong, Z., & Pinghua, Z. (2024). Effect of waste plastic fiber on the printability and mechanical properties of 3D-printed cement mortar. *Journal of Building Engineering*, 83, 108439.
4. Kostro, R., Kosior-Kazberuk, M., Krassowska, J., Protchenko, K., & Belay, A. (2024). Selected mechanical properties of basalt microbars reinforced concrete. *Materiały Budowlane*, 623(7), 5–8.
5. EN 196-1:2016 *Methods of testing cement – Part 1: Determination of strength*.



Influence of resin type, concrete grade and anchorage depth on the pull-out load-bearing capacity of anchors

Agnieszka Jabłońska-Krysiewicz¹, Dariusz Tomaszewicz²

¹*Białystok University of Technology, Poland, a.krysiewicz@pb.edu.pl*

²*International Academy of Applied Sciences in Łomża, Poland, dt542@lomza.mans.edu.pl*

Keywords: resin, anchors, pull-out, load-bearing capacity

1. Introduction

The phenomenon of adhesion of steel anchors to concrete via resin has been known in Poland for more than a century [1]. Testing the pull-out resistance of embedded anchors in concrete is an important issue in structural and materials engineering. Methods for checking adhesion stresses include: the analytical method according to ETAG 001 (now EAD), EN 1992-4 (Eurocode 2 part 4), the experimental method (in situ or laboratory tests), the numerical method (FEM simulations) and the method according to the manufacturer's ETA.

When it comes to the use of threaded bonded anchors in external three-layer walls in large-panel slab buildings or in other general construction systems, an important factor affecting the load-bearing capacity of bonded anchors is the method of attachment [2].

2. Influence of anchorage depth on load-bearing capacity of embedded anchors

The results of experimental research should be contrasted with numerical simulations [3] and theoretical estimates of the load carrying capacity of bonded anchors [4, 5].

2.1. Single 90-degree bonded anchors

Experimental tests have confirmed that for concrete of class C30/37, increasing the anchorage depth from $h_{ef} = 2$ cm to $h_{ef} = 6$ cm results in a 70% increase in anchorage capacity. In the case of concrete class C12/15, increasing the anchorage depth from $h_{ef} = 2$ cm to $h_{ef} = 6$ cm leads to a 35% increase in anchorage capacity. Therefore, a significant increase in anchor capacity can be observed; however, this occurs only



when the anchorage depth is sufficiently large, i.e., approximately five times the diameter of the anchor.

2.2. Single anchors bonded at angles of 60, 45 and 30 degrees

When comparing the load-bearing capacity of bonded inclined anchors installed at angles of 60° and 45° in concrete of class C12/15 with an identical embedment depth of $h_{ef} = 4 \text{ cm}$, it was found that the load-bearing capacity of anchors inclined at 60° was more than twice as high as that of those inclined at 45°. Similar results were obtained for bonded inclined anchors installed at 60° and 45° in concrete of class C30/37.

On the other hand, a comparison of the load-bearing capacity of bonded anchors installed at angles of 60° and 30° in C12/15 concrete showed that the 30° anchors had an embedment depth almost 2.5 times greater – **9.5 cm** compared to **4 cm** at 60°. Despite this, the load-bearing capacities were very similar. Therefore, in order to achieve a load-bearing capacity comparable to that of anchors bonded at 60°, when using anchors at 30°, it is necessary to ensure a significantly greater embedment depth – at least **eight times the anchor diameter**.

In general, it can be stated that the load-bearing capacity of anchors inclined at smaller angles decreases rather sharply. To ensure sufficient capacity, significantly greater embedment depths must be used.

2.3. Anchor groups in two- and three-anchor systems

Load-bearing capacity tests of two- and three-anchor systems have led to the following conclusions:

- a) The use of single inclined anchors at an angle of 60° in concrete of class C12/15 and stronger resin provides higher load-bearing capacity than three-anchor systems. However, in concrete of class C30/37 and when using weaker resin, three-anchor systems are significantly more advantageous.
- b) The use of single inclined anchors at an angle of 45° in concrete of class C12/15 with stronger resin, and in concrete of class C30/37 with weaker resin, results in lower load-bearing capacity compared to two-anchor systems.
- c) The use of single inclined anchors at an angle of 30° generally provides higher load-bearing capacity than two-anchor systems in nearly every case.

Inclined anchors are recommended for use when anchoring in structural layers of limited thickness.

3. Conclusions

The pull-out capacity of bonded anchors depends on many contributing factors. The type of resin used and the class of the concrete substrate do not have as direct



an impact on the load-bearing capacity of bonded anchors as the effective embedment depth. These component factors affect the value of adhesion stress between concrete and steel [6].

References

1. Grabowski, K. (1908). About the adhesion of concrete to iron. *Przegląd Techniczny*, XLVI, 521–522.
2. Tomaszewicz, D. (2024). The work of single bonded anchors into the three layer walls of large slab panel buildings. *Materiały Budowlane*, 628(12), 155–162. <https://doi.org/10.15199/33.2024.12.17>
3. Tomaszewicz, D., Jablonska-Krysiewicz, A., & Gryniewicz, M. (2021). Pull-out tests and numerical simulations of bonded threaded anchors in concrete blocks with thermal insulation layer. *Springer Nature Switzerland AG*.
4. Szlendak, J. K., & Tomaszewicz, D. (2021). Load capacity of anchors embedded into concrete and multi-layer façade slabs. In *Modern trends in research on steel, aluminium and composite structures* (pp. 363–369). <https://doi.org/10.1201/9781003132134-46>
5. Tomaszewicz, D., Czech, K., Szlendak, J. K., & Baryłka, A. (2024). Load-bearing capacity of single and multi-anchor connections – theory vs results of experimental research (Part I). *Safety Engineering of Anthropogenic Objects*, 3, 98–110. <https://doi.org/10.37105/iboa.224>
6. Kijania, M. (2015). The methods for computation of the bond stress between concrete and steel reinforcement. *Przegląd Budowlany*, 6, 38–42.

Response of the masonry wall to horizontal prestressing

Dominik Pernecký, Ladislav Klusáček

Brno University of Technology, Czech Republic Dominik.Pernecky@vutbr.cz, Ladislav.Klusacek@vut.cz

Keywords: masonry construction, horizontal prestressing, wall deformation, analysis

1. Introduction

Reinforcement of masonry walls by horizontal post-tensioning is increasingly used in current construction practice, especially in reconstruction or statically faulted structures. However, due to the lack of comprehensive research, a deeper understanding of masonry behaviour during prestressing is still lacking, and design approaches are mainly based on practical experience.

2. Aim of the work

The aim of this paper is to experimentally verify the method of prestress distribution in clay brick walls during horizontal prestressing and to analyse its effect on the deformation of the structure along the wall length.

This method of stiffening and strengthening of structures is suitable for stabilization of collapsed load-bearing structures, e.g. according to *Fig. 1*. This is a villa from the early 20th century, partially disturbed by subsidence of the foundations due to long-term roof leakage.



FIG. 1. Example of failure

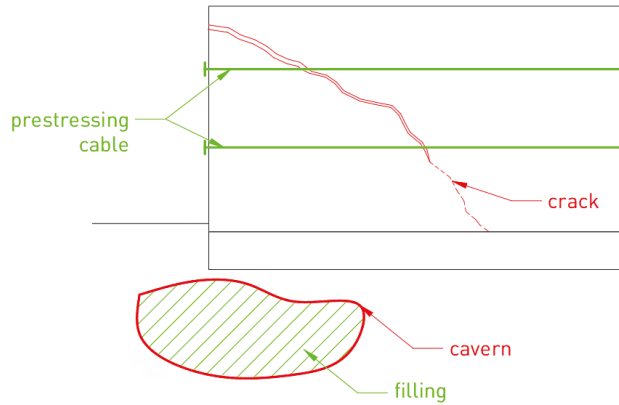


FIG. 2. Failure solution using horizontal post tensioning

3. Methodology

The experiment was performed on a test wall made of clay brick masonry 2 m high and 450 mm thick. The wall was prestressed with 2 external cables of MONOSTRAND type placed in the horizontal axis and anchored in the spreader plate. The wall was vertically prestressed in order to achieve the effect of the load from the higher floors. The wall strains were measured at three height levels and at three positions along the length of the wall: **Section 0** at the face, **Section 1** at a quarter of the length and **Section 2** at the midpoint. Horizontal deformations were monitored to determine the effectiveness of the prestressing force and its distribution along the length of the wall.



FIG. 3. Tensiometer placements



FIG. 4. Measurement of deformations on the wall face

4. Results

Early results show that the stress is not distributed uniformly in the structure, but with a clear decrease in intensity away from the point of force application. The largest deformations were observed at the level of the wall face, with a gradual decay towards the centre. The measured values indicate a possible relationship between the height of the measurement level and the prestressing force effectiveness. In addition, the deformation along the wall height was found to depend on the wall bearing at the head and footing, as well as on the loading of the wall under consideration from the structures of higher floors.

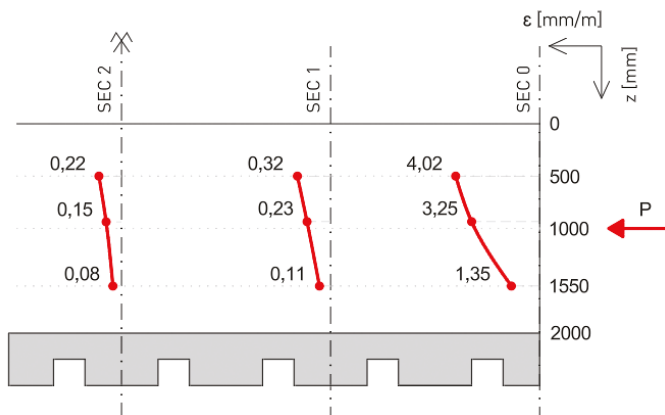


FIG. 5. Measured strain values



TABLE 1

z [cm]	ε [mm/m]		
	SEC 0	SEC 1	SEC 2
50	4,02	0,32	0,22
93,5	3,25	0,23	0,15
155	1,35	0,11	0,08

5. Discusion and meaning

The obtained results provide new insights into the mechanisms of prestressing force transfer in clay masonry walls, which have not been described in detail in the literature so far. The findings will be further used to refine masonry models or masonry performance characteristics. This measurement can contribute to the development of more reliable design methods for strengthening masonry and improving the safety of building structures.

References

1. Peknik, R., & Klusacek, L., Long-action of additional horizontal prestressing on masonry. *Procedia Engineering*, 195, 67–72. <https://doi.org/10.1016/j.proeng.2017.04.525>



Characterisation of the interfacial transition zone

Shivani Sharma, Sudhanshu Sharma, Dhiman Basu

Indian Institute of Technology, India shivanis@iitgn.ac.in, ssharma@iitgn.ac.in, dbasu@iitgn.ac.in

Keywords: ITZ Characterisation, SEM-EDS, Si/Ca ratio, Optical Microscopy

1. Introduction

Concrete is the most widely used construction material globally. The compressive strength of concrete is one of the major target parameters used in the mix design. The potential failure mode of concrete can be controlled with a carefully engineered mix design [1], yet in the absence of such a framework, the failure occurs due to crack generation in the weakest zones. The interfacial transition zone (ITZ) between the aggregate and the matrix often acts as this weakest link [2, 3], where the crack tends to initiate and propagate. Hence, measurement and mitigation of ITZ plays a vital role in improving the compressive strength of concrete [4] and establishing control over the potential failure modes.

This study presents a unique characterization method for the measurement of ITZ thickness by integrating optical microscopy with Scanning Electron Microscopy (SEM) and Energy Dispersive Spectroscopy (EDS). ITZ thickness is measured along three directions, each separated by 120°, and the average value is represented as the overall ITZ thickness. This approach provides a basis for estimating a uniform ITZ thickness and its assessment in a heterogeneous material (concrete).

2. Methodology

2.1. Hypothesis and approach

Based on existing literature, the Si/Ca ratio is a critical indicator that varies significantly with distance from the aggregate. The hypothesis formulated suggests that Calcium Hydroxide (CH) tends to accumulate in the pores adjacent to the aggregate due to the wall effect. As a result, the Si/Ca ratio is expected to be highest near the aggregate and gradually decrease towards the matrix. A distance is defined at which the Ca/Si ratio decreases by half from its initial value or approaches the Si/Ca ratio for the matrix. This distance from the aggregate is considered as the ITZ thickness.

2.2. Sample preparation and testing

Concrete samples are cast using Normal Strength Concrete (NSC) without Supplementary Cementitious Material (SCM) and High Strength Concrete (HSC) with SCM. The samples are visualised under an optical microscope, where the presence of CH is confirmed. The results reveal that abundant CH is present in case of NSC, whereas only traces of CH are detected in HSC. This is attributed to the pozzolanic reaction, whereby the SCM utilizes CH to convert it into Calcium Silicate Hydrate (CSH) gel and other pozzolanic products. Next, a SEM+EDS analysis is carried out on the samples. As illustrated in Figure 1, the process involves measurement of the Si/Ca ratio at three equidistant directions (120° apart) from the aggregate surface into the matrix using the EDS technique. These measurements allow the estimation of ITZ thickness and assessment of its uniformity.

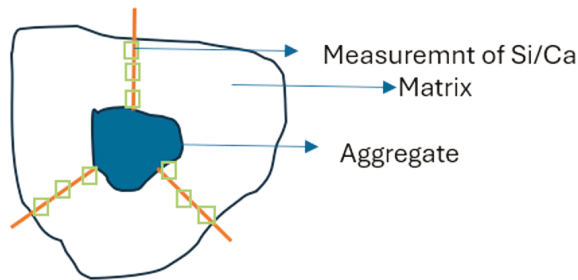


FIG. 1. Characterisation of ITZ

3. Experimental results

This is an ongoing experimental test. Preliminary data indicate the following Si/Ca ratios:

Element	Si/Ca ratio
Coarse Aggregate	2–4
Fine aggregate	1–4
Concrete Matrix (NSC without SCM), (HSC with SCM)	3–5, 0.1–1
ITZ	>5–20

These results show that the ITZ consistently exhibits a significantly higher Si/Ca ratio compared to both the matrix and aggregate, supporting the hypothesis.



4. Discussion

The preliminary observations confirm that Si/Ca ratio is highest in the ITZ, decreasing gradually towards the matrix. The three-directional measurements ensure a uniform and reliable estimation of ITZ thickness, minimizing bias due to material heterogeneity.

5. Conclusion and future work

This study presents a novel approach for characterizing the ITZ in concrete by combining optical microscopy, SEM, and EDS measurements. The initial findings validate the proposed hypothesis. Further detailed experimental testing is underway to substantiate these results and develop a comprehensive model for ITZ thickness estimation in both NSC and HSC.

Acknowledgments

The authors would like to acknowledge the manpower provided by the PMRF grant to support this research. The help of the CIF facility staff at IIT Gandhinagar is also acknowledged.

References

1. Basu, D., Mushtaq, S. M., Sharma, S., & Tripathi, S. (2024). Enhancing quality control in the mix design of high-strength concrete using a capacity-based approach. *International Journal of Concrete Structures and Materials*, 18(1), 78. <https://doi.org/10.1186/s40069-024-00722-8>
2. Liao, K. Y., Chang, P. K., Peng, Y. N., & Yang, C. C. (2004). A study on characteristics of interfacial transition zone in concrete. *Cement and Concrete Research*, 34(6), 977–989.
3. Hu, J., & Stroeven, P. (2004). Properties of the interfacial transition zone in model concrete. *Interface Science*, 12(4), 389–397.
4. Duan, P., Shui, Z., Chen, W., & Shen, C. (2013). Effects of metakaolin, silica fume and slag on pore structure, interfacial transition zone and compressive strength of concrete. *Construction and Building Materials*, 44, 1–6.



Design of reinforced concrete cylindrical tanks using numerical and analytical methods

Jan Klimasara, Jolanta A. Prusiel

Bialystok University of Technology, Poland, j.klimasara@pb.edu.pl, j.prusiel@pb.edu.pl

Keywords: reinforced concrete, cylindrical tanks, Finite Element Method (FEM), structural analysis

1. Introduction

The design of reinforced concrete tanks is a crucial aspect of modern civil engineering due to their wide application in water management, the chemical industry, energy production, and municipal infrastructure. Traditionally, the design of tank structures was based on analytical methods derived from the classical theory of cylindrical shells. These methods, developed in the first half of the 20th century, were the primary design tool for engineers, allowing relatively accurate determination of structural characteristics in a theoretical framework. Analytical formulas were used to calculate the distribution of hoop forces, vertical forces, and bending moments, forming the basis for reinforced concrete design. With the development of computer technology and numerical tools, particularly the Finite Element Method (FEM), analytical approaches were gradually replaced by computational simulations. FEM enables flexible structural modeling, consideration of complex geometries, nonlinear material behavior, and diverse boundary conditions and loads.

2. Description and analysed models

This paper presents a comparison of internal force calculations for reinforced concrete cylindrical tanks obtained using both analytical [1–4] and numerical methods. Numerical models were created in Autodesk Robot Structural Analysis 2026 and Dlubal RFEM 6, with identical assumptions regarding geometry, material properties, and loading conditions. The comparative analysis showed that differences between the two numerical environments were small, not exceeding 5%, confirming the consistency and reliability of both programs. In parallel, analytical calculations were performed based on classical shell theory to estimate and compare level of values with numerical methods.

3. Comparison of numerical and analytical calculations

The results lead to several important conclusions

1. FEM-based software significantly improves the efficiency of the design process by providing results quickly and under realistic structural conditions.
2. The small discrepancies between different software packages confirm the stability and repeatability of modern computational tools.
3. Classical analytical methods, though rarely used as a primary design tool, remain valuable as independent verification methods. They are particularly relevant in educational contexts and during preliminary conceptual studies.

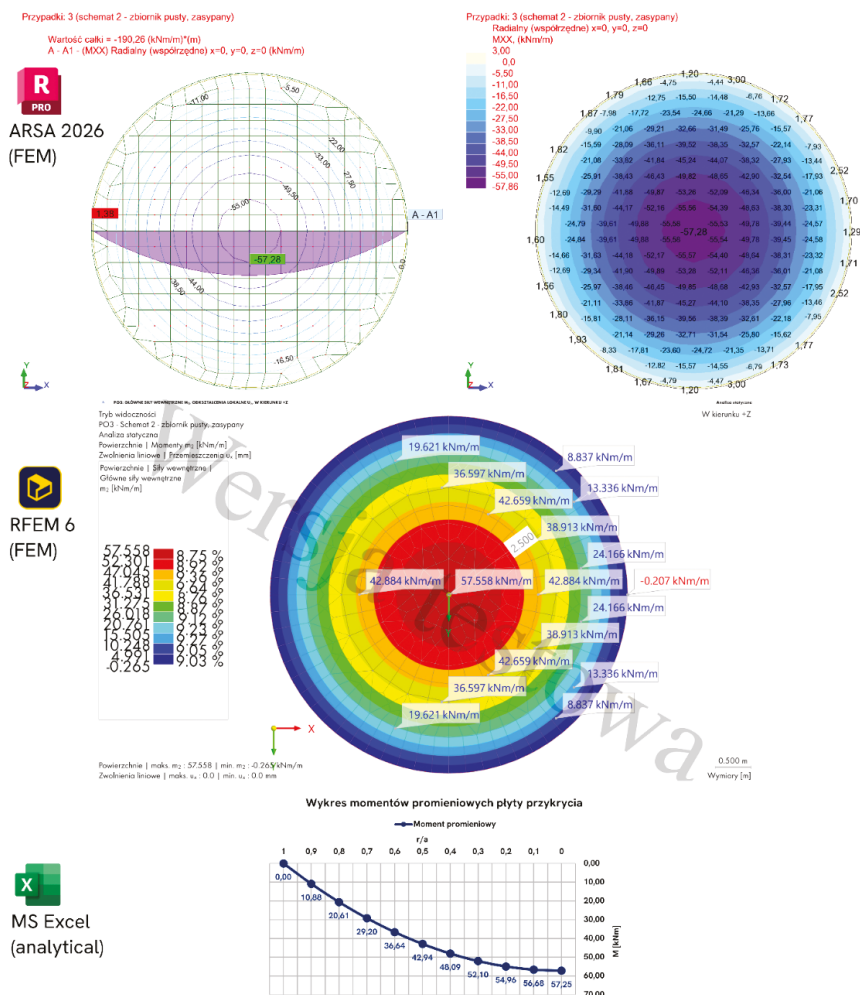


FIG. 1. Static analysis for tank cover slab – radial moments, Scheme II – empty tank, embedded in the ground, level 1 – Autodesk Robot Analysis 2026 (FEM), level 2 – Dlubal RFEM 6 (FEM), level 3 – analytical method (classical shell theory)



In summary, the comparative analysis of numerical and analytical approaches in the design of reinforced concrete cylindrical tanks confirms the high accuracy and reliability of modern FEM tools while emphasizing the continuing importance of analytical methods as supporting instruments in the design process. The findings may serve as a basis for further research on the optimization of tank design and the definition of practical limits of different calculation methods in engineering practice.

References

1. Kobiak, J., & Stachurski, W. (1991). *Konstrukcje żelbetowe* (Vol. IV). Arkady.
2. Halicka, A., & Franczak, D. (2023). *Projektowanie zbiorników żelbetowych* (Vol. 2). *Zbiorniki na ciecz*. PWN.
3. PN-88/B-02014 *Obciążenia budowli. Obciążenia gruntem*.
4. PN-EN 1991-4:2008 *Eurokod 1 – Oddziaływania na konstrukcje. Część 4: Silosy i zbiorniki*.



Low carbon recycled binder from concrete waste as a more ecoefficient alternative in earth stabilisation

José A. Bogas, Ricardo Cruz, Maria Gomes

*CERIS-Civil Engineering Research and Innovation for Sustainability,
Instituto Superior Técnico, Universidade de Lisboa, Av. Rovisco Pais, 1049-001 Lisbon, Portugal,
abogas@civil.ist.utl.pt;ricardojtcruz@tecnico.ulisboa.pt; maria.gloria.gomes@tecnico.ulisboa.pt*

Keywords: stabilised earth, compressed earth blocks, recycled cement, sustainability

Due to the urgent need to reduce the carbon footprint of cement-based materials, and the consequent search for alternatives to Portland cement (PC), extensive research has been conducted at Instituto Superior Técnico, University of Lisbon (IST-UL), focusing on the development of new low-carbon binders. Since 2018, one of the main research focuses has been the development of recycled cement (RC) obtained through the low-temperature thermoactivation of the cementitious fraction of concrete waste [1]. The goal is to recover the binding properties of old cement using a process that minimizes thermal energy consumption and avoids significant CO₂ emissions [2]. The thermoactivation at around 650–700 °C prevents the decarbonation phase, resulting in CO₂ emission reductions exceeding 60% compared to conventional clinker production [3]. Moreover, RC production also mitigates natural resource depletion while promoting the effective reuse of lowvalue construction and demolition waste (CDW). Several studies, including those conducted by the authors, have demonstrated the excellent hydration capacity of RC, which tends to develop hydration products of the same type and volume as PC [2, 4]. Additionally, concretes with up to 40% RC replacing PC have shown similar performance to reference mixes, with only minor differences in strength and durability [5, 6]. The main limitation of RC is its high water demand [2]. Nevertheless, C25/30-grade concretes could be produced using RC as the sole binder in the mix [5].

Despite the significant advances achieved in this field, one major challenge remains: the industrial production of RC can only be feasible if the cementitious fraction is first separated from the concrete debris, a task that the construction industry has not yet been able to solve effectively. In this context, the main author developed an innovative method that enables the individualisation of the cementitious fraction from aggregates [7]. This patented method makes it possible to obtain high-quality recycled sand (HQRS) with less than 3 wt% adhered paste, and cement waste of over 75 wt% purity. Thanks to these advances, a new generation of “green” cement-based building products has been developed at IST-UL, including rendering mortars, concretes, adhesive cements, and more recently RC-stabilised earth materials, which are discussed next.

Due to the growing demand for more sustainable materials, earth has regained relevance in construction, particularly for small dwellings. However, despite its very low embodied energy, high availability, and affordable cost, earthen materials exhibit poor mechanical strength and durability when exposed to outdoor environments [8]. Therefore, they typically require chemical stabilization, with PC being the most common and effective stabilizing agent. Nevertheless, as previously mentioned, PC is a highly energy-intensive binder, which considerably increases the embodied energy and carbon footprint of earth-based construction, thereby offsetting its ecological benefit [8]. Consequently, there is a need for alternative stabilizers capable of maintaining the eco-efficiency of earth while providing comparable performance to PC. Several studies have explored alternative stabilizers such as fly ash and agricultural wastes, but these have generally shown limited stabilisation efficiency, availability, and cost-effectiveness for large-scale use.

Thus, RC has been explored at IST as an alternative low-carbon binder for earth stabilization (Fig. 1). Specifically, compressed stabilized earth blocks (CSEB) were produced, combining both mechanical and chemical stabilization to achieve water-resistant materials. In this communication, key results regarding the mechanical and durability performance of RC CSEB are presented, and compared with unstabilized reference blocks (UCEB) and PC-stabilized blocks. CSEB were produced with up to 8% stabilizer, 20–100% RC, and with up to 40% of the earth replaced by CDW to further enhance sustainability. Mechanical strength had a strong correlation with total porosity, which was generally higher in RC CSEB due to its high water demand. Nevertheless, compared to UCEB, the mechanical strength of RC CSEB increased more than twofold. Moreover, unlike UCEB, RC CSEB, even at only 4% stabilizer content, proved to be water-resistant, withstanding 72 hours of immersion and 1 hour of severe water erosion at 2.5 bar pressure without significant deterioration (Fig. 2). In fact, the durability of RC CSEB was comparable to that of PC CSEB. Therefore, RC has demonstrated itself as a viable and ecofriendlier alternative to PC for earth stabilization, maintaining the integrity of CSEB even under very adverse exposure conditions.



FIG. 1. Eco-efficient blocks with RC and CDW



FIG. 2. Water resistant RC CSEB

Acknowledgments

The authors wish to thank the Portuguese Foundation for Science and Technology (FCT) for funding this research under project Eco+RCEB, ref. PTDC/ECI-CON/0704/2021, and under unit project UID/6438/2025 (CERIS), as well as Oficinas do Convento, Vimajas, Portuguese Air Force and Cobert for supporting the experimental work. The second author would also like to thank FCT for the doctoral scholarship 2023.05651.BD.

References

1. Site of the CDWValue group: <https://cdwvalue.eu> (accessed: October 2025).
2. Carriço, A., Bogas, J. A., & Guedes, M. (2020). Thermoactivated cementitious materials – a review. *Construction and Building Materials*, 250, 118873. <https://doi.org/10.1016/j.conbuildmat.2020.118873>
3. Real, S., Sousa, V., Meireles, I., Bogas, J. A., & Carriço, A. (2022). Life cycle assessment of thermoactivated recycled cement production. *Materials*, 15, 6766. <https://doi.org/10.3390/ma15196766>
4. Bogas, J. A., Real, S., Carriço, A., Abrantes, J. C. C., & Guedes, M. (2022). Hydration and phase development of recycled cement. *Cement and Concrete Composites*, 127, 104405. <https://doi.org/10.1016/j.cemconcomp.2022.104405>
5. Real, S., Bogas, J. A., Carriço, A., & Hu, S. (2021). Mechanical characterisation and shrinkage of thermoactivated recycled cement concrete. *Applied Sciences*, 11, 2454. <https://doi.org/10.3390/app11062454>
6. Carriço, A., Real, S., & Bogas, J. A. (2021). Durability performance of thermoactivated recycled cement concrete. *Cement Concrete Composites*, 124, 104270. <https://doi.org/10.1016/j.cemconcomp.2021.104270>
7. Carriço, A., Bogas, J., Hu, S., Real, S., & Pereira, M. (2021). Novel separation process for obtaining RC and HQRS from waste concrete. *Journal of Cleaner Production*, 309, 127375. <https://doi.org/10.1016/j.jclepro.2021.127375>
8. Bogas, J., Real, S., Cruz, R., & Azevedo, B. (2023). Mechanical performance and shrinkage of CSEB with thermoactivated RC. *Journal of Building Engineering*, 79, 107892. <https://doi.org/10.1016/J.JOBE.2023.107892>



Development of sustainable cement-based materials using recycled concrete aggregate and expansive agent

Benoit Bissonnette¹, Luc Courard², Andrzej Garbacz³

¹*Laval University, Quebec city (QC), Canada, benoit.bissonnette@gci.ulaval.ca*

²*University of Liège, Liège, Belgium, luc.courard@uliege.be*

³*Warsaw University of Technology, Warsaw, Poland, andrzej.garbacz@pw.edu.pl*

Keywords: expansive agent, mortar, recycled concrete aggregates, shrinkage cracking

1. Introduction

The construction industry is confronted with two pressing challenges: the depletion of natural aggregates, particularly sand, and the growing accumulation of construction and demolition waste (CDW). Global demand for aggregates is projected to reach 63 billion metric tons by 2024, up from 43 billion in 2016, with sand consumption increasing at an annual rate of approximately 5% [1]. This surge in demand, coupled with environmental concerns related to extraction, underscores the urgency of developing sustainable alternatives. Concurrently, CDW represents a significant secondary resource that, if properly processed, can contribute to circular economy in construction [2].

2. Recycled sand as an alternative

Recycled sand obtained from CDW offers a promising substitute for natural sand in cement-based materials. However, its physical and chemical properties differ markedly from those of natural aggregates. Recycled sands typically exhibit lower density (1,970–2,140 kg/m³) and higher porosity, resulting in water absorption rates between 3 and 10%, compared to 0.2–2% for natural sand [3]. These characteristics influence workability, water demand, and mechanical performance. Studies indicate that incorporating up to 20% recycled fine aggregates in concrete has negligible impact on strength, whereas full replacement can reduce compressive strength by 10–20% [4]. Durability assessments reveal that carbonation and capillary absorption remain comparable to conventional concrete when recycled sand content does not exceed 30% [5]. Washing processes have been shown to improve material quality by reducing fines and residual cement paste, thereby lowering water absorption [6].



3. Shrinkage and expansive agents

Shrinkage in cement-based materials, driven by moisture loss and chemical reactions during hydration, is a major concern, particularly when using recycled sand, which tends to increase shrinkage and cracking susceptibility. Expansive agents are introduced to counteract these effects by inducing controlled expansion during early curing stages. The main expansive systems currently in use include calcium sulfoaluminate (CSA)-based (type K, M), lime-based (type G), and magnesium oxide-based systems [7]. Experimental results highlight significant differences in expansion kinetics among these systems. Type G agents exhibit rapid expansion, achieving better dimensional balance under limited curing conditions, whereas type K and MgO-based systems expand more gradually and require prolonged moist curing to reach their full potential [8]. The effectiveness of shrinkage-compensating systems depends on proper restraint and curing conditions, as insufficient curing can drastically reduce expansion and compromise performance.

4. Sustainability and standards

The integration of recycled sand and shrinkage-compensating technologies aligns with global sustainability objectives by reducing the environmental footprint of construction materials. Shrinkage-compensating concretes enhance structural durability, minimize cracking, and extend service life, thereby lowering maintenance costs and resource consumption. These benefits translate into reduced life-cycle impacts and contribute to green building certifications such as LEED. Additionally, CSA cements used in expansive systems offer environmental advantages, including 30–50% lower CO₂ emissions and reduced energy consumption compared to Portland cement, due to lower calcination temperatures and reduced limestone requirements [9].

Despite these advantages, the widespread adoption of recycled sand and shrinkage-compensating systems faces regulatory and technical barriers. Current standards provide limited guidance on dimensional behavior and rate of volume change, making it difficult to compare products and ensure performance consistency. Harmonized testing protocols and stricter requirements for reporting dimensional stability are essential to support the development and acceptance of these sustainable materials.

5. Conclusions

The use of recycled sand in cement-based materials represents a significant step towards achieving circular economy in the construction sector. While its higher porosity and water demand pose challenges, these can be mitigated through proper processing and mix design. The incorporation of expansive agents further enhances the performance of recycled aggregate concretes by reducing shrinkage and cracking, thereby



improving durability and sustainability. To fully realize these benefits, regulatory frameworks must evolve to include clear specifications and performance criteria for recycled aggregates and shrinkage-compensating systems. This combined approach offers a pathway to more sustainable, durable, and environmentally responsible construction practices.

References

1. UEPG, European Aggregates Association. (2021). *Annual Review 2020–2021*.
2. Peduzzi, P. (2014). Sand, rarer than one thinks. *Environmental Development*, 11, 208–218.
3. Silva, R. V., de Brito, J., & Dhir, R. (2014). Properties and composition of recycled aggregates from construction and demolition waste suitable for concrete production. *Construction and Building Materials*, 65, 201–217.
4. Tam, V. W. Y., Soomro, M., & Evangelista, A. C. J. (2018). A review of recycled aggregate in concrete applications (2000–2017). *Construction and Building Materials*, 172, 272–292.
5. Etxeberria, M., Gonzalez, A., & Valero, I. (2012). *Application of low grade recycled aggregates for non-structural concrete production in the city of Barcelona* [Conference presentation]. Third International Conference on Sustainable Construction Materials and Technologies, Kyoto, Japan.
6. Hubert, J., Zhao, Z., Michel, F., & Courard, L. (2023). Effects of crushing method on the properties of recycled concrete aggregates. *Buildings*, 13(9), 2217.
7. American Concrete Institute. (2021). ACI PRC-223: *Shrinkage-compensating concrete – Guide*.
8. Bissonnette, B., Essalik, S. J., Lamothe, C., Jolin, M., Courard, L., Gagné, R., & Morin, R. (2018). *Characterization tools for shrinkage-compensating repair materials*. ICCRRR 2018.
9. Thomas, R. J., Maguire, M., Sorensen, A. D., & Quezada, I. (2018). Calcium sulfoaluminate cement. *Concrete International*, 40(4), 65–69.



From obligation to opportunity US Buy Clean policies to decarbonize concrete

Tien Y. Peng

GreenPlum Street LLC, Seattle, Washington, USA, typ@greenplumstreet.com

Keywords: Procurement, embodied carbon, declarations

1. Introduction

In the past few years, ambitious climate policies have been passed on both sides of the Atlantic. Governmental entities seeking to reduce their industrial environmental impacts have established emissions disclosure and performance standards for construction materials. European Union Member States have deployed green industrial policies to cut emissions to meet the Green Deal. Meanwhile in the United States, several states and local jurisdictions have enacted Buy Clean laws to transform the marketplace. With carbon emissions from construction representing significant greenhouse gas contributions annually, low carbon solutions in public procurement policies address the emissions of cement and concrete.

1.1. Embodied carbon

Currently, buildings account for 42% of energy related global CO₂ emissions, demonstrating the importance of the building and construction sector in fulfilling these ambitions. Of this sector's contribution, 28% comes from operational carbon with 11% arising from the energy used to produce building and construction materials [1], usually referred to as embodied carbon (EC). Most of a building's total EC is released *upfront* in the production stage at the beginning of a building's life. Unlike with operational carbon, which was the focus of earlier climate policies, there is no chance to decrease EC with updates in efficiency after the building is constructed.

1.2. Buy Clean

One policy solution being adopted in the US is Buy Clean. The element that distinguishes this policy from earlier US climate policies, such as the clean power and fuel efficiency standards, is the strategic focus on construction materials. Essentially, Buy Clean is a green procurement mechanism by which entities seek to reduce the environmental impact of construction material supply chains by establishing emissions disclosure and performance standards for key products in the construction sector.



Government agencies adopting Buy Clean have committed to seeking lower-carbon materials, including cement and concrete, in state-funded projects.

The focus for this study is the analysis of Buy Clean programs in the US which require environmental disclosure and establishment of maximum allowable global warming potential (GWP) values for varying classes of eligible concrete material. By assessing different programs with established emissions limits and quantifying the reductions against the industry benchmarks, the goal is to provide decision-useful guidance to meet embodied carbon reduction goals for the sector. With Buy Clean policies, the manufacturer, architects and structural engineers have a unique opportunity to become key players in global carbon dioxide removal efforts using current and developing carbon-efficient materials.

1.3. Implementation

These Buy Clean policies emphasize reducing its GWP measured in $\text{kgCO}_2\text{e/m}^3$, specifically the cradle-to-gate embodied carbon impact, by identifying emissions in the products using reporting tools. The burden is placed on the bidding contractor to deliver environmental disclosure reports called environmental product declarations (EPD) and select material providers with lower GWP impacts than the “maximum acceptable” GWP limits to be considered for contract bidding. The type of limit to be set by the agency may also vary depending on the policy design.

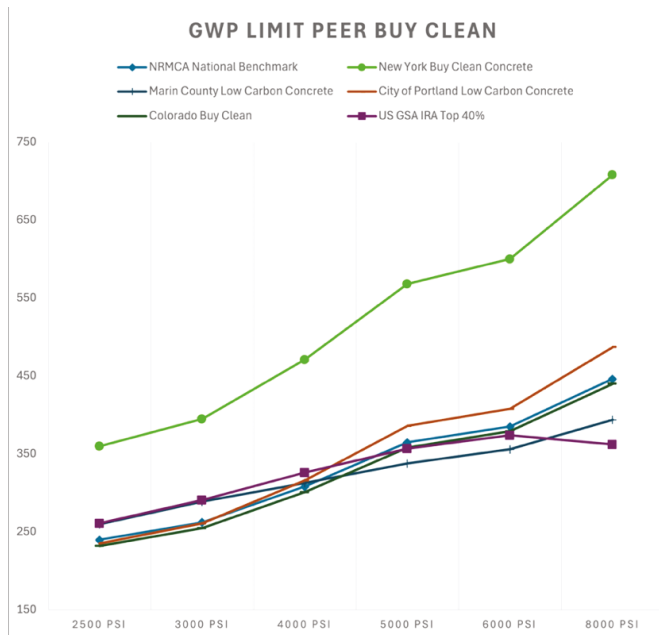


FIG. 1. Peer Buy Clean Maximum Acceptable GWP Limits compared to NRMCA Benchmark ($\text{kgCO}_2\text{e/m}^3$)



Two components that are key to understanding the requirements:

- **Disclosure:** Requirement to disclose the carbon footprint of eligible material using facility-specific EPDs.
- **GWP Limits:** Requirements that a product's carbon footprint be below a maximum acceptable GWP value (a.k.a. limit) established by a government agency.

1.4. Limitations with Buy Clean

While the contractor is responsible for reporting, it is the architects and structural engineers that must address embodied carbon along with other key performance requirements in the contract documents. It is tempting to definitively compare the results of EPDs conducted by different reporting entities. Making effective use of it and avoiding the pitfalls of overconfidence in its precision requires an understanding of its limitations and inherent uncertainties.

Done right, procurement policies such as Buy Clean, Green Claims Directive and EU Fit-for-55 can increase the ability of governments to deal with the impacts of climate change, and make finance flows consistent with a low greenhouse gas emissions and climate-resilient pathways. Conversely, deficient policies can hinder competition, impede innovation and stall efforts of the carbon-intensive construction industry.

References

1. Rempher, A., Esau, R., & Weir, M. (2023). *Embodied Carbon 101: Building Materials*. RMI. <https://rmi.org/embodied-carbon-101>



Analysis of the potential use of waste in the form of powders and fine aggregates in cement composites

Teresa Rucińska, Olga Borziak

*West Pomeranian University of Technology in Szczecin, Poland,
trucinska@zut.edu.pl, olga.borziak@zut.edu.pl*

Keywords: sustainable cement composites, waste materials, waste aggregates, waste powders

1. Abstract

The dynamic increase in the volume of construction waste represents a significant environmental challenge, necessitating the implementation of effective resource management strategies. In this context, cement-based material technologies, such as mortars and concretes, demonstrate a high capacity for incorporating secondary raw materials derived from recycled construction waste. Previous studies conducted by national and international research institutions confirm the feasibility of using recycled materials, although their technical properties do not always match those of materials produced from virgin raw resources.

However, the diversity of technical requirements depending on the application allows for the effective use of materials with slightly lower performance characteristics, while still adhering to the principles of sustainable development. Both the results of original research and literature analysis confirm the potential for utilizing waste materials in the form of powders and aggregates in cement composite technologies. Powders typically serve as cement substitutes or fillers, whereas waste aggregates, once properly processed into suitable fractions, can partially or fully replace natural aggregates.

In the conducted experiments, cement mortars in which fine natural aggregate was replaced with waste aggregate of equivalent granulometry (in volumetric proportions of 10%, 20%, and 30%, and in the case of glass cullet – 50% and 100%) demonstrated suitability for use as masonry mortars and floor screeds. The addition of powders at 2% of the cement mass, excluding powder derived from incinerated municipal sewage sludge, did not adversely affect the mechanical properties of the cement matrix. The reduced performance observed with the sewage sludge powder is attributed to the presence of phosphate ions, which delay the hydration process and consequently slow down strength development.

The obtained results clearly indicate the validity of research focused on the use of recycled materials in cement composite technologies, contributing to the reduction of natural resource extraction and supporting environmental protection efforts.

References

1. Giergiczny, E., & Góralna, K. (2008). Mielony granulowany żużel wielkopiecowy – dodatek do betonu typu II. *Stowarzyszenie Producentów Cementu. Budownictwo, Technologie, Architektura*, 1, 56–59.
2. Ortega, J. M., Pastor, J. L., Albaladejo, A., Sánchez, I., & Climent, M. A. (2014). Durability and compressive strength of blast furnace slag-based cement grout for special geotechnical applications. *Materiales de Construcción*, 64(313), e003.2014.
3. Mirza, J., Mirza, M., Roy, V., & Saleh, K. (2002). Basic rheological and mechanical properties of high-volume fly ash grouts. *Construction and Building Materials*, 16(6), 353–363.
4. Lee, S. T., Moon, H. Y., & Swamy, R. N. (2005). Sulfate attack and role of silica fume in resisting strength loss. *Cement and Concrete Composites*, 27, 65–76.
5. Oliveira, D. R. B., Leite, G., Possan, E., & Filho, J. M. (2023). Concrete powder waste as a substitution for Portland cement for environment-friendly cement production. *Construction and Building Materials*, 397(5), 132382. <https://doi.org/10.1016/j.conbuildmat.2023.132382>
6. Bordy, A., Younsi, A., Aggoun, S., & Fiorio, B. (2017). Cement substitution by a recycled cement paste fine: Role of the residual anhydrous clinker. *Construction and Building Materials*, 132, 1–8.
7. El-Dieb, A. S., & Kanaan, D. M. (2018). Ceramic waste powder an alternative cement replacement – Characterization and evaluation. *Sustainable Materials and Technologies*, 17, e00063.
8. Gautam, L., Kumar Jain, J., Alomayri, T., Meena, N., & Kalla, P. (2021). Performance evaluation of self-compacting concrete comprising ceramic waste powder as fine aggregate. *Materials Today: Proceedings*, 43.
9. Subaşı, S., Öztürk, H., & Emiroğlu, M. (2017). Utilizing of waste ceramic powders as filler material in self-consolidating concrete. *Construction and Building Materials*, 149.
10. Gołek, Ł., & Kapeluszna, E. (2013). Zastosowanie stłuczki szklanej i popiołów fluidalnych do produkcji spoiw. *Świat Szkła*, 5.
11. Tremiño, R. M., Real-Herraiz, T., Letelier, V., Branco, F. G., & Ortega, J. M. (2021). Effects after 1500 hardening days on the microstructure and durability-related parameters of mortars produced by the incorporation of waste glass powder as a clinker replacement. *Sustainability*, 13, 3979.
12. Chin, S. C., Ing, D. S., Kusbiantoro, A., & Wan Ahmad, S. (2016). Characterization of sewage sludge ASH (SSA) in cement mortar. *Journal of Engineering and Applied Sciences*, 11(4), 2242–2247.
13. Li, L. G., Zhuo, Z. Y., Zhu, J., Chen, J. J., & Kwan, A. K. H. (2019). Reutilizing ceramic polishing waste as powder filler in mortar to reduce cement content by 33% and increase strength by 85%. *Powder Technology*, 355, 119–126.
14. Garcés, P., Pérez Carrión, M., García-Alcocel, E., Payá, J., Monzó, J., & Borrachero, M. V. (2008). Mechanical and physical properties of cement blended with sewage sludge ash. *Waste Management*, 28(12), 2495–2502.
15. Krejcirikova, B., Ottosen, L. M., Kirkelund, G. M., Rode, R., & Peuhkuri, R. Characterization of sewage sludge ash and its effect on moisture physics of mortar. *Journal of Building Engineering*, 21, 396–403.



16. Lotfy, A., & Al-Fayez, M. (2015). Performance evaluation of structural concrete using controlled quality coarse and fine recycled concrete aggregate. *Cement and Concrete Composites*, 61, 36–43.
17. Chen, H.-J., Yen, T., & Chen, K.-H. (2003). Use of building rubbles as recycled aggregates. *Cement and Concrete Research*, 33, 125–132.
18. Ray, S., Haque, M., Sakib, Md. N., Mita, A. F., Rahman, M. D. M., & Tanmoy, B. B. (2021). Use of ceramic wastes as aggregates in concrete production: A review. *Journal of Building Engineering*, 43, 102567.
19. Sivakumar, A., Srividhya, S., Sathiyamoorthy, V., Seenivasan, M., & Subbarayan, M. R. (2021). Impact of waste ceramic tiles as partial replacement of fine and coarse aggregate in concrete. *Materials Today: Proceedings*.
20. Sikora, P., Horszczaruk, E., Skoczylas, K., & Rucinska, T. (2017). Thermal properties of cement mortars containing waste glass aggregate and nanosilica. *Procedia Engineering*, 196, 159–166.
21. Sikora, P., Augustyniak, A., Cendrowski, K., Horszczaruk, E., Rucinska, T., Nawrotek, P., & Mijowska, E. (2016). Characterization of mechanical and bactericidal properties of cement mortars containing waste glass aggregate and nanomaterials. *Materials*, 9(8), 701.
22. Rucińska, T. Sustainable cement mortars. *E3S Web of Conferences*, 49, 00090, 1–8.



Mechanical and economic evaluation of recycled aggregate self-compacting concrete in the context of large panel buildings deconstruction

Seweryn Malazdrewicz

*Wroclaw University of Science and Technology, Poland,
seweryn.malazdrewicz@pwr.edu.pl*

Keywords: Recycled Coarse Aggregate, Self-Compacting Concrete, Large Panel System buildings, Recycled Aggregate Concrete

1. Introduction

The ongoing transformation of urban infrastructure in Central and Eastern Europe has led to a growing need for sustainable strategies in the management of obsolete prefabricated large panel system buildings (LPS), constructed extensively in the post-war era. In countries such as Germany and Poland, these structures are increasingly approaching the end of their service life, which can end up in generating large volumes of concrete waste [1, 2]. This research addresses this challenge by exploring the mechanical and economic viability of reusing structural elements from demolished LPS, specifically focusing on the production of self-compacting concrete (SCC) incorporating recycled coarse aggregate (RCA) derived from such buildings.

2. Materials and methods

The research was divided into several complementary stages: (1) a comprehensive literature survey identifying scientific, technological, and environmental gaps in the reuse of precast concrete elements; (2) a material-focused investigation into the properties of RCA extracted from a dismantled LPS panels; (3) the design and optimization of SCC mixtures with 0%, 10%, 20% and 30% RCA replacement levels. Special emphasis was placed on analysing the interfacial transition zone (ITZ) using SEM and XRD techniques and on monitoring dynamic stiffness using the innovative EMM-ARM (Elastic Modulus Measurement through Ambient Response Method); (4) a detailed mechanical and microstructural evaluation of fresh and hardened SCC; and (5) a techno-economic assessment of the proposed solution compared to traditional concrete technologies.

3. Results and discussion

The RCA obtained from LPS demolition exhibited 15–20% lower water absorption and 10% lower bulk density compared to typical RCA reported in the literature [3, 4]. In terms of fresh concrete properties, SCC mixtures with up to 30% RCA maintained slump flow in class SF2 (730–745 mm) and viscosity within class VS2, meeting EFNARC requirements [5].

Mechanical testing confirmed that compressive strength was only slightly reduced:

- Reference series (only natural coarse aggregate): f_{cm} , after 28 days = 68.9 MPa,
- 10% RCA: 68.4 MPa,
- 20% RCA: 65.9 MPa,
- 30% RCA: 64.7 MPa.

All mixtures were thus classifiable as C50/60 or higher according to PN-EN 206+A2. Abrasion resistance (Bohme disc) remained within acceptable ranges, with only 5–9% mass loss.

Microstructural analysis confirmed the existence of a weaker ITZ in RCA-based mixtures. However, the presence of mineral admixtures (fly ash) reduced porosity and partially mitigated ITZ-related strength loss.

The EMM-ARM method revealed consistent trends in the evolution of the elastic modulus during the first 7 days, demonstrating its potential as a complementary diagnostic tool. The experimental campaign also enabled the identification of practical thresholds for water demand and setting time variability in fresh mixes.

4. Economic assessment

From an economic standpoint, a comparative analysis revealed that, despite the additional processing cost of RCA, the proposed solution is economically justifiable in urban demolition scenarios, particularly when factoring in avoided landfill fees and reduced demand for virgin aggregates. The developed framework aligns with EU strategies for circular construction and highlights the potential of integrating recycled materials into high-performance concretes. While RCA processing added ~10–15% cost relative to natural coarse aggregate, avoided landfill fees and reduced extraction of virgin aggregates balanced the expenses. For the reference slab case study ($6.0 \times 3.0 \times 0.2$ m), incorporating 30% RCA enabled a reduction of 135 kg CO₂ emissions, 0.9 GJ primary energy savings, and substitution of >1 t of natural coarse aggregate.



5. Conclusions and outlook

The findings contribute to the optimization of sustainable concrete technologies and offer clear guidelines for practitioners aiming to implement RCA-based SCC in structural and non-structural applications. The study also sets the groundwork for future research in RCA surface treatment methods, ITZ enhancement, and long-term performance modelling. Future research should address:

- CO₂ mineralization treatments for RCA,
- combined use of RCA with dispersed fibre reinforcement,
- long-term durability (freeze-thaw, alkali silica reaction resistance, creep and shrinkage),
- comparative analysis of RCA from different LPS systems (e.g., OWT, WUF, Wk-70 in Poland).

References

1. Huuhka, S., Kaasalainen, T., Hakanen, J. H., & Lahdensivu, J. (2015). Reusing concrete panels from buildings for building: Potential in Finnish 1970s mass housing. *Resources, Conservation and Recycling*, 101, 105–121.
2. Romano, E., Iuorio, O., Nikitas, N., & Negro, P. (2018). A review of retrofit strategies for Large Panel System buildings. In *Proceedings of The Sixth International Symposium on Life-Cycle Civil Engineering*.
3. Panda, K. C., & Bal, P. K. (2013). Properties of self compacting concrete using recycled coarse aggregate. *Procedia Engineering*, 51, 159–164.
4. Duan, Z., Singh, A., Xiao, J., & Hou, S. (2020). Combined use of recycled powder and recycled coarse aggregate derived from construction and demolition waste in self-compacting concrete. *Construction and Building Materials*, 254, 119323.
5. BIBM, Cembureau, EFCA, EFNARC, & ERMCO. (2005). *The European guidelines for self-compacting concrete*.



Durability, deterioration patterns and life cycle costs of hollow concrete blocks partitions: A comparative study

Igal M. Shohet^{1,2} Monica Paciuk³, Alon Uralainis⁴, Gili Lifshitz Sherzer⁴

¹*Ben-Gurion University of the Negev, Israel, igals@bgu.ac.il*

²*Chaoyang University of Technology*

³*National Building Research Institute, Technion, Israel*

⁴*Ariel University, Israel, alonu@ariel.ac.il, gilil@ariel.ac.il*

Keywords: hollow concrete blocks, deterioration, durability, life cycle costs

1. Introduction

This study explores the life expectancy (LE) and life cycle costs (LCC) of hollow concrete block partitions versus alternative interior partitions in residential units, such as gypsum board and autoclaved aerated concrete (AAC) block partitions. Sustainability and economy of hollow concrete blocks are contrasted against light-weight partitions subject to occupancy and service conditions. Three contrasting service conditions were evaluated: Standard (built without faults), Inherent Defect Conditions (with initial, non-progressing flaws), and Failure Conditions (incurring flaws as time progresses). Occupancy condition effect was evaluated employing six 'Negative Occupancy Factors' identified as the central root cause of partition degradation: non-ownership, lack of maintenance, high residential density, presence of young children, domestic pets, and furniture density. They characterize four occupancy condition classes: Light, Moderate, Standard, and Intensive. This study reveals that hollow concrete block partitions proved to be the most long-lasting, lasting more than 100 years under light or moderate occupancy conditions. Gypsum board partitions, although economical, show lower life expectancy and require replacement in 11–27 years under intensive occupancy conditions. Autoclaved concrete blocks present moderate life expectancy as those of equal cost to hollow blocks under standard occupancy conditions. This study presents the effect of service and occupancy on interior partitions life cycle and performance and recommends evidence-based partition alternative selection depending on the service regime.

2. Methodology

The study uses a structured framework to evaluate durability, performance, and life-cycle costs of gypsum, AAC, and hollow concrete block partitions. Field surveys

recorded construction quality, defects, maintenance, and occupancy, with partitions rated on a 1–5 Component Performance (CP) scale, considering flatness, alignment, cracking, peeling, joint integrity, and electrical stability.

Initial Component Performance (ICP): Reflects inherent construction quality

$$ICP = \frac{\sum_{i=1}^n CP_i}{n}, \quad n = 5, \quad (1)$$

Standard Condition Performance (SCP): Measures deterioration under normal service without major failures:

$$SCP = \frac{\sum_{i=1}^n CP_i}{n}, \quad n = 6, \quad (2)$$

Failure Condition Performance (FCP): Accounts for deterioration from specific failure mechanisms. Weighted performance combines initial state, standard deterioration, and failure impact:

$$WPF = -\alpha \cdot Age + \beta - \frac{(100 - ICP)}{n} - \sum_{m=1}^M \frac{(100 - FCP_m)}{m} \quad (3)$$

where: α, β are regression coefficients, n the number of standard indicators, and M the number of failure mechanisms.

Occupancy Conditions Six negative factors define four categories: light (0), moderate (1–2), standard (2–4), and intensive (≥ 4). **Service Life Prediction:** The typical deterioration path (TDP) was derived by regression of SCP against partition age. Service life (SLE) is defined at the intersection of TDP and the minimum required component performance (MRCP60%). The Life Expectancy Limiting Coefficient (LELC) quantifies the effect of failures on SLE. **Lifecycle Cost (LCC):** Includes initial investment, replacement, maintenance, and residual value over a 50-year horizon. Components are replaced only if residual life exceeds half of predicted service life.

3. Field survey and results

The study surveyed 133 partitions in Israel – 33 gypsum, 30 AAC, and 41 hollow concrete blocks. Initial Component Performance averaged 82.7%, 88.8%, and 91.0%, respectively, with gypsum degrading fastest and hollow blocks slowest. Predicted service life (MRCP60%) ranges from 95 to 11 years for gypsum, 72 to 18 for AAC, and 164 to 38 for hollow blocks across light to intensive occupancy. Inherent construction defects reduce life expectancy by 3–11%, with hollow blocks least affected. Common failures include cracks at wall, ceiling, and door junctions, surface cracks,



and electrical instability, with cumulative impacts quantified via LELC: 0.20–0.40 for gypsum, 0.19–0.38 for AAC, and 0.47–0.55 for hollow blocks.

Lifecycle Cost Analysis (LCC) Assuming a 50-year building lifecycle, 5% interest, and annual maintenance of 0.5% of asset value, components are replaced only if their residual life exceeds half of the predicted service life [1, 2]. Gypsum boards have the lowest initial cost at \$94.2/m² and a replacement cost of \$152.7/m², with a life expectancy of 11 years under intensive occupancy and a lifecycle cost of \$52.6/m². AAC blocks cost \$131.3/m² initially, \$157.6/m² for replacement, last 18 years under intensive conditions, and have a lifecycle cost of \$53.6/m². Hollow concrete blocks have the highest initial and replacement costs (\$154.8/m² and \$185.8/m²) but the longest life expectancy of 38 years in intensive occupancy and the lowest lifecycle cost at \$38.4/m². Gypsum boards are economical in light to moderate conditions but require frequent replacement under intensive occupancy, hollow concrete blocks remain the most durable and cost-efficient in demanding conditions, and AAC blocks perform at an intermediate level.

4. Discussion and conclusions

Hollow concrete blocks have the longest service life and most stable performance, gypsum boards degrade fastest under intensive conditions, and AAC blocks are moderately durable. Service life and costs depend on occupancy and construction quality, emphasizing material selection for sustainable, cost-effective design.

References

1. Santos, R., Costa, A. A., Silvestre, J. D., Vandenberg, T., & Pyl, L. (2020). BIM-based life cycle assessment and life cycle costing of an office building in Western Europe. *Building and Environment*, 169.
2. Plebankiewicz, E., Zima, K., & Wieczorek, D. (2016). Life cycle cost modelling of buildings with consideration of the risk. *Archives of Civil Engineering*, 62(2).



Underwater structural investigation: Scour monitoring around bridge piers

Łukasz Topczewski¹, Paweł Mikołajewski^{2, 3}

¹*West Pomeranian University of Technology in Szczecin, Poland, Lukasz.Topczewski@zut.edu.pl*

²*Maritime University of Szczecin, Poland, p.mikolajewski@pm.szczecin.pl*

³*ESCORT TECHNOLOGY, Poland, pawel.m@escort.com.pl*

Keywords: scour, riverbed erosion, sonar investigation, bridge piers inspection

1. Introduction

The technical condition of bridges must be assessed comprehensively, taking into account both the structural integrity of bridge piers and the condition of the riverbed surrounding them. One of the most critical processes affecting bridge stability is scour, a localized form of riverbed erosion occurring around bridge piers, particularly near outer riverbanks [1].

2. Mechanisms of scour formation

Scour is a complex erosional process caused by interactions between river flow dynamics, sediment transport, and structural geometry. Two main types are distinguished: global scour where large-scale riverbed erosion is shaping the main channel and local scour, where concentrated erosion is occurring near individual piers, abutments, or structural obstacles. The formation and severity of scour depend on multiple factors, including: flow velocity and turbulence, water depth and seasonal fluctuations, channel width between piers, pier geometry and orientation relative to flow, riverbed bathymetry, soil composition and sediment size, natural or artificial obstructions (e.g., ice, debris, woody material) [1], [4], [5].

3. Scour monitoring techniques

Monitoring scour around bridge piers is crucial for ensuring structural safety. A combination of traditional field surveys, sonar imaging, and remote sensing techniques is commonly used:

- bathymetric surveys: provide precise measurements of riverbed elevation and scour depth;

- sonar inspections: enable detailed visualization of submerged structures using sonograms [1], [2];
- remote sensing: allows continuous monitoring during high-flow events.

Figure 1 presents an example of underwater sonar imaging performed by ESCORT TECHNOLOGY. Such visualizations are vital for assessing the technical condition of submerged bridge elements.

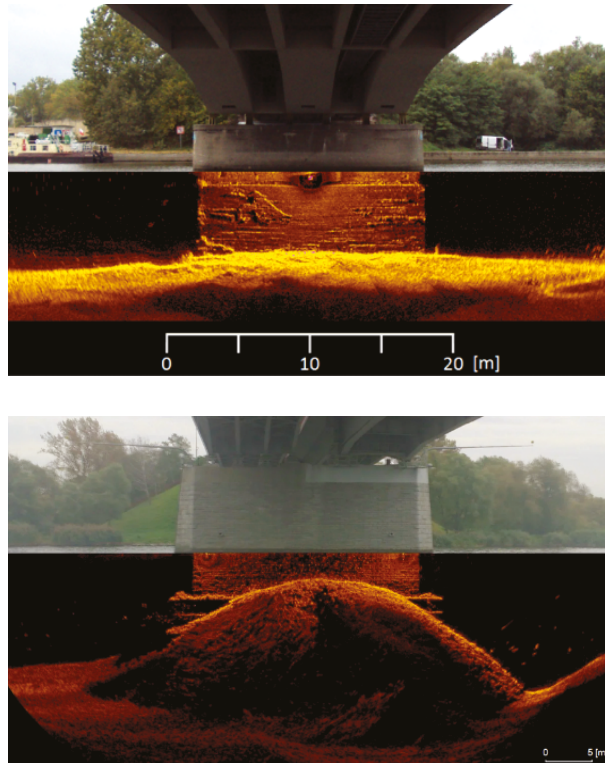


FIG. 1. Underwater Sonar Investigations – ESCORT TECHNOLOGY survey report

4. Case study: MOPMO project

The MOPMO project implemented a permanent scour monitoring system designed to observe changes in riverbed morphology during high-water events. Sonar-based sensors recorded scour depth variations in real time, allowing engineers to identify critical moments of structural vulnerability. Figure 2 shows the monitored locations and the progression of scour development during extreme flow conditions.

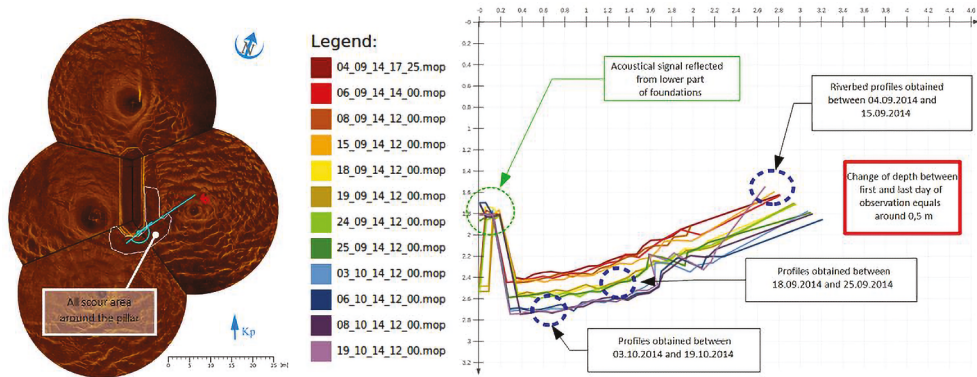


FIG. 2. Location of scour and long term observations [3]

5. Conclusions

Underwater investigations using sonar imaging and bathymetric surveys provide effective tools for assessing the safety of bridge structures. This study demonstrates that integrating continuous monitoring systems, such as those applied in the MOPMO project, significantly improves early detection of scour and enables timely implementation of preventive measures. Future research should focus on combining sonar observations with hydrodynamic modeling to improve scour risk prediction.

Acknowledgments

Special thanks are directed to all team members engaged in the MOPMO project: specialists and engineers from IBDiM and to ESCORT TECHNOLOGY Company.

References

1. Topczewski, Ł., Jarominiak, A., Cieśla, J., Markowski, Z., Mikołajewski, P., Rafalski, L., Rymśa, J., & Zajbert, A. (2015). *Guidelines for the bridge scour monitoring in the proximity of bridge supports*. https://escort-technology.com/wp-content/uploads/WYTYCZNE_Lukasz.pdf
2. Markowski, Z., & Mikołajewski, P. (2011). *Akustyka pomaga w inspekcji budowli wodnych*. Miejskie Obiekty Mostowe – IV Seminarium.
3. Topczewski, Ł., Cieśla, J., Mikołajewski, P., Adamski, P., & Markowski, Z. (2016). Monitoring of scour around bridge piers and abutments. *Transportation Research Procedia*, 14, 3963–3971.
4. Florida Department of Transportation. (2024). *Bridge scour manual*.
5. Jarominiak, A. (2016). Zabezpieczenie przed rozmyciem dna cieków przy filarach mostów. *Drogownictwo*, 10.



Simulations of wire ropes used in prestressed concrete. Model validation based on archival complex experiment

Marcin Gryniewicz¹, Michał Dzun¹, Julita Krassowska¹, Zhihua Chen², Dai Wang³

¹*Bialystok University of Technology, Poland,*

mgryniewicz@pb.edu.pl, mdzun@pb.edu.pl, j.krassowska@pb.edu.pl

²*Tianjin University, China, zhchen@tju.edu.cn*

³*Tianjin Chengjian University, China, wgd@tcu.edu.cn*

Keywords: wire rope, prestressing, concrete, Finite Element Method

1. Introduction

Wire ropes used in prestressed concrete structures transfer prestressing forces by means of adhesion. Some of their most important properties are tension stiffness and resistance. Compared to material strength, which is clear, these properties may depend on wire geometry: particularly wire cross-section area and their configuration, creating a rope. Considering basic solutions only, which are under discussion here, this configuration is usually a helical strand around a single steel core. This paper describes the numerical modelling of wire ropes with various geometries. It was essential to perform a parametric analysis, and prove it by an archival complex experiment which has a wide scope and relates perfectly to the study.

2. Experiment description

It has to be noted clearly that the experiment on which the study described in this paper is based was undertaken in the 1970s [2]. Regardless of age, its wide scope cannot remain neglected. Tested ropes were made of typical geometry comparable to those according to DIN3052 [1] (but 1 x 7 wire ropes). A total of 12 configurations of ropes were tested with 6 repetitions (64 tests for the main experiment). Additionally, the main experiment of ropes was accompanied by material testing of single wires (strands and cores), in a total of 36 tests, to obtain a stress-strain relationship.

The main experiment was divided into two main groups – ropes made of drawn wires of diameter 2,8 mm (resistance $R_m = 2197$ MPa) and 5,5 mm (resistance $R_m = 1668$ MPa). Then, ropes with 6 different values of helix pitch were prepared

within each group. The number of tests, their variability, and detailed archival documentation allowed reconstruction of the experiment numerically. This is sufficient to initially prove the presented method's accuracy.

3. Applied methods

The Finite Element Method is usually an adequate choice for considerations about structural optimisations. The chosen environment is ANSYS LS-DYNA software with a geometry prepared in the SpaceClaim module. This set is suitable for parametric analysis of steel wire ropes where the overall geometry is constant and only two variables are changing (helix pitch and the strands diameter).

It was possible to automate the process of preparing a geometry. The main idea was to use Python scripting within SpaceClaim to build an algorithm which creates the wires. Its logic was based on helical solids generation using a built-in function "RevolveFaces – ByHelix" (described in the accompanying paper where helical strands pitch was under research). Boundary conditions are applied as zero displacement at one rope end and a displacement value at the opposite end to create a quasi-axial load to the ropes. Mesh size was set between 0,8 mm and 1,5 mm (Fig. 1). The implicit type solver has been used for analysis.

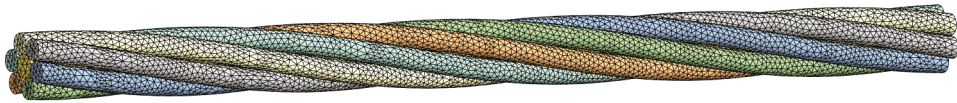


FIG. 1. Example of rope meshing (1x5,5 + 6x5,0)

4. Results and discussion

The outcomes from the numerical analysis gave a satisfactory match to the archival tests, which can be clearly visible on the selected charts in Fig. 2. The main conclusion is that geometry generation using "RevolveFaces – ByHelix" feature provides a good quality input for FEM simulations. Then it can be efficiently solved by the LS-DYNA implicit solver. Additional checks proved that results are comparable to those which could be obtained via Ansys Mechanical. However, model preparation in Mechanical requires more user preparation, especially with contact definitions, when in LS-DYNA it appears to be more intuitive, even by utilisation of default settings.

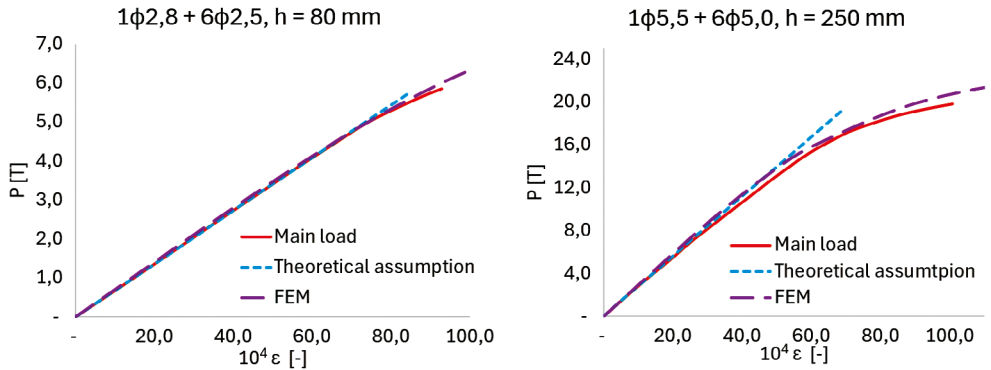


FIG. 2. Selected results of the experiment and simulations (where h is the pitch of the helix)

Acknowledgments

This work is a part of the project no LIDER14/0206/2023 financed by the National Centre for Research and Development in Poland, and the project no WZ/WB-III/6/2023 at the Białystok University of Technology under financing from the Ministry of Science and Higher Education of the Republic of Poland.

References

1. DIN 3052:1972-03 *Steel wire ropes; spiral rope 1×7*.
2. Kuś, S. (1971). *Sploty jako ciężna w konstrukcjach strunobetonowych. Analiza teoretyczna. Badania i zastosowanie* (in Polish). Instytut Techniki Budowlanej.



Effect of fresh and spent FCC catalyst (ECAT) on the mechanical and microstructural properties of eco-friendly ultra-high-performance concrete

Hassan Abdolpour, Jennifer Udebunu, Benedykt Mrosek, Michał Pachnicz

*Wrocław University of Science and Technology, Poland,
Hassan.abdolpour@pwr.edu.pl, jennifer.udebunu@pwr.edu.pl,
benedykt.mrosek@pwr.edu.pl, michal.pachnicz@pwr.edu.pl*

Keywords: Ultra high-performance concrete, recycled steel fiber, spent catalyst, micro-computed tomography (μ CT).

1. Introduction

The reuse of industrial by-products like Fluid Catalytic Cracking catalyst (Ecat) in concrete aligns with sustainable construction practices. While prior studies have explored its pozzolanic potential, limited work exists on its comparative performance when used in fresh versus spent form. This research aims to bridge this gap by combining mechanical testing with 3D microstructural analysis.

2. Materials and methods

2.1. Mix composition

Four concrete mixes were prepared with Ecat content of 0%, 10%, 20%, and 30% by mass of cement. Two series were produced:

- FRESH: Containing unused (fresh) Ecat.
- USED: Containing spent Ecat collected from refinery operations.

2.2. Mechanical testing

Load-CMOD [1] curves were analysed to determine peak strength, stiffness (initial slope) as shown below. All mixes show an initial sharp increase in load with CMOD (crack mouth opening displacement), followed by a peak and then a descending branch. R3-E20-USED (20% ECAT): Exhibits the highest peak load among the used ECAT mixes, showing better load-carrying capacity. Spent ECAT performs better than Fresh ECAT at all replacement levels, offering higher load capacity and more stable fracture response. However, increasing ECAT content still reduces peak load while enhancing ductility.

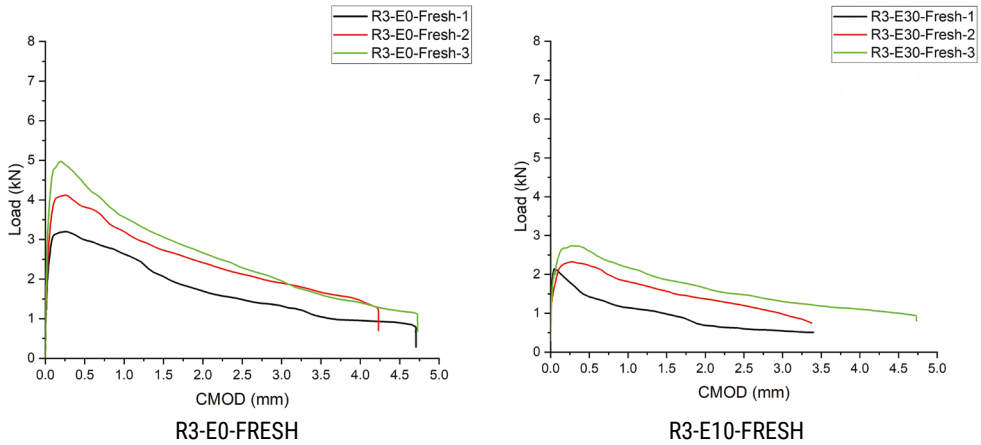


FIG. 1. Load vs. CMOD for Fresh ECAT

2.3. Micro-CT analysis high-resolution μ CT

Micro-CT Analysis High-resolution μ CT scans were conducted on representative samples from both series. Morphometric parameters including porosity, pore connectivity, and degree of anisotropy were quantified [2–3].

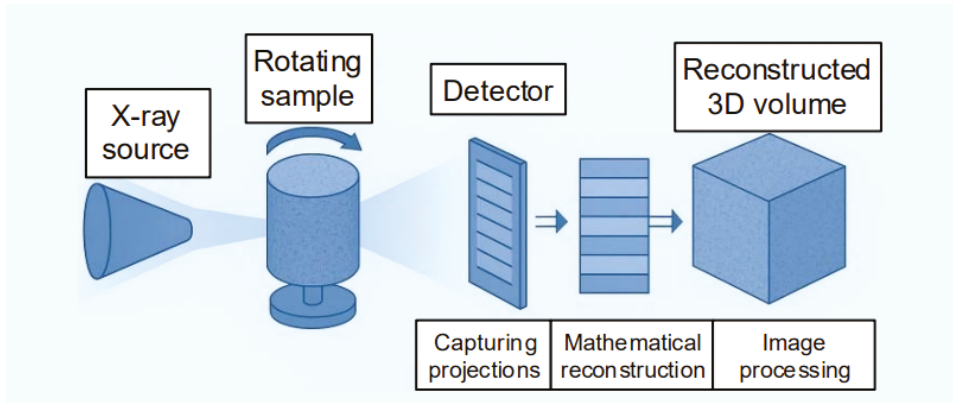


FIG. 2. Schematic representation of the μ CT scanning process, illustrating the X-ray source, rotating concrete sample, digital detector capturing a series of 2D projections, and the resulting reconstructed 3D volume used for microstructural analysis



3. Results and discussion

Comparative Performance: Fresh vs. Spent ECAT

A direct comparison between fresh and spent ECAT highlights the following key observations:

1. Strength retention – Spent ECAT mixes achieved higher peak loads than Fresh ECAT mixes, irrespective of the replacement level.
2. Ductility enhancement – Both fresh and spent ECAT improved ductility at higher replacement levels, with Spent ECAT providing more stable crack propagation.
3. Optimal replacement – At 20% replacement, mixes balanced strength and fracture resistance most effectively.

The results highlight the trade-off between strength and ductility when substituting OPC with ECAT. While higher ECAT replacement reduces peak load capacity, it enhances fracture resistance and post-cracking toughness. Spent ECAT demonstrates superior mechanical performance compared to Used ECAT, suggesting that its reactivity contributes positively to the matrix. An optimum balance is achieved at around 20% ECAT replacement, where both strength and ductility are retained at practical levels.

References

1. Rilem T. (2002). 162-TDF. Test and design methods for steel fibre reinforced concrete. *Materials and Structures*, 35(9), 579–582.
2. Feldkamp, L. A., Davis, L. C., & Kress, J. W. (1984). Practical cone-beam algorithm. *JOSA A*, 1(6), 612–619. <https://doi.org/10.1364/JOSAA.1.000612>
3. Katsevich, A. (2002). Theoretically exact filtered backprojection-type inversion algorithm for spiral CT. *SIAM Journal of Applied Mathematics*, 62(6), 2012–2026.



Advanced engineering of eco-efficient UHPFRC using recycled steel fibres and pozzolanic petrochemical waste

Hassan Abdolpour

hassan.abdolpour@pwr.edu.pl

Keywords: ultra-high-performance concrete (UHPFRC), recycled steel fibres, spent equilibrium catalyst, sustainable construction materials

Abstract

Innovative ultra-high performance fiber-reinforced concretes (UHPFRCs) that incorporate recycled materials have been developed in response to the need for high-performance and environmentally friendly building materials. This was possible with the use of two important industrial byproducts – spent equilibrium catalyst (Ecat) waste from petrochemical refining and recycled steel fibers (RSFs) taken from end-of-life tires. This work offers a unified research framework aimed at creating a new class of eco-friendly, self-compacting, ultra-high performance mortar and concrete mixes. These substances have the combined benefit of improving cementitious composites' mechanical qualities and drastically lowering their environmental impact.

The rheological, mechanical, microstructural, and fracture behavior of UHPFRCs with different ratios of RSF (1–3% by volume) and Ecat (5–20% by weight) were examined in a number of experimental and numerical investigations. The results consistently showed that adding RSF improves flexural toughness and crack-arresting ability by converting brittle matrix behavior into ductile post-cracking response. At the same time, a pozzolanic aluminosilicate called Ecat enhanced the hydration process, strengthened the microstructure, and permitted a 15% cement substitution without sacrificing durability or compressive strength. These improvements came at the expense of 5–15% reductions in CO₂ emissions and production costs.

The mini-slump cone and flow tests were used to assess the workability of self-compacting mixes. While Ecat lowered fluidity because of its high surface area and water absorption capacity, the incorporation of RSF somewhat decreased flowability (up to 22% at 3% RSF). However, by tailoring the dosage of the superplasticizer, the necessary self-compatibility was maintained. The mortars' potential for structural applications was demonstrated by their attainment of compressive strengths above 180 MPa and flexural strength increases of up to 21% at 28 days.

Fracture propagation and post-peak behavior under various loading conditions were successfully reproduced by advanced finite element modeling using the Concrete Damage Plasticity (CDP) model together with element deletion techniques.



The suggested constitutive models' dependability was validated using experimental data, which also showed how well hybrid reinforcement techniques reduce brittle failures. The best technique for predicting shear strength across various compositions was determined to be ridge regression.

Scanning electron microscopy and X-ray diffraction microstructural analyses showed that Ecat-modified mortars had a denser matrix and more C–S–H and C–A–S–H gel formation. The interfacial transition zone (ITZ) improved and porosity decreased, especially in mixtures that contained both RSF and Ecat. Additionally, these materials improved repair capabilities and interfacial bonding in substrate-overlay systems with flexible polyurethane joints.

The comprehensive lifecycle analysis highlighted the ecological and economic viability of this approach. The use of waste-derived steel fibres and catalysts diverts substantial waste from landfills, reduces dependency on virgin resources, and contributes to carbon neutrality objectives in the construction sector. Moreover, these UHPFRC mixes are ideal for high-performance infrastructure applications, such as seismic retrofitting, impact-resistant overlays, military structures, and nuclear facilities.

This integrated research contributes a pioneering approach to eco-efficient material engineering by merging high mechanical performance with waste valorization. It presents a robust pathway to large-scale deployment of green UHPFRCs, aligning structural innovation with global sustainability goals.



Probabilistic maintenance optimization of concrete culverts: Integrating corrosion-driven deterioration and structural simulation

Gili Lifshitz Sherzer¹, Igal M. Shohet^{2,3}

¹Ariel University, Israel, gilil@ariel.ac.il,

²Chaoyang University of Technology, Taiwan, igals@bgu.ac.il

³Ben-Gurion University of the Negev

Keywords: corrosion-induced deterioration, FDEM, probabilistic maintenance, transition matrix

1. Introduction

Culverts are critical for roadway and water management networks, yet they often receive insufficient attention in long-term maintenance planning. In this research, a comprehensive framework is presented to optimize the maintenance of culverts based on probabilistic modelling and field-validated deterioration analysis. An extensive field survey was carried out to create empirical deterioration patterns, and an exponential degradation model showed a good fit ($R^2 = 0.94$). A Markovian transition probability matrix was established to model transition in performance states along time and derive an optimal maintenance strategy. In addition, numerical modelling was carried out to compare the structural response of corroding culverts. A local-to-global modelling strategy was used to monitor the cracking progression according to the corrosion severity. The simulation considered significant mechanical loads, such as positive and negative bending moments, live and dead load shear, and hydrostatic and geostatic pressure due to water and soil [1]. In the numerical simulation using the finite-discrete element method (FDEM), we applied the effects of electrochemical corrosion by modelling the resulting radial pressure as a mechanical response, enabling us to capture the successive phases of crack initiation and propagation [2]. The computed damage pattern versus site observation exhibited notable differences, highlighting the role of unmodeled influences such as construction quality, waterproofing breakdown, and local environment and highlighting the requirement for multi-parameter evaluation in real culvert management.

2. Results

2.1. Damage

Fracture patterns and structural damage were assessed through FDEM simulations. The extent of damage was measured as the proportion of the affected area relative to the volume of the central block in which the fracturing process was modelled. The findings are represented as a percentage (see Fig. 2, left) and categorized into five distinct damage grades: 1 – minimal, 2 – up to 5%, 3 – 5–20%, 4 – 20–50%, and 5 – severe (>50%). Fig. 2 (right) illustrates the evolution of the damage over time.

Fig. 1 shows that the crack growth stays steady for around 58 years before undergoing a profound acceleration. There is a period of unstable growth after around 60.5 years. Stages 1 and 2 last similarly, while Stage 3 is substantially prolonged.

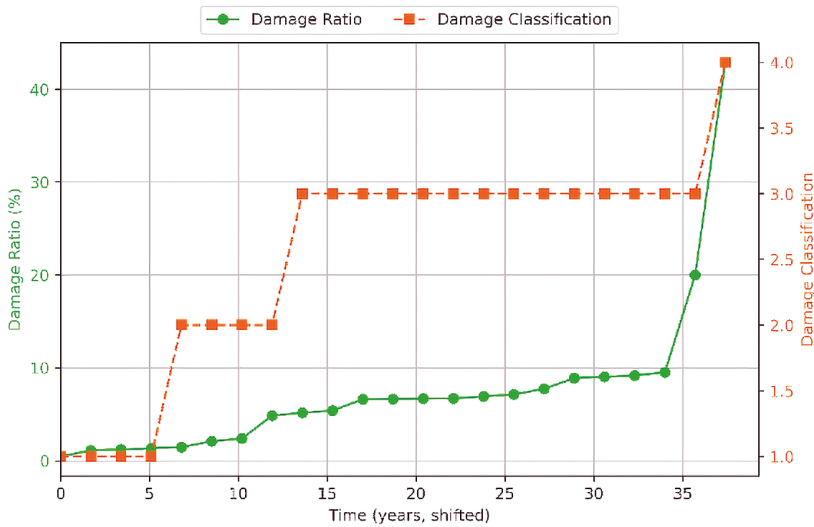


FIG. 1. Damage assessment over time: (left) percentage of damage and (right) classification scale 1–5

2.2. Regression analysis

The survey data were utilized to harmonize culvert age and performance to determine a suitable deterioration model. Three types of regressions, namely linear, logarithmic, and exponential, were tested, and the exponential model exhibited the most appropriate fitting of the apparent degradation trend (Fig. 2). The model showed good validity, given the value of the coefficient of determination of $R^2 = 0.9416$, thus supporting its stability.

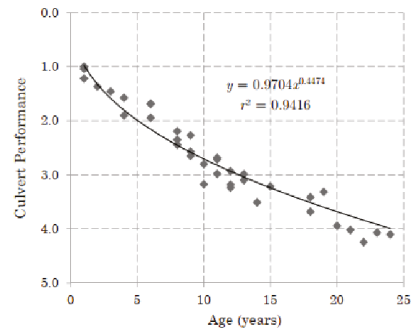
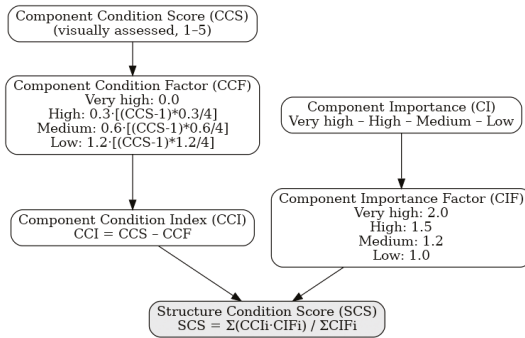


FIG. 2. (left) Structure Condition Score framework; (right) Culvert survey data points with fitted exponential deterioration model

Exponential models have been effective in forecasting culvert deterioration [3]. A χ^2 (chi-squared) test was conducted on culvert performance ratings (1–5) in four groups for cross-validation of field data. With four degrees of freedom, the test provided a 92% likelihood of a normalized distribution, supporting its usage under the exponential deterioration model application. There is, however, a discrepancy between simulation results and field data. It begins to deteriorate after steel depassivation (≈ 20 years), while inspections often show damage in the first year of operation. Such early damage is likely due to construction defects, poor work, or unaddressed issues such as waterproofing or joint failures, and not only because of corrosion cracking.

References

1. Lifshitz Sherzer, G., & Shohet, I. M. (2025, June 11–13). *Probabilistic optimization of culverts maintenance: Analyzing corrosion-induced deterioration and structural performance* [Conference presentation]. International Conference on Digital Frontiers in Buildings and Infrastructure (DFBI 2025), Delft University of Technology, Delft, Netherlands.
2. Urlainis, A., Lifshitz Sherzer, G., & Shohet, I. M. (2024). Multi-scale integrated corrosion-adjusted seismic fragility framework for critical infrastructure resilience. *Applied Sciences*, 14(19), 8789. <https://doi.org/10.3390/app14198789>
3. Andrade, C., Alonso, C., & Molina, F. J. (1993). Cover cracking as a function of bar corrosion: Part I – Experimental test. *Materials and Structures*, 26(8), 453–464. <https://doi.org/10.1007/BF02472805>

Static analysis of the post-tensioned SPP truss girder

Petr Moštěk, Ladislav Klusáček

Brno University of Technology, Czech Republic, petr.mostek@vutbr.cz

Keywords: truss girder, analysis, post-tensioned concrete

1. Introduction

In the second half of the 20th century, prestressed concrete was primarily used in buildings where long spans without internal supports were required. Although steel was commonly used for these structures, over time prestressed concrete became more widely used. To make truss girders economically viable despite their labor intensity, they had to be produced as prefabricated elements and in large series. For this reason, they were mainly used in countries of Eastern Europe, such as Czechoslovakia, Poland, Hungary and others. They were manufactured either as one piece or in segments, which were connected on site. As with other post-tensioned structures from that period, this type of construction is often affected by corrosion of the prestressing tendons, mainly due to poorly executed or completely missing grouting of the prestressing ducts. In fact, there have been recent cases of structural failures involving these systems in the Czech Republic and Slovakia (Fig. 1) [1].



FIG. 1. Truss girder collapse in the Czech Republic from 2023 [1]

For this reason, the risks associated with these structures should not be underestimated. The topic of concrete truss girders is primarily focused in terms of structural assessment, the design of new systems, and the optimization of these structures with respect to their carbon footprint. The aim of this article is to analyse this type of structure using various methods, compare them with one another, and assess their suitability. The methods considered include a historical calculation approach, a simplified beam model, a more accurate beam model, and a shell model.

2. Methodology

The structure under investigation is an SPP truss girder, which was mass-produced in the former Czechoslovakia. It is a segmented, post-tensioned concrete truss girder (Fig. 2).

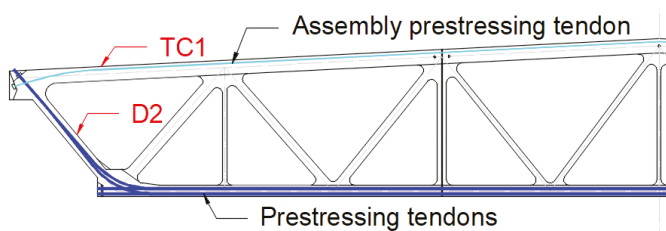


FIG. 2. SPP 6-18/6 truss girder TC1 = top chord, D2 = edge diagonal member

Three types of loads on the truss were considered: self-weight, load from the roof cladding, and prestressing. Roof cladding load was applied as a uniformly distributed load along the top chord. Prestressing was modeled using the method of equivalent loads induced by the prestressing tendons.

In historical design procedures, internal forces in truss structures were calculated using a simplified approach, assuming pinned joints at the nodes. The effects of non-nodal loads on the truss were considered either by modeling it as a continuous beam or as a beam with fixed supports at both ends, with the fixity assumed at the nodal points.

A simplified beam model was created in RFEM5 (Fig. 3); calculation was performed as a linear analysis.

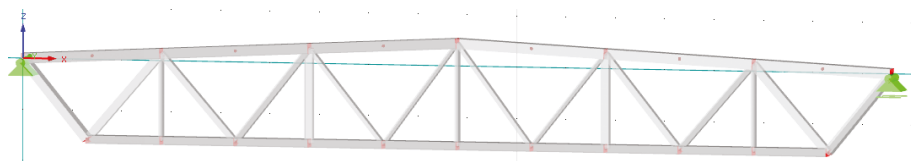


FIG. 3. Numerical model in RFEM

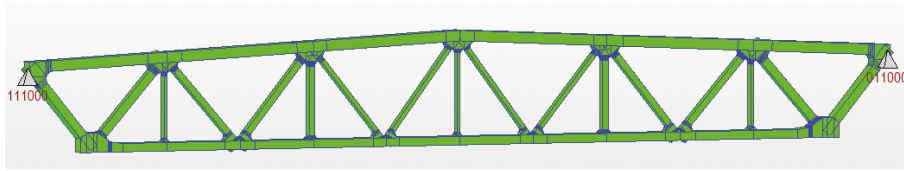


FIG. 4. Numerical model in MIDAS CIVIL

A more refined beam model was created using MIDAS CIVIL (Fig. 4). Compared to the simplified beam model, this model includes the accurate geometry of the truss, taking into account the nodal regions. Another difference is that a nonlinear analysis was performed.

3. Results

To evaluate the different analytical variants, an interaction diagram $N + M$ was created for each member. The comparison was made by determining the corresponding bending resistance M_{Rd} for a given normal force $N_{Rd} = N_{Ed}$. The calculated moment M_{Ed} was then divided by M_{Rd} . The resulting M_{Ed}/M_{Rd} ratios for the top chord 1 (TC1) and diagonal 2 (D2) are shown in Figs. 5 and 6.

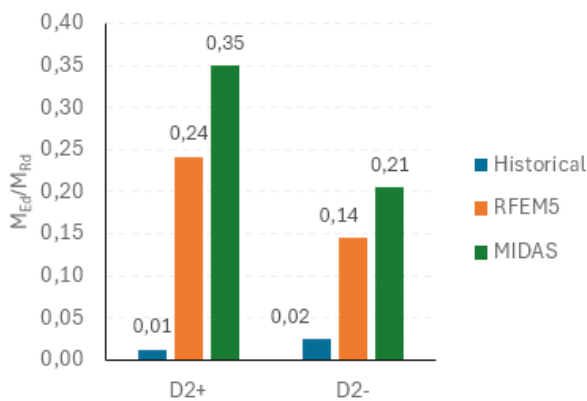


FIG. 5. Comparison of analytical models for D2

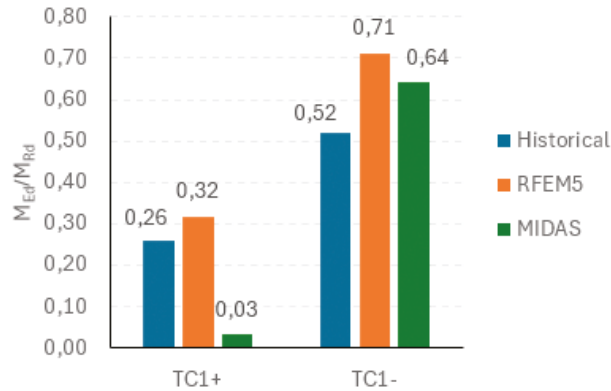


FIG. 6. Comparison of analytical models for TC1

4. Conclusion

Figure 5 clearly shows that the historical methods are not capable of accounting for the frame behavior of the structure. Figure 6 demonstrates that moment effects can be partially considered in the TC model using manual calculation and shows an anomaly for TC1+ when using MIDAS CIVIL. This anomaly will be examined more closely in the next phase of the analysis.

Until now, this type of structure appears more dangerous than we initially assumed.

References

1. Bureš, V., Mynarčík, P., Čítek, D., Hlaváček, A., & Čapek, K. (2024). *Zkušenosti z průzkumů dodatečně předpjatých vazníků průmyslových hal* (in Czech). Konstrukce. <https://bit.ly/konstrukceczclanek1484>



Influence of casting method on bond performance and self-compacting concrete properties

Milena Kucharska, Piotr Dybel

AGH University of Krakow, Poland, kucharska@agh.edu.pl, dybel@agh.edu.pl

Keywords: casting technology, self-compacting concrete, bond, strength properties

1. Introduction

The process of casting the concrete mixture from the bottom of the formwork is a technique exclusive to self-compacting concretes. It has been demonstrated that this method is particularly effective in enhancing the efficiency of self-venting, which, in turn, has a number of beneficial outcomes. Primarily, it leads to an improvement in the surface and structural quality of the concrete elements. Consequently, it can be assumed that this technology will improve the quality of the reinforcing bar cover and, therefore, the steel-concrete bond.

2. Materials and methods

A deep beam test element measuring $1440 \times 640 \times 160$ mm was designed and subdivided into modular specimens intended for bond strength (10 samples), compressive strength (13 samples), splitting tensile strength (9 samples), and computed tomography (CT) analysis (4 core samples). Steel reinforcement bars with a diameter of 16 mm (class B500SP) were embedded in the specimens designated for both bond and CT tests. The bars were positioned to represent good and poor bond conditions at distances of 8 and 56 cm from the top surface of the element. Two casting methods were employed to build test elements: top-down (TD) and bottom-up (BU) concreting. All elements were produced using self-compacting ready-mix concrete (SCC). A pull out method was used for bond tests [1].

3. Results and discussion

3.1. Concrete properties

The mixture satisfied the requirements for SCC mixtures, grading into classes SF1 (slump-flow), VS2 (viscosity) and PL2 (passing ability). The mean compressive strength of the SCC determined for samples from the test elements was 73.7 MPa and 79.7 MPa for the element produced using top-down and bottom-up casting, respectively.

Meanwhile, the mean splitting tensile strength ascertained on specimens extracted from the test elements was determined to be 3.8 MPa and 4.4 MPa for the TD and BU element, respectively. The higher results of concrete samples made using bottom-up casting technology is attributed to the improved self-venting associated with the flow of the mix in the formwork. The mix injected from the bottom valve displaces the previously placed mix in the formwork without disrupting its venting process.

3.2. Bond properties

The pull-out tests enabled the determination of the local relationship between the bond stress and the slip of the rebar (Fig. 1 – left). This approach provides a comprehensive evaluation of the bond behaviour, encompassing both bond strength and stiffness. A comparison of the behaviour of equivalent rebars in the TD and BU elements allows the conclusion to be drawn that the technology of casting the SCC mixture bottom-up ensures high bond stiffness and bond strength results. In accordance with international concrete design standards [2], in areas of poor bond conditions, bond stresses are reduced. This must be counterbalanced by extending the anchorage length. In the analysis of the casting position factor, i.e. the ratio of the bond strength of the bottom and top bars, it can be observed that there are smaller differences between them in the BU element. This suggests that the bond conditions for this concreting technology are more uniform.

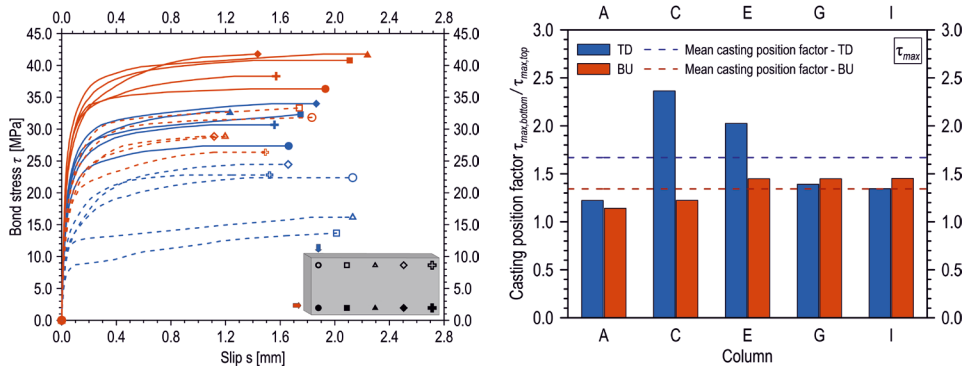


FIG. 1. Bond test results: bond-slip relationships (left) and casting position factor (right) in the deep-beam elements

3.3. Quality of steel-concrete bond zone

The quality of the concrete cover was evaluated on the basis of tomographic imaging, which allows the internal structure of the material to be visualised and the voids around the reinforcing bars to be distinguished. As illustrated in Fig. 2, the three-dimensional images demonstrate an occurrence of voids beneath the top rebars of TD and BU elements. A continuous void was formed under the top bars of the TD element

due to plastic settlement and bleeding effects. It is notable that no such void is formed around the top bars of the BU element, and that only increased porosity in comparison to the cover of the bottom bars is observed.

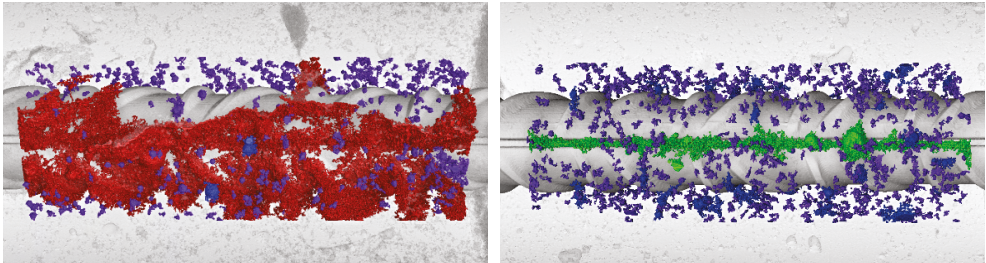


FIG. 2. Tomographic view of concrete cover of top rebars in TD (left) and BU (right) element

Acknowledgments and funding

This research was financially supported by grant No. 2023/49/N/ST8/01835 of the National Science Centre, Poland. Authors would like to acknowledge Steel Quality Promotion Centre (CPJS) and Doka GmbH for material support.

References

1. EN 10080:2015 *Steel for the reinforcement of concrete*.
2. EN 1992:2024 *Eurocode 2 – Design of concrete structures – Part 1-1: ‘General rules, rules for buildings, bridges and civil engineering structures’*.

Experimental assessment of crushed prefabricated fibre-reinforced concrete rings

Agnieszka Głuszko, Lidia Buda-Ożóg

Rzeszow University of Technology, Poland, agluszko@prz.edu.pl, lida@prz.edu.pl

Keywords: FRC, concrete rings, crushing strength,

1. Introduction

Prefabricated concrete rings are structural elements widely used in sewerage and drainage systems. In conventional solutions, steel reinforcement is applied to provide adequate load-bearing capacity. However, its durability is significantly reduced in aggressive environments containing chlorides, sulfates, and organic compounds. Steel corrosion leads to structural degradation, shortening of service life, and the need for costly repairs. An alternative to conventional reinforcement is fibre-reinforced concrete (FRC), in which synthetic macrofibres are uniformly dispersed within the cementitious matrix. The dispersed fibres enhance ductility and crack resistance, thereby improving the durability of prefabricated elements.



FIG. 1. Prefabricated concrete ring prepared for crushing testing with the application of an optical displacement measurement system

The aim of the study is to compare the experimental results of prefabricated fibre-reinforced concrete rings and conventionally reinforced concrete rings with an internal diameter of 1500 mm subjected to crushing tests. The analysis focuses on the cracking mechanism and failure modes of the elements under axial loading.

2. Crushing tests

The research program comprised full-scale compression tests of prefabricated rings made of C45/55 concrete modified with synthetic polymer fibres. For comparison, concrete elements without dispersed reinforcement but strengthened with conventional steel reinforcement were also tested. The tests were carried out in a vertical position in accordance with the requirements of PN-EN 1917 [1] and PN-EN 476 [2]. The specimens had an internal diameter of 1500 mm, a wall thickness of 150 mm, and a height of 500 mm. The test setup included steel loading plates with elastomer pads, linear displacement transducers, strain gauges, and the Aramis optical measurement system (*Fig. 1*). During the tests, the load-displacement response, crack initiation and propagation, as well as the failure mechanism of the elements were recorded.



FIG.2. Failure crack in a fibre-reinforced concrete ring after the crushing test

3. Conclusions

The experimental tests confirmed that prefabricated fibre-reinforced concrete rings meet the standard requirements for compressive strength with a considerable safety margin. The average ultimate load exceeded 37 kN, which is three times higher than the minimum crushing load F_n of 12.5 kN specified in PN-EN 1917 [1]. The recorded



load-displacement curves exhibited a linear response up to the first cracking. After cracking, a distinct strain-hardening phase was observed, during which the load-bearing capacity of the elements continued to increase despite growing displacements. The failure process was ductile, without a sudden break, and was characterised by a clear plastic plateau accompanying the development of deformations (*Fig. 2*). The observed differences in the load-displacement curves can be attributed to the random distribution of fibres within the concrete matrix and the inherent material heterogeneity. In comparison, the steel-reinforced rings reached significantly lower ultimate load values and showed a less favourable structural behaviour. Their failure mechanism was more brittle, with sudden crack propagation and limited deformation capacity. The results clearly indicate that fibre-reinforced concrete rings provide higher load-bearing capacity and a significantly more ductile behaviour compared to plain concrete rings.

Acknowledgments

“The Regional Centre of Excellence in Engineering for Quality of Life and Technological Development”, funded by a subsidy from the Minister of Science and Higher Education under “The Regional Initiative of Excellence” program (project no. RID/SP/0032/2024/01)

References

1. Polish Committee for Standardization. (2004). *Studzienki włączowe i niewłączowe z betonu niezbrojonego, betonu zbrojonego włóknem stalowym i żelbetowe* (PN-EN 1917:2004).
2. Polish Committee for Standardization. (2012). *Wymagania ogólne dotyczące elementów stosowanych w systemach kanalizacji deszczowej i sanitarnej* (PN-EN 476:2012).

Assessment of second-generation Eurocode 2 in predicting shear resistance of FRP-reinforced lightweight concrete members

Agnieszka Wiater, Tomasz Wojciech Siwowski

Rzeszow University of Technology, Poland, wiater@prz.edu.pl, siwowski@prz.edu.pl

Keywords: shear strength, lightweight concrete, FRP reinforcement, Eurocode 2

1. Introduction

The use of lightweight concrete (LWC) leads to a reduction in structural dead weight by 25–30% relative to conventional concrete. Nevertheless, LWC's increased permeability facilitates the penetration of aggressive agents, thereby accelerating degradation, increasing maintenance demands, and shortening the structure's lifespan. For structures exposed to such conditions, fibre-reinforced polymer (FRP) reinforcement is preferred over traditional steel bars due to its corrosion resistance. Shear resistance constitutes a governing limit state in the structural design of such elements, ensuring compliance with safety requirements and achieving the prescribed reliability levels.

2. Shear resistance according to the second-generation Eurocode 2

Annex R of EN 1992-1-1 [2] contains rules for the design of new structures reinforced with GFRP or CFRP bars. Regarding shear strength, the basic equation used for steel reinforcement is modified by replacing the yield strength of steel with the characteristic tensile strength of FRP bars. Additionally, a reduction factor E_{fR}/E_s is introduced. These modifications can be summarized as follows:

$$\tau_{RC} = \max \left[11 \cdot \sqrt{\frac{f_{ck}}{f_{fR0}} \cdot \frac{E_{fR}}{E_s} \cdot \frac{d_{dg}}{d}}; 0.66 \left(100 \cdot \rho_l \cdot \frac{E_{fR}}{E_s} \cdot f_{ck} \cdot \frac{d_{dg}}{d} \right)^{\frac{1}{3}} \right] \quad (1)$$

$$d_{dg} = \begin{cases} \min \left(16 + a_g \cdot \left(\frac{60}{f_{ck}} \right)^2 ; 40 \right) & \text{for } f_{ck} > 60 \text{ MPa} \\ \min(16 + a_g ; 40) & \text{for } f_{ck} \leq 60 \text{ MPa} \end{cases} \quad (2)$$

where: ρ_l is the FRP reinforcement ratio, a_g is the maximum aggregate size, d is the distance from extreme compression fibre to centroid of tension reinforcement, f_{ck} is the compressive strength of concrete, f_{fR} is the characteristic tensile strength of FRP reinforcement, E_{fR} is the modulus of elasticity of FRP reinforcement and E_s is the modulus of elasticity of ordinary reinforcing steel.

Equation (1) do not account for material safety and partial factors (whose values in the relevant formulas were assumed to be 1.00). It should be noted that this Annex does not apply to the use of FRP reinforcement in lightweight concrete. However, this study attempts to assess the applicability of the proposed equation for such elements. The results obtained from Eq. (1) were taken into consideration, and a similar modification was applied as for steel-reinforced lightweight concrete, based on Annex M [2], where the parameter d_{dg} is assumed to be 16 mm.

3. Assessment of procedure

To assess the prediction of shear resistance, a database of 50 LWC/FRP elements was created based on a literature review [1, 3–7]. Of the 50 test specimens nine are slab specimens and 41 are beam specimens. The test specimens were made of three different lightweight concretes. Most specimens (in four works) were made of lightweight sand concrete. All-lightweight concrete was used only in one study [3] and only one study utilised fibre-reinforced lightweight concrete [7]. Finally, the analysed studies utilised three different types of FRP composite bars. Most of the research was conducted on GFRP bars. In one study, BFRP bars were used [5] and one test was partially performed on CFRP bar-reinforced elements [3]. The results of comparing shear resistance calculations (τ_{RC}) with values obtained from experimental research (τ_{exp}) are presented qualitatively and quantitatively in Figure 1 as ratio τ_{exp}/τ_{RC} . The individual designations are as follows: the type of composite reinforcement (blue-GFRP; red-CFRP; green-BFRP) and the type of lightweight concrete (black marker stroke-sand lightweight concrete; green bold marker stroke-all-lightweight concrete; red double line marker stroke-fibre-reinforced lightweight concrete). The results of the tests of slabs and beams were compiled together because the code procedures for these elements are identical (however, the diagrams distinguish the type of tested elements as well, circle for beams and triangular for slabs).

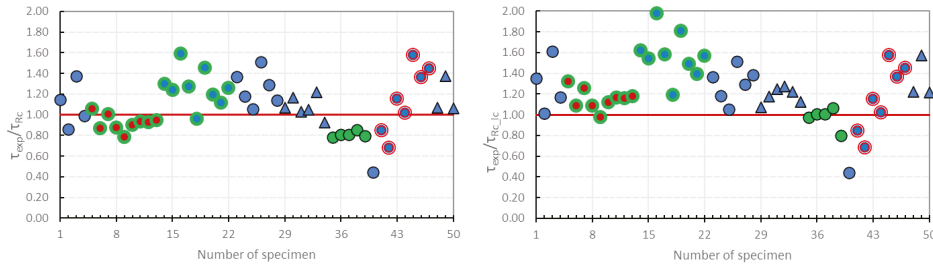


FIG. 1. Ratio of experimental to calculated results without (left) and with (right) consideration of lightweight concrete

An evaluation of the whole database showed an average ratio of 1.08 without considering lightweight concrete, and 1.24 when lightweight concrete was taken into account, with standard deviations of 0.24 and 0.28, respectively. Further analyses were conducted regarding element type, concrete type, and FRP type; however, these results are not presented here due to abstract length limitations.

References

- [1] Bengar, H. A., Zarrinkolaei, F. A., & Bozorgnasab, M. (2021). Shear capacity of lightweight concrete beam reinforced with glass fiber-reinforced polymer bars. *Iranian Journal of Science and Technology, Transactions of Civil Engineering*, 45, 1565–1574. <https://doi.org/10.1007/s40996-020-00457-y>
- [2] European Committee for Standardization. (2023). *Eurocode 2: Design of concrete structures – Part 1–1: ‘General rules and rules for buildings, bridges and civil engineering structures’* (EN 1992-1-1:2023).
- [3] Kim, C. H., & Jang, H. S. (2014). Concrete shear strength of normal and lightweight concrete beams reinforced with FRP bars. *Journal of Composites for Construction*, 18, 04013038.
- [4] Liu, R., & Pantelides, C. P. (2013). Shear strength of GFRP reinforced precast lightweight concrete panels. *Journal of Composites for Construction*, 48, 51–58.
- [5] Mehany, S., Mohamed, H. M., & Benmokrane, B. (2022). Flexural strength and serviceability of GFRP-reinforced lightweight self-consolidating concrete beams. *Journal of Composites for Construction*, 26, 04022020. [https://doi.org/10.1061/\(ASCE\)CC.1943-5614.0001208](https://doi.org/10.1061/(ASCE)CC.1943-5614.0001208)
- [6] Vakili, S. E., Homami, P., & Esfahani, M. R. (2019). Effect of fibers and hybrid fibers on the shear strength of lightweight concrete beams reinforced with GFRP bars. *Structures*, 20, 290–297. <https://doi.org/10.1016/j.istruc.2019.04.006>
- [7] Wiater, A., & Siwowski, T. (2020). Serviceability and ultimate behaviour of GFRP reinforced lightweight concrete slabs: Experimental test versus code prediction. *Composite Structures*, 239, 112020. <https://doi.org/10.1016/j.compstruct.2020.112020>



Effect of perforation in CFRP tubes on load-bearing capacity of short concrete columns

Oliwia Sikora¹, Krzysztof Adam Ostrowski²

¹*Cracow University of Technology, CUT Doctoral School, Poland, oliwia.sikora@doktorant.pk.edu.pl*

²*Cracow University of Technology, Poland, krzysztof.ostrowski.1@pk.edu.pl*

Keywords: Strengthening, Perforation, CFRP tubes, Concrete columns

1. Introduction

The growing interest in composite materials in the construction industry offers a compelling alternative to traditional structural solutions. Fiber Reinforced Polymers (FRPs), due to their high tensile strength, low self-weight, design flexibility, and resistance to aggressive environmental conditions, help mitigate corrosion and external degradation. Among them, Carbon Fiber Reinforced Polymers (CFRPs) exhibit the most favourable mechanical properties, making them a valuable option in structural engineering applications. However, a significant drawback of CFRPs lies in their poor performance at elevated temperatures. The epoxy resins typically used for bonding CFRP laminates becomes plasticized at a temperature of about 60°C, which under intense solar exposure may lead to material degradation and, consequently, structural failure.

In response to this challenge, the presented research explores the improvement of the interaction between concrete and composite components through the use of internally placed perforated CFRP tubes. As part of the SONATA-19 grant (2023/51/D/ST8/01795), the influence of perforation distribution in the perforated CFRP tubes on the compressive strength of concrete columns was analyzed. A literature review [1] revealed a notable research gap concerning the use of CFRP as internal strengthening for concrete columns, particularly with respect to the influence of perforations on load-bearing capacity and damage propagation mechanisms.

2. Experimental research

The aim of the study was to determine which perforation pattern in CFRP tubes provides better load-bearing capacity under uniaxial compression and to determine the dominant failure modes. The designed variants differed in perforation arrangement (*Fig. 1*). The perforations were intended to improve the cooperation between

the concrete core and the outer concrete shell. For comparison, reference samples without composite strengthening were also prepared.

The materials used in this study included self-compacting concrete (SCC) and SikaWrap-230C carbon fiber mats soaked with Sikadur-300 resin. CFRP tubes were made of 1 layer of CFRP with 30% overlap. Cylindrical specimens (150x300 mm) were tested after 28 days of curing. The viscosity and consistency classes of fresh SCC were VS2 and SF3, respectively. Uniaxial compression tests were performed on reference specimens (SCC) and CFRP-strengthened samples with two perforation schemes (I and II), four specimens in each group. The average compressive strengths were: reference – 49.06 MPa, Scheme I – 61.04 MPa, and Scheme II – 49.29 MPa. This corresponds to a 24.4% increase in compressive capacity for Scheme I compared to the unstrengthened specimens, while Scheme II did not provide significant improvement. During testing, the reference specimens failed in a typical concrete crushing mode, characterized by longitudinal cracking and surface spalling, whereas the strengthened samples exhibited localized cracking initiating from the perforations and propagating diagonally between successive holes. After surface cracking, the outer concrete layer failed first, followed by the load transfer to the confined concrete core within the CFRP tube. In several cases, the upper or lower perforation remained intact, suggesting a non-uniform stress distribution within the tube wall. The considerably lower strength of Scheme II is likely due to the weakening of the mid-height region, which acted as a critical failure zone.

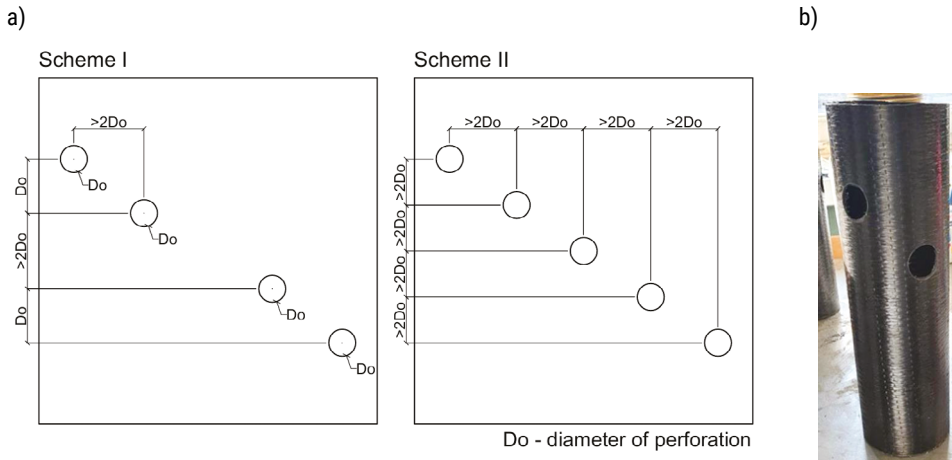


FIG. 1. (a) Layout of perforations in CFRP tubes: Scheme I and Scheme II; (b) View of a CFRP tube with perforations



3. Conclusion

The application of perforated CFRP tubes as internal elements in concrete columns demonstrates a beneficial effect on axial compressive strength, while maintaining adequate material interaction. Among the tested variants, Scheme I exhibited a 24% higher load-bearing capacity compared to the reference specimens, confirming that an optimized perforation layout can enhance the confinement effect and ensure better cooperation between the concrete core and the composite shell.

Observed damage patterns confirmed that failure initiated around the perforations and propagated diagonally between adjacent openings. These results also suggest that the use of a single circumferential CFRP layer may be insufficient to strengthen the concrete core, as local fiber displacement and stress concentrations can occur near perforations, limiting the strengthening efficiency. Despite these promising results, a comprehensive evaluation of the effectiveness of this strengthening approach and the associated failure mechanisms induced by perforations requires further investigation. Future studies will focus on key parameters such as CFRP tubes wall thickness and column slenderness. These variables may significantly affect the stress distribution and the overall performance of the strengthened structural elements.

Acknowledgments

This research was funded from a project supported by the National Centre of Science, Poland [Grant no. 2023/51/D/ST8/01795 “Experimental evaluation of the effect of perforating the composite profiles on the load-bearing behavior of concrete elements”].

The authors would like to express their gratitude to the companies that supported the research by providing materials: Sika Poland Sp. z o.o., Centrum Technologiczne Betotech Sp. z o.o., and Bioeko Grupa TAURON Sp. z o.o.

References

1. Sikora, O., & Ostrowski, K. A. (2025). A review of external confinement methods for enhancing the strength of concrete columns. *Materials*, 18, 3222. <https://doi.org/10.3390/ma18143222>

Experimental verification of rigid plastic bond model in the design of composite steel concrete columns

*Bartosz Grzeszykowski¹, Magdalena Szadkowska¹,
Maciej Lewandowski-Szewczyk², Elżbieta Szmigiera¹*

¹*Warsaw University of Technology, Poland bartosz.grzeszykowski@pw.edu.pl,
elzbieta.szmigiera@pw.edu.pl, magdalena.szadkowska@pw.edu.pl*

²*Gdańsk University of Technology, Poland maciej.szewczyk@pg.edu.pl*

Keywords: push-out test, concrete shrinkage, natural bond, rigid-plastic model, composite column

1. Introduction

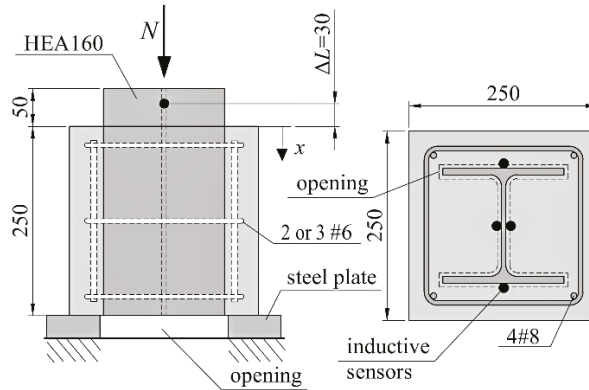
There is no consensus in the literature on whether the bond modulus is a real steel-concrete interface property or if it serves as a model parameter regularizing the rigid plastic or frictional contact model [1]. The methodology adopted in EN1994-1-1:2004 tends to favor the latter, establishing the rigid plastic law as its standard model for the natural bond in the design of composite columns [2]. The interface design shear strength τ_{Rd} , which is the only defining parameter of the model, varies based on the type of cross-section. For the completely concrete encased steel cross-sections, which are the focus of this study, $\tau_{Rd} = 0.3 \text{ N/mm}^2$. Two questions arise: does this design interface strength specified in the code include the effects of concrete shrinkage? And does the rigid-plastic model describe the natural bond behavior with adequate accuracy, allowing for the safe design of the load introduction to concrete encased composite columns?

2. Research program, results and discussion

To answer the above questions we carried out standard push-out experiments, cf. Fig.1a. The notation of the specimens is as follows: SCC and W denote self compacting and regular vibrated concrete mix, respectively; 2 or 3 denotes the number of stirrups used, cf. Fig.1a and the suffix S indicates samples that were tested 8 months after casting, to increase concrete shrinkage effects. Specimens that lack this suffix were tested 28 days from casting. Four inductive sensors measured, for a given axial load N , the change in the distance between the concrete's upper surface and a cross-section positioned $\Delta L = 30 \text{ mm}$ above it, cf. Fig.1a. Consequently, the slip between steel and concrete at the top concrete surface $s(0)$ is: , with Aa and Ea representing the HEA160 cross-sectional area and Young modulus, respectively. For each specimen the readings from four sensors were averaged. To investigate the shear transfer

mechanism, an analytical model with linear elastic constitutive relations for both steel and concrete and two types of natural bond laws were investigated: rigid plastic and elastic plastic. The interface stiffness k (in N/mm²) of the latter was iteratively adjusted to match the global initial stiffness K_{ini} (N/mm) obtained from the experiment, cf. Fig. 1b. Then the interface stiffness was calculated assuming uniform distribution of stresses along the perimeter of the steel profile ρ : $\kappa = k/\rho$ (in N/mm³). Rigid-plastic model was used to calculate the global response of specimens according to EN1994-1-1:2004, cf. red dash-dotted line in Fig. 1b. The point where the linear extrapolation of experimentally determined equilibrium paths intersects the rigid-plastic bond model establishes the slip demand s_d , functioning as the critical threshold beyond which the EN1994-1-1:2004 model no longer guarantees design safety. $n_u = N_u/(H\rho)$ denotes the normalized maximum force obtained in the experiment, where H and N_u denote the interface height and maximum load, respectively. Results obtained in each experimental group were averaged and gathered in Table 1.

a)



b)

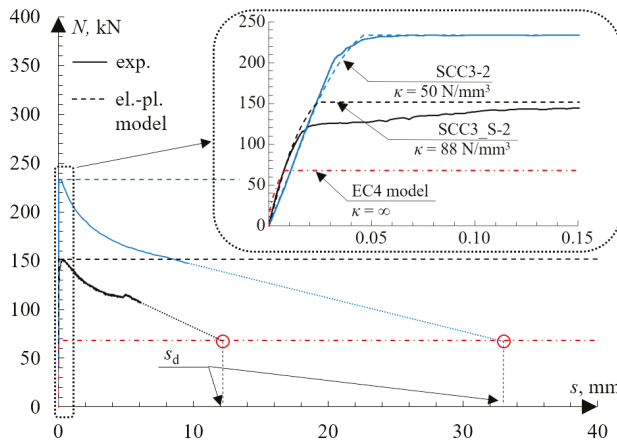


FIG. 1. Scheme of push-out specimens: a) experimental; b) model equilibrium paths

TABLE 1. Results averaged over each experimental group

	After 28 days			After 8 months		
	SCC2	SCC3	W2	SCC2_S	SCC3_S	W2_S
κ_{avg} , N/mm ³	49	50	92	52	70	77
$s_{D,avg}$, mm	19	34	29	17	12	14
$n_{U,avg}$, N/mm ²	0.50	0.90	0.64	0.48	0.46	0.44

3. Conclusions

Shrinkage decreases substantially the normalized ultimate force n_U , but there is lack of correlation between the interface stiffness κ and shrinkage. The microgaps at the steel-concrete interface, which are the aftermath of the shrinkage, deteriorate the adhesive mechanism that drives the ultimate force observed for very small slips, cf. Fig. 1b. Shrinkage causes contractions towards the center of mass of the concrete block on either side of the wide flange web that produce these microgaps, hence reduce the effective adhesion area. The fitted interface stiffness values $\kappa \in \sim (50 \div 90)$ N/mm³ produce the global response that tends to the rigid-plastic EN1994-1-1:2004 model solution, cf. Fig. 1b. Therefore, the rigid plastic model is indeed suitable to describe the initial response of tested specimens, especially as there are fluctuations of κ test results and the lack of substantial dependence of concrete shrinkage on interface stiffness. Additionally, $s_{D,avg}$ obtained for each specimen exceeds 6 mm, the slip demand required by EN1994-1-1:2004 to consider a shear connection as ductile. Thus, for completely concrete encased steel cross-sections of tested proportions, the rigid-plastic model has an adequate margin of safety, provided that the calculated design slip does not exceed 6 mm.

References

1. Grzeszykowski, B., Lewandowski-Szewczyk, M. J., & Niedośpiał, M. (2023). Load introduction to composite columns revisited – Significance of force allocation and shear connection stiffness. *Engineering Structures*, 295, 116800.
2. Walraven, J., & Bigaj-van Vliet, A. (Eds.). (2010). *fib model code for concrete structure 2010*. E&S.



Torsional strength and stiffness of concrete elements: An experimental approach

*Magdalena Lewandowska¹, Michał Demby¹,
Szymon Wojciechowski², Robert Studziński¹*

*¹Poznań University of Technology, Poland,
magdalena.lewandowska@put.poznan.pl,
michal.demby@put.poznan.pl*, robert.studzinski@put.poznan.pl
²Pekabex BET S.A., szymon.wojciechowski@pekabex.com*

Keywords: torsional capacity, torsional stiffness, concrete sections, experimental approach

1. Abstract

The torsion phenomenon in concrete structures, although not as common as bending or shear, is one failure mechanism which should be the subject of scientific consideration [3]. The aim of the study was to determine the torsional strength and stiffness of selected cross-sections of concrete elements and to compare the obtained results with those from analytical calculations. The analysis aimed to assess how accurately theoretical approaches reflect the actual behaviour of elements subjected to pure torsion.

Eight prefabricated concrete beams made of high-strength self-compacting concrete (C70/85) were tested. Three types of cross-sections were used: solid rectangular (P_01: width 120 mm, height 240 mm), I-shaped (T_01: height 240 mm, flange width 120 mm, flange thickness 50 mm, web width 48 mm), and slender rectangular (I_01: width 48 mm, height 240 mm).

The tests were carried out using a laboratory setup that allowed the introduction of a torsional moment through an actuator acting on an intermediate element. The system generated torsion by rotating a loading disc while the opposite end of the specimen was fixed [4]. The applied force and displacement increments of six points along the length of the beam were recorded.

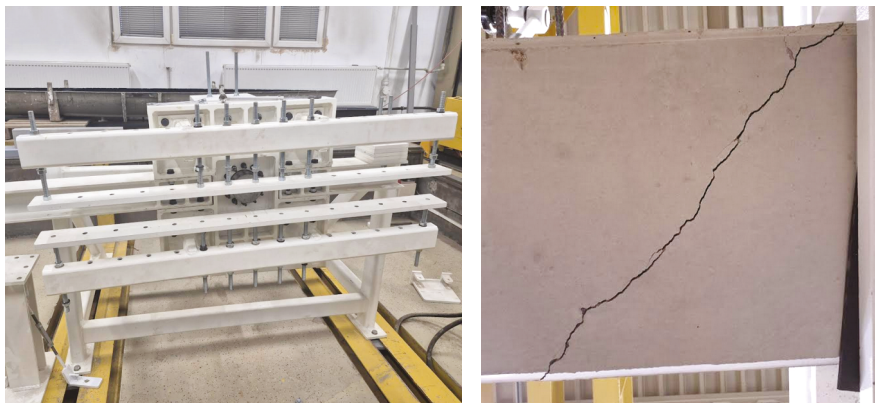


FIG. 1. Rotary support of the testing rig (on the left) and an example failure mechanism of the specimen (on the right)

Classical analytical solutions were used for the theoretical analysis of the concrete cross-sections: the elastic model by Prandtl and the plastic model by Nadai.

A comparison of the torsional capacities obtained experimentally and those calculated using analytical models is presented in Fig. 2. The Prandtl analogy significantly underestimated the torsional strength for all tested cross-sections. Better agreement was observed for the Nadai analogy, which closely matched the results for rectangular cross-sections (P_01 and I_01), falling within the range of standard deviation. For the I-shaped cross-section (T_01), the result was also close to the experimental value, although still slightly underestimated. It can therefore be concluded that the plastic model provides a good representation of the behavior of torsionally loaded concrete members. However, as noted in the literature [1], it does not account for the size effect, which may lead to underestimation for small specimens and overestimation for large elements.

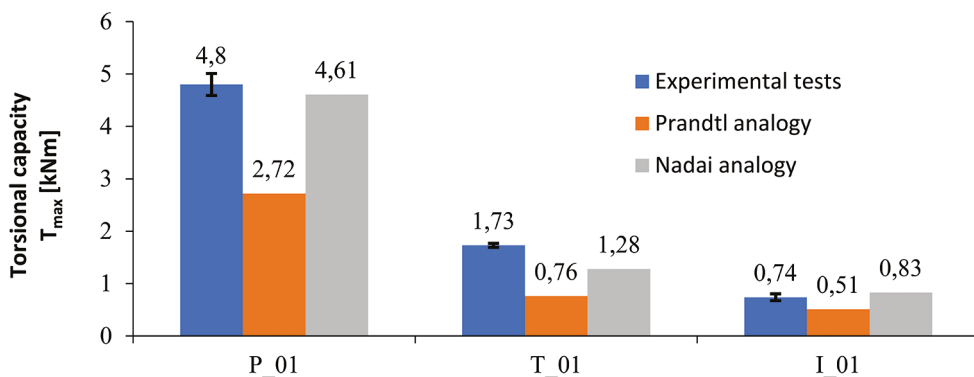


FIG. 2. Torsional capacity – experimental results and analytical models

As part of the analysis, the response of the T_01 and I_01 specimens was evaluated based on torque–twist angle diagrams, developed from measured displacements. Two distinct stages can be identified in the behavior of the elements: an initial linear range corresponding to the elastic behavior of concrete, and a nonlinear range associated with the initiation and propagation of microcracks. In the first phase, according to Saint-Venant's theory, the torsional stiffness can be approximately determined as the product of the shear modulus and the torsional moment of inertia of the cross-section (). However, the assumptions of this theory indicate that this relationship is valid only within the elastic range, before the onset of material damage. According to the literature [1], it is possible to extend its applicability to the entire torque range by considering the tangent modulus of elasticity, determined for a stress level corresponding to approximately . This can be approximately done using the modified formula provided in Eurocode 2 [2].

References

1. Hsu, T. T. C. (1984). *Torsion of reinforced concrete*. Van Nostrand Company Inc.
2. Polski Komitet Normalizacyjny. (2008). *Eurokod 2 – Projektowanie konstrukcji z betonu – Część 1-1: Reguły ogólne i reguły dla budynków* (PN-EN 1992-1-1).
3. Rahal, K. N. (2000). Torsional strength of reinforced concrete beams. *Canadian Journal of Civil Engineering*.
4. Wojciechowski, S. (2022). *Analiza doświadczalna, numeryczna i teoretyczna skręcanych statycznie paneli warstwowych o sztywnych okładzinach i podatnym rdzeniu*. Instytut Analizy Konstrukcji, Politechnika Poznańska.



Limitations of simplified methods for determining second-order effects in high-slenderness rc cantilever columns

Dawid M. Zmysłony, Czesław Bywalski, Roman J. Wróblewski

*Wrocław University of Science and Technology, Poland,
dawid.zmyslony@pwr.edu.pl, czeslaw.bywalski@pwr.edu.pl, roman.wroblewski@pwr.edu.pl*

Keywords: second-order effects, RC columns, nonlinear analysis, general method

1. Introduction

Modern design standards, exemplified by Eurocode 2 [2], provide simplified methods for the assessment of second-order effects. Although these methods are widely used in engineering practice, their applicability to the analysis of very slender columns has been increasingly questioned [3, 4]. As slenderness and axial force increase, major discrepancies appear between results from different design codes [5] and between code-based methods and nonlinear analyses [1].

The objective of this study is to quantify these discrepancies using the General Method (GM) in nonlinear finite element analysis, accounting for material nonlinearities in concrete and steel.

2. Calculation assumptions and scope of comparison

The analysis covers three cantilever RC columns with lengths of 8.0 m, 10.5 m, and 13.0 m, corresponding to slenderness of $\lambda = 123, 162$, and 200, respectively. A total reinforcement ratio of 3.0% was assumed in a symmetrically reinforced 450×450 mm cross section. Each column is subjected to an axial compressive force $N_{Ed} = 500$ kN ($n = N_{Ed} / (A_c f_{cd} + A_s f_{yd}) \approx 0.05$). The bending moment changes linearly from $M_{01} = 10$ kNm to $M_{02} = 100$ kNm over the column length (Fig. 1). Concrete C50/60 and steel B500B ($f_{yk} = 500$ MPa) were used. The structural configuration corresponds to a cantilever column (Fig. 1), representative of members in an unbraced structural system.

Three methods were compared: Nominal Stiffness Method (NSM), Nominal Curvature Method (NCM), and the General Method (GM). Each accounts differently for governing physical phenomena influencing second-order effects in a distinct manner.

In GM, apart from geometric nonlinearity, material nonlinearity is considered, including cracking, creep ($\varphi(\infty, t_0) = 1.5$), and stress–strain relations for concrete and steel. Geometric imperfections, biaxial bending, and tension stiffening were excluded. The analyses were performed in SOFiSTiK 2025. NSM uses constant nominal stiffness, ignoring cracking explicitly. NCM utilises curvature increments without incorporating local degradation. Creep is included in both models with an effective coefficient $\varphi_{ef} = 0.3$.

3. Results and analysis

Both simplified methods overestimate the second-order effects (Fig. 1) when compared to the values obtained using GM. The magnitude of these discrepancies increases with slenderness of the column. Both approaches result in a significant exaggeration of the second-order moments, with the NCM resulting in significantly higher overestimations in comparison to the NSM. The sudden increase in the design moment M_{Ed} in the NSM for the column with $\lambda = 200$ is due to the axial force N_{Ed} approaching the critical buckling load N_B .

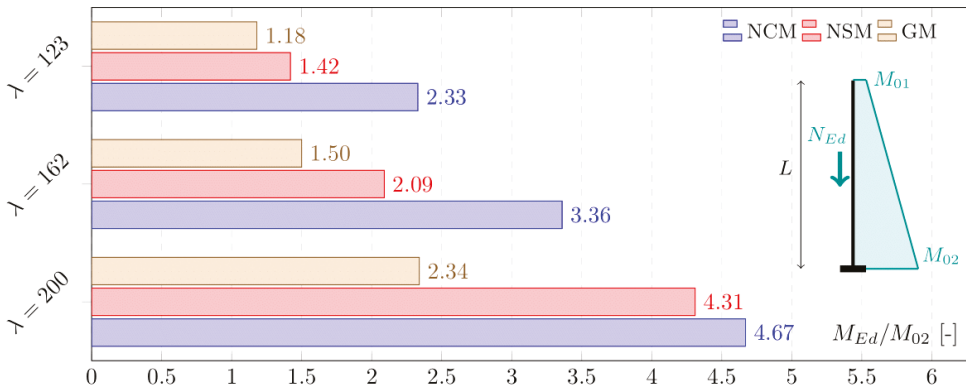


FIG. 1. Design moments M_{Ed} incorporating first and second-order effects, relative to the first-order moment M_{02} (without imperfections), as obtained using the NCM, NSM, and GM methods, along with the force and moment diagram adopted for the analysis

4. Conclusions

The results of the analysis allow for the formulation of the following practical conclusions:

- Both NSM and NCM overestimated second-order bending moments in the analysed very slender cantilever columns, irrespective of the slenderness considered, which is suboptimal from an economic standpoint.



- Increasing slenderness amplifies discrepancies between GM and the simplified methods, reaching approximately 84% to 100% for $\lambda = 200$.
- It was demonstrated that NSM exhibits a stronger correlation with GM in the column with the lowest analysed slenderness $\lambda = 123$. At this point, the overestimation was found to be approximately 20%.
- The observed discrepancies underscore the necessity to develop engineering-level methods for the estimation of second-order moments in high-slenderness columns, which are extensively used in contemporary industrial building design.

References

1. Dobrý, J., Čuhák, M., Čížek, P., & Benko, V. (2019). Nonlinear analysis and comparison of design methods for slender concrete columns with their impact on economy and reliability. *Solid State Phenomena*, 292, 197–202.
2. CEN, European Committee for Standardization. (2023). *Eurocode 2 – Design of concrete structures – Part 1-1: ‘General rules – Rules for buildings, bridges and civil engineering structures’* (EN 1992-1-1).
3. Kijania, M., Seruga, T., & Rewers, I. (2013). Effect of some factors on second order effects in reinforced concrete columns. *Technical Transactions*, 110, 41–58.
4. Pędziwiatr, J., & Musiał, M. (2023). Calculation of second-order effects in columns – applications and examples. *Archives of Civil Engineering*, 69, 271–286.
5. Zmysłony, D., Bywalski, C., & Wróblewski, R. (2025). Review of simplified code-based methods for the consideration of second-order effects in slender RC columns. *Materiały Budowlane*, accepted for publication (in Polish).



Flexural moment distribution in hollow core floors. Code provisions in light of new experimental data

Miłosz Jeziorski^{1,2}, Wit Derkowski^{3,4}

¹*Consolis Group Technology Development Centre, milosz.jeziorski@consolis.com*

²*Cracow University of Technology, CUT Doctoral School, milosz.jeziorski@doktorant.pk.edu.pl*

³*Cracow University of Technology, Chair of Reinforced, wit.derkowski@pk.edu.pl*

Concrete and Prestressed Concrete Structures

⁴*Linnæus University, Department of Building Technology, wit.derkowski@lnu.se*

Keywords: hollowcore, precast concrete, prestressed concrete, load distribution


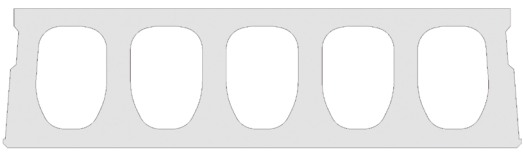
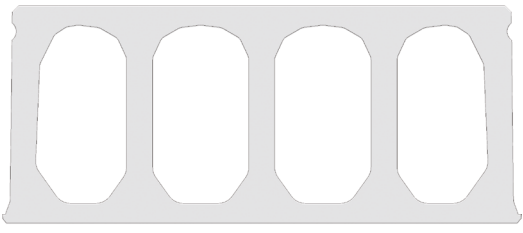
1. Introduction

Cast-on-site joints between precast prestressed hollow core (HC) slabs forming entire floors allow cooperation between unevenly loaded individual units loaded vertically by point loads. Due to this, the bending moment in directly loaded slab can be significantly decreased allowing more economical design. The European Standard EN 1168 [1] provides load distribution graphs based upon which mentioned phenomenon can be taken into account. Previous works regarding this subject [2–4] highlighted that the above mentioned standard can provide questionable results which, due to the lack of sufficient experimental data, was until now difficult to validate. In this work, the authors analysed the distribution of flexural bending moments based on measurements performed during novel experiments on three full scale hollow core floors.

2. Experiments on full scale hollow core floors

Each experiment consisted of six identical HC slabs, in which three types of hollow core slabs were used, different in each floor, and a constant span-to depth ratio was kept in each experiment. Table 1 summarizes the geometry of each floor, Figure 1 presents its scheme.

TABLE 1. Geometry of each floor experiment

Floor	HC Cross-section	Span L [m]	Depth H [m]
1		4.44	0.15
2		9.44	0.32
3		14.95	0.50

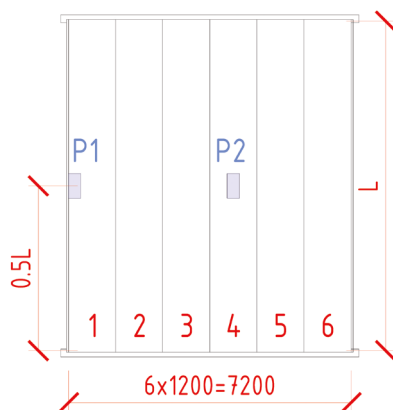


FIG. 1. Scheme of the experimental setups

The slabs were interconnected by pre-cracked cast on site joints, supported through a neoprene layer on steel plates which rested through roller bars and load cells with spherical bearings on precast T-beams. Reinforced concrete tying beams were casted on supports and free edges. Point loads were applied in several loading

cycles in two locations, denoted as P1 and P2, see Fig. 1. Constant measurements of applied force, reaction force on one support, displacements and strains were performed. The strain was measured by distributed fibre optic sensors (DFOS) glued to the top and bottom surface of the floor in both longitudinal and transverse direction.

3. Distribution of flexural bending moments

The DFOS measurements were used to obtain the bending moment diagrams. Knowing the slabs geometry and measured elasticity modulus, and assuming a linear elastic behaviour, peak bending moments were calculated. These were further used to obtain α factors indicating fraction of the total moment in the considered slab. Results are compared to EN 1168 by plotting them together with experimentally obtained values visible in Figures 2 and 3.

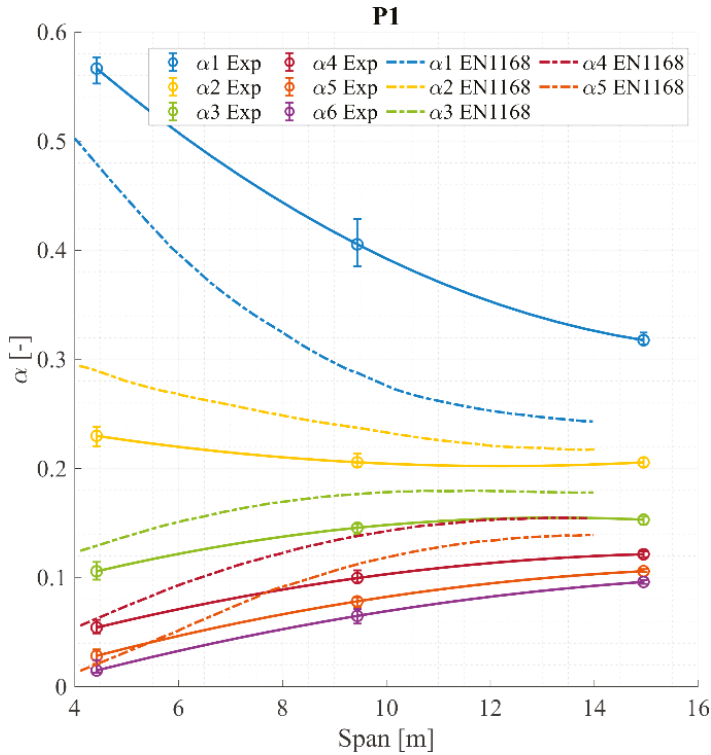


FIG. 2. Bending moment distribution – P1

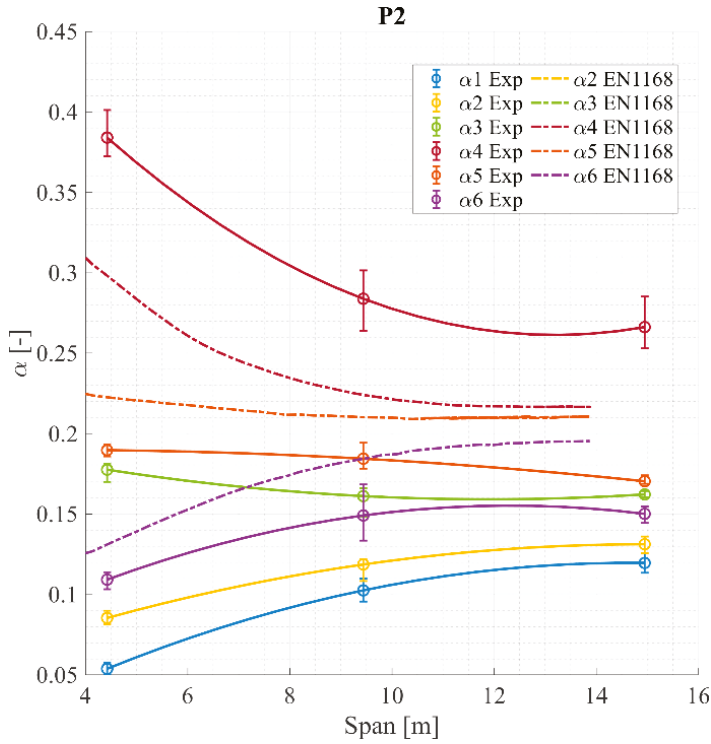


FIG. 3. Bending moment distribution – P2

4. Conclusions

The obtained experimental data shows, in line with EN 1168, that the bending moment distribution improves with the distance from the free edge and is strongly correlated with a floor's span. In contrary to code provisions, more than 5 elements can be considered in the floor analysis. The contribution of a 6-th element is limited in case of P1 but visible in P2. The experiments provide evidence that code provisions can lead to overestimated flexural bending moment distribution.

Acknowledgments

The authors wish to gratefully acknowledge financing and support by the International Prestressed Hollowcore Association as well as the valuable contribution of Construction Engineering Research Group of Hasselt University and SHM System, Nerve-Sensors companies.



References

1. EN 1168:2005+A3:2011 *Precast concrete products – Hollow core slabs*. CEN: 2011.
2. Jeziorski, M., & Derkowski, W. (2022). Comparative study of various provisions on load distribution in hollowcore slabs. In S. Stokkeland, H. C. Braarud (Eds.), *Concrete innovation for sustainability: Proceedings for the 6th fib International Congress 2022 held in Oslo, Norway, June 12–16, 2022, fib Symposium Proceedings* (Vol. 59, pp. 2658–2667). Fédération Internationale du Béton.
3. Jeziorski, M., Derkowski, W., & Michelini, E. (2024). Vertical load distribution in precast hollow core floors: State of the art and future perspectives. *Structural Concrete*, 25, 3412–3429. <https://doi.org/10.1002/suco.202301150>
4. Jeziorski, M., & Derkowski, W. (2022). Wątpliwości dotyczące nośności stropu z płyt kanałowych obciążonego siłą skupioną. *Inżynieria i Budownictwo*, 78(5–6), 263–268.



Comparative finite element analysis of sunk wells lowering in varying soil

Anna Szymczak-Graczyk, Tomasz Garbowski

*Poznan University of Life Science, Poland,
anna.szymczak-graczyk@up.poznan.pl, tomasz.garbowski@up.poznan.pl*

Keywords: sunk wells, axisymmetric finite element analysis, lateral earth pressure, groundwater uplift.

1. Introduction

The design and construction of sunk wells for civil and environmental infrastructure projects –such as stormwater systems, tunnels, and foundations – demand a careful assessment of interactions between structural elements [1, 2] and the surrounding ground environment. These challenges are amplified when construction is conducted in heterogeneous or saturated soils [6–8]. Unpredictable soil reactions, buoyancy effects, and uneven stress distributions can compromise the sunk well’s structural integrity if not adequately addressed. While full-scale field testing is rarely feasible in the early design stages, numerical modeling offers a powerful tool for simulating performance under variable loading and environmental conditions.

In practical engineering, it is rarely feasible to assess all possible geotechnical scenarios through field testing [4]. Instead, numerical simulations offer a valuable tool [3, 5] to test multiple design configurations, evaluate risk factors, and identify vulnerable loading conditions that may result in structural failure. In the case of sunk well construction, it is particularly important to understand how different depths, groundwater levels, and surrounding soil compositions influence internal stress distributions in the sunk well.

2. Methods and materials

This study investigates the behavior during lowering of a reinforced concrete sunk well during lowering under diverse soil conditions using a custom-built axisymmetric finite element model implemented in MATLAB. The sunk well, with an internal diameter of 6 meters, a depth of 6 meters, and a wall thickness of 30 cm, is reinforced on both faces with a mesh of $\phi 12$ bars spaced every 15 cm. The model simulates the stepwise lowering of the sunk well into the ground. While the surrounding soil is not explicitly modeled using continuum mechanics, its effects are introduced through external loading: self-weight of the sunk well, lateral earth pressure, hydrostatic water pressure (in selected cases), and frictional interaction along the sunk well-soil interface.



Several dozen configurations were evaluated, including dry and saturated conditions, multi-layered soil profiles, and variations in groundwater levels. For each variant, lateral pressure and base uplift due to buoyancy were applied using analytical expressions. The mechanical response of the sunk well was analyzed at each depth increment, with focus on stress distributions and the identification of critical zones of tensile and compressive stresses. Particular attention was paid to the most unfavorable configurations potentially leading to cracking or structural instability.

In the absence of an explicitly modeled soil continuum, the following formulas were used to define the loads:

- lateral earth pressure (active): $\sigma_h = K_a \cdot \gamma \cdot h$
- base uplift pressure (in presence of groundwater): $p_w = \gamma_w \cdot h_w$
- frictional force on sunk well sidewall: $F_f = \mu \cdot \sigma_v \cdot A_{contact}$

Where:

- γ is the unit weight of soil,
- γ_w is the unit weight of water,
- h is the current embedment depth,
- h_w is the water table level below the ground surface,
- μ is the friction coefficient,
- K_a is the active earth pressure coefficient.

Boundary conditions were adjusted dynamically during sunk well sinking, simulating the progressive exposure to increased loading. Frictional forces and earth pressure were applied as surface loads.

3. Preliminary findings

The most unfavorable stress states occurred in highly stratified soils with soft interlayers and high groundwater levels.

Dry, dense sand yielded the most favorable configurations in terms of uniform sunk well during lowering and low stress peaks.

Groundwater significantly contributed to uplift pressure, particularly in the initial stages of sunk well embedment, emphasizing the need for buoyancy-resistant design.

These findings provide valuable guidance for the design and execution of sunk well sinking projects in complex geotechnical settings.

References

1. Garbowski, T., Borecki, P., Rutkowski, J., & Szymczak-Graczyk, A. (2024). Optimal design of rectangular tank walls with ribs using numerical models and global optimization. *Civil and Environmental Engineering Reports*, 34(4), 293–306. <https://doi.org/10.59440/ceer/195601>
2. Garbowski, T. Pawlak, T. G., & Szymczak-Graczyk, A. (2024). Efficient load-bearing capacity assessment of a degraded concrete manhole using sectional homogenization. *Materials*, 17, 5883. <https://doi.org/10.3390/ma17235883>
3. Garbowski, T., Szymczak-Graczyk, A., & Rutkowski, J. (2024). Optimization of rectangular tank cross-section using trust region gradient method. *Inżynieria Mineralna*, 1(2). <https://doi.org/10.29227/IM-2024-02-99>
4. Pawlak, T. G., Szymczak-Graczyk, A., & Garbowski, T. (2024). Three-layer repair coating system for manholes, pump stations, and tanks in aggressive sulfate environment. *Civil and Environmental Engineering Reports*, 35(1), 1–19. <https://doi.org/10.59440/ceer/196751>
5. Szymczak-Graczyk, A., Garbowski, T., & Ksit, B. (2024). Influence of geometric parameters on internal forces in the walls of rectangular tanks. *Inżynieria Mineralna*, 1(2). doi.org/10.29227/IM-2024-02-27
6. Szymczak Graczyk, A. (2024). Metody obliczania studni opuszczanych. *Przegląd Budowlany*, 95(4), 91–94. <https://doi.org/10.5604/01.3001.0054.6393>
7. Szymczak-Graczyk, A. (2023). Selected aspects of the design and construction of reinforced concrete sunk wells. *Acta Scientiarum Polonorum – Architectura, Budownictwo*, 21(3). doi.org/10.22630/aspa.2022.21.3.21
8. Szymczak-Graczyk, A. (2021). *Żelbetowe studnie opuszczane. Kształtowanie, obliczenia, wykonawstwo, przykłady realizacji*. Wydawnictwo Uniwersytetu Przyrodniczego w Poznaniu.



Two-variable individual-layer nonlocal model of static bending of asymmetric sandwich plate with laminate facings

Stanisław Karczmarzyk

Warsaw University of Technology, Poland, stanislaw.karczmarzyk@pw.edu.pl

Keywords: asymmetric sandwich plate, individual-layer kinematics, transverse flexibility of the core, two-variable nonlocal model

1. Introduction

There are at least two groups of composite surface girders. One of them includes laminated shells and plates consisting of thin layers glued together with resins. The second group includes sandwich structures, in particular plates. They are structurally very diverse and much more complex than the laminated structures. The simplest sandwich structure consists of three connected homogeneous continuous layers. The outer layers are called ‘facings’ and the middle one is called ‘core’.

It is emphasized that there is a wide variety of more complex sandwich structures in the literature and engineering applications. For example, the sandwich plates with laminated facings are more complex than their counterparts with homogeneous outer layers. The most complex sandwich structures have a discontinuous, cellular or corrugated core. All classical sandwich structures are constructed according to the fundamental idea that the facings are relatively thin and stiff in tension and the core is relatively thick and susceptible to stretching.

The literature on sandwich structures and in particular on their modelling is very extensive. Here are mentioned some exemplary articles on the topic. Applications of sandwich plates and shells in various industries are outlined in the review papers [1–3]. Paper [4] presents a simple nonlocal, four-variable static model of bending of asymmetric sandwich plate with laminated facings, that satisfies the interlayer compatibility equations for displacements and stresses but neglects the transverse flexibility of the core. Articles [5, 6] are devoted to very complex sandwich structures with non-continuous, corrugated cores. In paper [7] the reader will find a theory for asymmetric sandwich plate about its middle plane. This theory was obtained without the need of finding the location of the neutral surface in the sandwich plate, but it is formally very complicated. The theory in [7] is based on kinematic assumptions with seventeen unknown functions of in-plane spatial variables (x , y). Applying this theory we must solve seventeen partial differential equations. Paper [8] contains a dynamic model of sandwich plate with cellular re-entrant core.

An efficient two-variable, nonlocal static model of the asymmetric sandwich plate with laminate facings is scheduled for presentation during this AMCM 2025 conference. This model is based on the kinematic assumptions individual for each layer. These kinematic assumptions are similar but essentially different than those applied in paper [4]. This model can directly be applied for the static analysis and extended for dynamic analysis of the precast concrete sandwich panels (PCSP) that are widely applied in the building industry [3].

It is noted that the nonlocal model for the asymmetric sandwich plate, presented here, is much less complicated than the theory proposed in [7] for such a plate. The kinematic assumptions in the model scheduled for the presentation within AMCM 2025 contain only four unknown functions. However, the final statement of the problem considered here contains in fact only two unknown functions of the in-plane spatial variables (x, y) , namely $w_b(x, y)$ and $w_s(x, y)$. Such reduction of the variables was possible due to a different approach than that in paper [4]. In the model presented here both warping and transverse flexibility of the core has been taken into account and all interlayer compatibility equations are satisfied.

2. Basic details of the efficient static model

The kinematic, geometric assumptions for the static model are as follows,

$$u_{xfk} = u_{x0}(x, y) - z \frac{\partial w_b}{\partial x} + u_{xk}(x, y) - z \frac{\partial w_s}{\partial x}, \quad u_{yfk} = u_{y0}(x, y) - z \frac{\partial w_b}{\partial y} + u_{yk}(x, y) - z \frac{\partial w_s}{\partial y},$$

$$u_{zfk} = w_b(x, y) + w_s(x, y), \quad k = 1, 2. \quad (1)$$

$$u_{xcn} = u_{x0}(x, y) - z \frac{\partial w_b}{\partial x} - f_{xcn}(z) \frac{\partial w_s}{\partial x}, \quad u_{ycn} = u_{y0}(x, y) - z \frac{\partial w_b}{\partial y} - f_{ycn}(z) \frac{\partial w_s}{\partial y},$$

$$u_{zcn} = w_b(x, y) + h_{cn}(z) w_s(x, y), \quad f_{xcn}(z) = A_{1x}z + A_{3xn}z^3,$$

$$f_{ycn}(z) = A_{1y}z + A_{3yn}z^3, \quad n = t, b. \quad (2)$$

Expressions (1), (2) determine displacements in directions x, y, z : (1) for two facings – subscripts f and $k = 1, 2$, and (2) for two parts (top and bottom) of the core – subscripts c and $n = t, b$, respectively. In expressions (1) all the functions of variables x, y are unknown. In expressions (2) the same unknown functions occur as in (1). Apart from that, the functions $hn(z)$ in formula for $uzcn$ contain four unknown constants. Also the coefficients $A_{1x}, A_{3xn}, A_{1y}, A_{3yn}$, ($n = t, b$) are unknown.

The model outlined above has been verified numerically, by comparisons of the predicted numerical results with results published elsewhere and obtained according to other models. Good agreement of the results compared has been observed.

3. Conclusion

A novel approach for modelling of the asymmetric sandwich plate, which is much simpler than that proposed in paper [7], has been shown in this work. This approach essentially differs from that in paper [4] and enables the acquisition of the final statement of the problem containing in fact two unknown functions of the in-plane spatial variables (x, y) , namely $wb(x, y)$ and $ws(x, y)$.

References

1. Birman, V., & Kordomateas, G. A., Review of current trends in research and applications of sandwich structures. *Composites Part B Engineering*, 142, 221–240.
2. Castanie, B., Bouvet, C., & Ginet, M. (2020). Review of composite sandwich structure in aeronautic applications. *Composites Part C*, 1, 100004.
3. O'Hegarty, R., & Kinane, O. (2020). Review of precast sandwich panels and their innovations. *Construction and Building Materials*, 233, 117145.
4. Karczmarzyk, S. (2020). An efficient four-variable I-L nonlocal static model of unsymmetrical sandwich rectangular plate with laminated facings. *Composite Structures*, 246, 112242.
5. Liu, R., Zhong, Y., Shi, J., & Shi, Z. (2021). Static buckling and free vibration analyses of composite sandwich plate with bi-directional trapezoidal cores using VAM-based reduced plate model. *Composite Structures*, 277, 114636.
6. Magnucka-Blandzi, E., & Rodak, M. (2017). Bending and buckling of a metal seven-layer beam with a lengthwise corrugated main core – comparative analysis with the sandwich beam. *Journal of Theoretical and Applied Mechanics*, 55, 41–53.
7. Mohammadimehr, M., & Mostafavifar, M. (2016). Free vibration analysis of sandwich plate with a transversely flexible core and FG-CNTs reinforced nanocomposite face sheets subjected to magnetic field and temperature-dependent material properties using SGT. *Composites Part B: Engineering*, 94, 253–270.
8. Peng, X., Zhong, Y., Shi, J., & Shi, Z. (2022). Free flexural vibration analysis of composite sandwich plate with reentrant honeycomb cores using homogenized plate model. *Journal of Sound and Vibration*, 529, 116955.

Stirrup-deficient post-tensioned concrete girders – shear failure mode and shear performance analysis

Rafał Walczak¹, Wit Derkowski^{1,2}

¹Cracow University of Technology, Poland, rafal.walczak@pk.edu.pl, wit.derkowski@pk.edu.pl

²Linnaeus University, Sweden, wit.derkowski@lnu.se

Keywords: post-tensioned concrete, shear, stirrup deficiency, finite element analysis

1. Introduction

Numerical analysis is increasingly used for refined assessment of structural members when full-scale testing is limited [1–4]. This study applies a previously developed finite-element model [5] to investigate the shear behaviour of typical post-tensioned concrete (PC), precast crane girders removed after more than 50 years of exploitation [6]. The investigation concerned a similar type of structural member, with the same modular span of 6 m, but with a smaller cross-section, used for lower load-bearing capacities. Due to the limited number of real-scale test specimens, the validated numerical model was used to reproduce a prior experiment [6] and extend the parametric analysis and the assessment. Three load cases, diversified by the shear span-to-depth ratio (a/d) were analysed (Fig. 1) to validate against experimental results. Comparison of the experimental and numerical ultimate loads shows good consistency of numerical mapping of the corresponding test results, see Fig. 2.

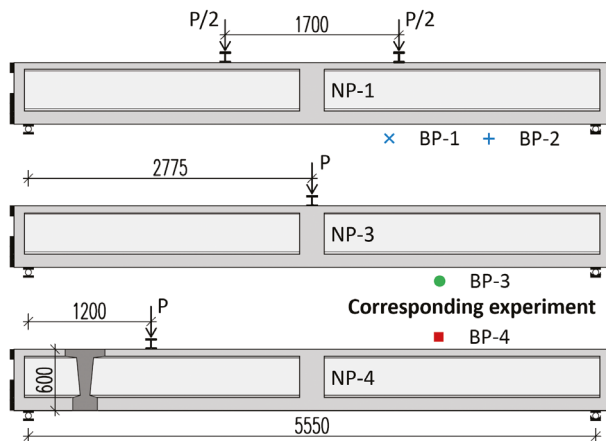


FIG. 1. Modelled girder geometry, analysed load cases and corresponding experiments

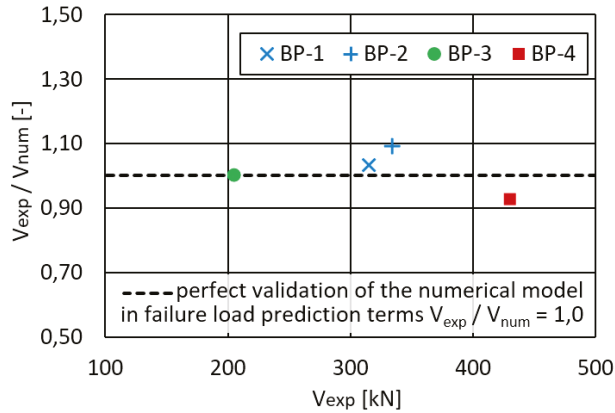


FIG. 2. Experimental ultimate transverse force versus numerical prediction

2. Transverse reinforcement parametric analysis

The study examined the effect of the transverse reinforcement ratio on shear capacity and failure mode of the analysed PC girders. The stirrup ratio of reference models corresponded to the designed value of 0.56%. However, models with a reduced stirrup ratio ($\rho_w = 0.28\%$ – marked ') represented the actual, lower-than-expected transverse reinforcement ratio observed in real-scale tested girders. *Figure 3* shows the load-deflection curves of the conducted analyses. A comparison of the obtained capacity results, in terms of the shear span-to-depth ratio, is shown in *Figure 4*.

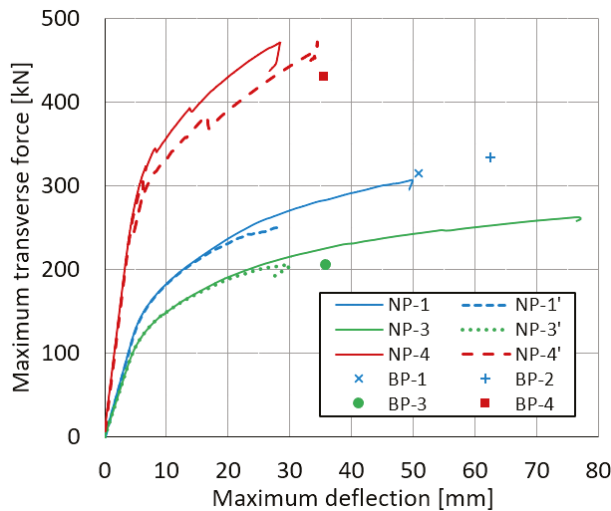


FIG. 3. Maximum transverse force versus maximum deflection

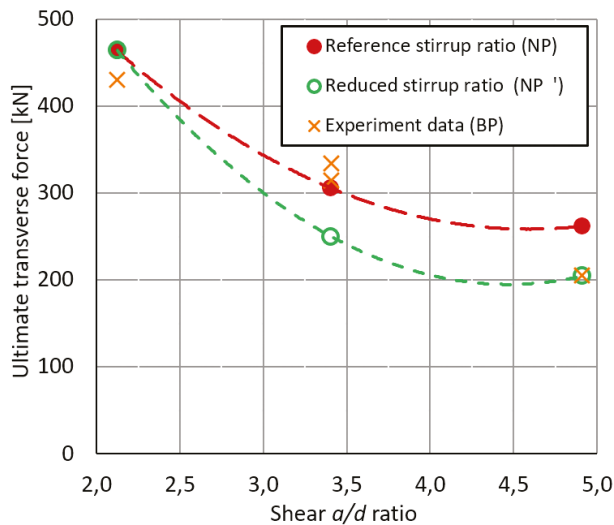


FIG. 4. Ultimate transverse force as a function of shear a/d ratio

3. Brief discussion on results and findings

Results indicate that for the NP-4 series (low a/d), capacity is governed by shear-compression failure and is only marginally affected by reduced stirrup ratio. On the other hand, the effect of the transverse reinforcement ratio on the load-bearing capacity is evident in the NP-1 and NP-3 series. Previously analysed girders [5] with the same span but greater depth, hence less slender members ($l/d = 7.3$), showed reduced sensitivity to transverse reinforcement deficiency. The failure modes of the beams reflected the bending and shear interaction, regardless of the stirrup ratio. However, the current analysis of more slender beams ($l/d = 9.8$) showed that the failure mode of the members directly relates to shear-tension (except NP-4 – low shear a/d ratio series). Also, the load-bearing capacity and behaviour of the beams are clearly dependent on the transverse reinforcement ratio. Consistent observations result from corresponding experiments, where all members failed due to shear, even in the typical three-point bending static scheme (BP-3 beam). These findings inform assessment and rehabilitation strategies for long-service post-tensioned concrete precast girders.

References

1. de Borst, R., Crisfield, M. A., Remmers, J. J. C., & Verhoosel, C. V. (2012). *Non-linear finite element analysis of solids and structures*. John Wiley & Sons
2. Zdanowicz, Ł., Seręga, S., Tekieli, M., & Kwiecień, A. (2020). Polymer flexible joint as a repair method of concrete elements: Flexural testing and numerical analysis. *Materials*, 13(24), 5732. <https://doi.org/10.3390/ma13245732>



3. Jeziorski, M., & Derkowski, W. (2025). Comprehensive numerical investigation of the concentrated load capacity in prestressed hollow core floors. *Engineering Structures*, 335, 120208. <https://doi.org/10.1016/j.engstruct.2025.120208>
4. Coronelli, D., & Gambarova, P. (2004). Structural assessment of corroded reinforced concrete beams: Modeling guidelines. *Journal of Structural Engineering*, 130(8), 1214–1224. [https://doi.org/10.1061/\(ASCE\)0733-9445\(2004\)130:8\(1214\)](https://doi.org/10.1061/(ASCE)0733-9445(2004)130:8(1214))
5. Walczak, R., & Derkowski, W. (2023). Numerical study on the shear capacity of PC crane beams in uncertain prestressing tendons anchorage conditions. *Lecture Notes in Civil Engineering*, 350. https://doi.org/10.1007/978-3-031-32511-3_4
6. Derkowski, W., & Walczak, R. (2019). Problem of condition assessment of precast, post-tensioned concrete crane beams in an extended period of use. In *Concrete innovations in materials, design and structures – 16th fib symposium 2019 proceedings* (pp. 1507–1514).



Diagnostics of cable post-tensioned concrete grinders – the effect of temperature

*Tadeusz Chyży¹, Czesław Miedziałowski¹, Krzysztof Czech¹, Marcin Orłowski¹,
Dai Wang², Hai Zhang², Jacek Karpiesiuk³*

¹Białystok University of Technology, Poland,

t.chyzyi@pb.edu.pl, c.miedzialowski@pb.edu.pl, k.czech@pb.edu.pl, m.orlowski@pb.edu.pl

²Tianjin Chengjian University, China, *wgd@tcu.edu.cn, zhanghai@tcu.edu.cn*

³Warsaw University of Life Sciences, Poland, *jacek_karpiesiuk@sggw.edu.pl*

Keywords: cable post-tensioned concrete girders, thermal load

1. Introduction

As a result of World War II, approximately 64.5% of Polish industry nationwide was destroyed. According to post-war estimates, 14,000 out of 22,000 industrial facilities were destroyed. In some branches, losses reached 90%. The 1950s and 1960s in Poland were a period of intensive rebuilding and industrial development, accompanied by a very high demand for hall-type industrial facilities. Technologies such as large-slab construction and cable post-tensioned concrete girders used for covering large-span halls originated in this period [1]. These technologies were an attempt to modernise and advance construction methods in post-war Poland.

Prestressed and post-tensioned structures require particularly careful workmanship and good quality materials, and this was not always the case in post-war Poland. At the same time, problems with improper maintenance of industrial halls during their exploitation were reported [2]. Ultimately, in the 1970s, the use of this type of construction solution was banned.

The main problems identified during inspections of industrial halls with cable-concrete girders were the aforementioned poor workmanship and mounting, and above all, problems with their improper maintenance [2].

2. Measurements of the deflection of cable post-tensioned concrete girders

In the diagnosis of cable post-tensioned concrete grinders, an important issue is the assessment of the safety of their further use. The safety of a grinder depends mainly on the technical condition of the post-tensioning cable, which may lose its

load-bearing capacity during operation. Loss of load-bearing capacity may be the result of pitting corrosion of the post-tensioning cables or damage to the anchorage zones.

The subject of analysis in this article are cable post-tensioned concrete girders type KBOS-24/66, which are the supporting structure of the roof of the POLMOS Bialystok industrial plant.

In the first instance, the anchoring zones of the girders were examined. No significant abnormalities were found, so it was natural to move on to examining the condition of the cables. At this point, the first problem arises: how to assess the actual technical condition of the cables? The great majority of experts in such cases use non-destructive testing, mainly consisting of deflection measurements. The tests are based on the assumption that a weakened cable (due to corrosion) will be signalled by an increase in the deflection of the entire girder. A nomogram (presented by Prof. L. Runkiewicz [4]) is often used as a criterion for assessing the condition of cables. It indicates the permissible increase in deflection of a cable post-tensioned concrete girder during its service life (Fig. 1). This approach is very useful and widely used.

Another problem arises at the stage of implementing measurement methods and interpreting results. In the analysed case, both geodetic methods and direct measurement of the distance between metal benchmarks mounted on the floor of an industrial hall and the lower surface of a cable post-tensioned concrete girder were used.

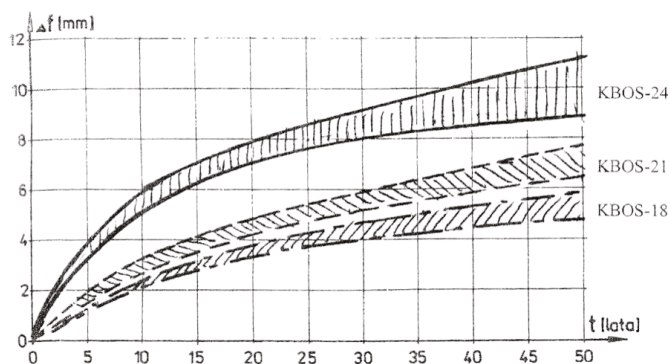


FIG. 1. Range of deflection increments of cable post-tensioned concrete girders [4]

As a result of many years of diagnostic monitoring, results were obtained in the form of changes in the deflection of cable post-tensioned concrete girders as a function of time. Example diagrams are shown in Fig. 2.

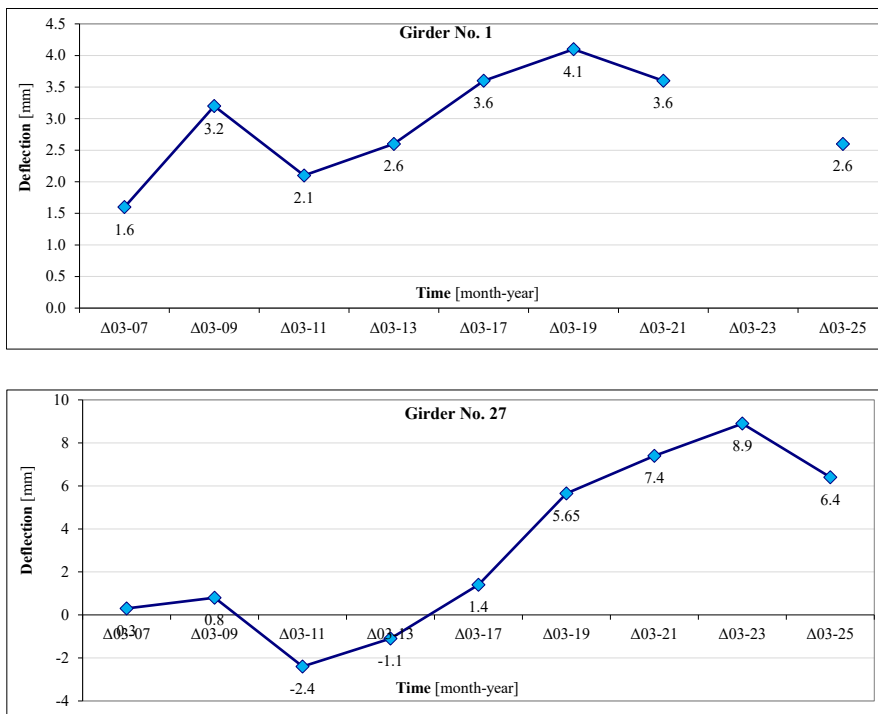


FIG. 2. Example graphs of deflection changes over time [3]

Analysing the variability of deflections, it can be seen that some girders show the expected direction of deflection (downwards) and some show the opposite.

The paper will present an analysis of the reasons for this history of deflection changes, mainly in terms of temperature effects.

References

1. Zieliński, A. (1962). *Prefabricated prestressed concrete girders*. Arkady Publishing House.
2. Han, Z. (1970). *Analysis of results obtained from inspections of cable-concrete structures in Poland*. ITB.
3. *Report on the technical condition of KBOS-24/66 cable-concrete girders at the POLMOS Białystok spirits and yeast factory, Białystok (1990–2025)*.
4. Runkiewicz, L. (2008). Assessment of the technical condition of prestressed roof girders in existing buildings. *Przegląd Budowlany*, 11.



Longitudinal forces in concrete structures. An ignored phenomenon which severely changes the structure behavior

Piotr Noakowski

TU Dortmund, Constructure GmbH, Germany, p.noakowski@constructure.de

Keywords: concrete structures, longitudinal forces, structure behavior

1. Introduction

Practical application of the stiffness-oriented design methods by the author is presented in this paper. Due to their closeness to reality these methods found wide acceptance in research, regulations and, most of all, in the complex engineering practice. To demonstrate the latter, a typical design task from the author's activities is analysed in this paper. All the investigations are based on the book *Statics of r/c Structures* by the author. The investigations are based on generally accepted design methods by the author which found entrance into research work, standards and engineering practice.

2. Significants of tension forces

Tension forces are present in practically every concrete element. The phenomenon is due to the loss of hydration heat, concrete shrinkage and temperature drop which produces virtual shortening of the affected components. As soon as such actions are constrained by adjacent building cores or walls, tension forces are activated and through cracks can appear. Such cracks frequently impair the structure behavior as follows:

- ground water intrusion due to the loss of tightness,
- large deflection due to the decrease of bending stiffness and
- decrease of the shear bearing capacity due to the vertical shift within the crack.

These facts indicate that tension forces should not be ignored in modern design.

3. Floor slabs subjected to bending and tension forces

In floor slab areas located between stiff stairwells, tension forces are activated in addition to the regular bending moments induced by loads. This phenomenon is due to constrained slab shortenings caused by the loss of hydration heat, shrinkage and cooling. In such structure areas, cracking occurs and results in the drop of stiffness, redistribution of moments and drop of imposed moments and forces. In case of insufficient reinforcement, not tight through cracks form and large deflections arise. A corresponding case of a beam fixed to stair wells and subjected to cooling is analyzed in the paper.

In this spirit, the following beams are analyzed:

System	Three span beam with fixed ends	
Concrete	Strength 25 MN/m ² or 50 MN/m ²	
Dimensions	Span 3 x 7.80 m, height 0.20 m and 0.40 m	
Actions	Dead load and service load	
	Uniform temperature drop of $0 < \Delta T < 20$ K capturing cooling and shrinkage	
Reinforcement	Determined conventionally without consideration of tension	
Internal Forces	Bending moments due to the external loads	
	Tension forces imposed by cooling and fixation	
Behavior criteria	Steel stress above the support	$\sigma_s < 400$ MN/m ²
	Crack width above the support	$w_k < 0,30$ mm
	Compression zone above support	$x_d > 50$ mm
	Deflection	$\delta < 15$ mm (l/500)

The most important findings result from the following three studies:

- STUDY 1: Slender slab $h = 0.20$ m → Steep increase of deflections δ along with cooling ΔT_m
 - Floors of low thickness 0.20 m and large span 7.80 m subjected to tension tend to high deflections.
 - The reason is formation of numerous cracks which successively decrease the slab stiffness.
 - This is especially the case at high concrete strength 50 MN/m² which doesn't matter after cracking.
- STUDY 2: Compact slab $h = 0.40$ m → High increase of crack width w along with cooling ΔT_m
 - Floors of large thickness 0.40 m and low span 3.90 m subjected to tension tend to wide cracks.
 - The reason is the weak reinforcement designed for low moments and large internal lever arm.
 - This reinforcement is not in the position to bear the additional tension forces.



- STUDY 3: Compact slab $h = 0.40$ m è Decrease of the compr. zone x_d along with cooling ΔT_m
 - Floors of large thickness 0.40 m and low span 3.90 m subjected to tension tend to through cracks.
 - The reason is low moments producing low eccentricity which leads to loss of x_d .
 - The wide separating cracks make the slab not tight and are not able to withstand shear forces.

4. Conclusions

Tension forces are activated in floor slab areas between stair wells due to the loss of hydration heat, shrinkage and sudden frost. The phenomenon changes unfavorably the behavior of the structure:

- Slender slabs develop extreme deflections due to the large drop of the overall stiffness.
- Compact slabs may lose the compression zones and therefore their tightness and shear bearing capacity.
- Cracking results in redistribution of the load-bound and reduction of constraint-bound moments.
- Cracking causes large moment-reductions in lowly loaded, weakly reinforced and tensioned beams.
- Extreme increase of deflections in highly loaded, weakly reinforced and tensioned beams.

All these examples prove that safe analysis of r/c structures is only possible if longitudinal tension and cracking are considered.



Numerical and experimental study on fiber content. Optimization of high-strength steel fiber-reinforced concrete cylinders

Gili Lifshitz Sherzer, Yuri Ribakov

Ariel University, Israel, gilil@ariel.ac.il, ribakov@ariel.ac.il

Keywords: SFRC, high-strength concrete, LDPM, energy dissipation and ductility

1. Introduction

This study investigates the influence of steel fiber content and distribution on the mechanical behaviour of high-strength steel fiber-reinforced concrete (SFRHSC) to optimize the fiber dosage for structural applications. Unlike the traditional volume-based measure, the weight ratio of fiber is adopted in pursuit of a more precise measurement of fiber content [1]. We based our study on experimental data on fifteen concrete cylinders with 0–60 kg/m³ fiber content. The outcomes determine the optimal 30 kg/m³ content, with improved compressive strength (85–90 MPa), improved ductility, increased Poisson's ratio, and enhanced energy dissipation capacity. The tests were complemented by simulations with the Lattice Discrete Particle Model (LDPM). The model parameters were initially calibrated with cube samples through uniaxial compression tests and verified with loading–unloading simulations. The model was calibrated and subsequently utilized to investigate the contribution of the fiber-driven cracking behaviour and the energy absorption for a range of strength grades. The coupled experimental-numerical strategy offers insight into SFRHSC design for specified mechanical performance in challenging structural applications.

2. Results and discussion

2.1. Fiber content effect

Cylindrical specimens with 0–60 kg/m³ fiber ratios were tested. Both experiments and simulations showed significant improvements in ductility and energy dissipation up to 30 kg/m³, after which performance declined. Figure 1 compares load–strain curves for selected fiber ratios.

2.2. Energy dissipation

Energy dissipated (W) was calculated from hysteresis loops. *Table 1* shows close agreement between experimental and simulated results, with minimal error at 30 kg/m³.

TABLE 1. Comparison of experimental and simulated energy dissipation

Fiber ratio (kg/m ³)	Exp. (kNm/m)	Sim. (kNm/m)	Error %
0	0	0.19	
20	1.08	0.83	22
30	1.89	1.71	9
40	1.63	1.44	12
60	0.31	0.82	62

2.3. Crack behavior

Simulations revealed distributed micro-cracks at 20–30 kg/m³, leading to higher energy dissipation. At higher contents, fiber clumping caused localized cracking and reduced ductility (see *Fig. 1*).

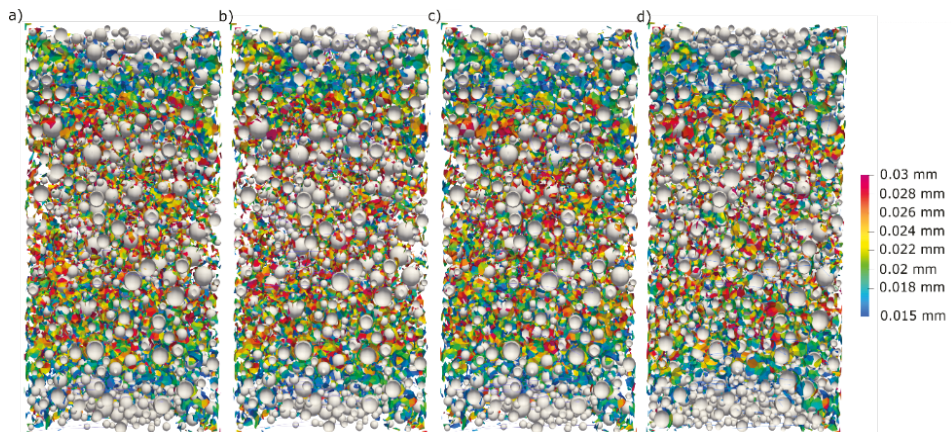


FIG. 1. Total crack opening values and patterns: a) 20 FWR, b) 30 FWR, c) 40 FWR, d) 60 FWR

2.4. Compressive strength effect

Simulations of 120 MPa concrete confirmed that 30 kg/m³ remained optimal, though higher strength mitigated the negative effect of excessive fiber contents.



3. Conclusions

- FRHSC cylinders achieve optimal ductility and energy dissipation at 30 kg/m³ fiber content.
- LDPM simulations reproduced experimental findings, providing insight into crack propagation and fiber pull-out mechanisms.
- Excessive fiber contents (>40 kg/m³) reduce ductility due to clumping and matrix saturation.
- Higher compressive strength moderates the loss of ductility at elevated fiber ratios but does not shift the optimal value.

This combined experimental–numerical approach supports rational optimization of FRHSC for advanced structural applications.

References

1. Holschemacher, K., Iskhakov, I., Ribakov, Y., & Mueller, T. (2012). Laboratory tests of two-layer beams consisting of normal and fibered high-strength concrete: Ductility and technological aspects. *Mechanics of Advanced Materials and Structures*, 19(7), 513–522. <https://doi.org/10.1080/15376494.2011.556840>



Impact of basalt minibars on the structural performance of BFRP bar reinforced concrete beams

Abel A. Belay, Marta Kosior-Kazberuk, Julita Krassowska
Bialystok University of Technology, Poland, abel.belay@sd.pb.edu.pl

Keywords: basalt minibars, BFRP bars, concrete beams, deflection

1. Introduction

BFRP bar reinforced concrete beams are now considered a promising alternative to conventional steel-reinforced beams, particularly in corrosive environments, owing to their excellent tensile strength, low density, and superior chemical resistance. Numerous studies have investigated their structural behavior, examining load-bearing capacity, deflection response, cracking patterns, and failure modes [1, 2, 3].

Despite these advantages, BFRP bars have a significantly lower modulus of elasticity compared to steel. This leads to notably higher deflections in reinforced concrete beams. For instance, Kosior-Kazberuk [3] reported deflections that were three to four times greater than those observed in steel-reinforced counterparts, a finding supported by other researchers [4, 5].

To address this serviceability concern, the aim of the present research is to investigate the effect of incorporating basalt minibars into concrete beams reinforced with BFRP bars. The study focuses on enhancing the mechanical performance and compares the results with beams reinforced solely with BFRP bars and with conventional steel reinforcement.

2. Materials

Two concrete mixtures were prepared: standard concrete and concrete modified with 3.5 kg/m^3 of basalt minibars (50 mm long, 1 mm in diameter). Both mixes contained 320 kg/m^3 of cement, a water-to-cement ratio of 0.5, 732 kg/m^3 of fine aggregate ($\leq 2 \text{ mm}$), and 1203 kg/m^3 of coarse aggregate ($\leq 8 \text{ mm}$). Additionally, 3.2 kg/m^3 of superplasticizer was added to improve workability.

To assess mechanical performance, compressive strength tests were carried out in accordance with EN 12390-3:2009, while tensile strength was measured following EN 12390-5:2019. The modulus of elasticity was determined using cylindrical



specimens per EN 12390-13:2013. The results, including average values, standard deviations, and coefficients of variation (CV), are summarized in Table 1

TABLE 1. Mechanical properties comparison of concrete with 3.5 kg/m³ basalt minibars and regular concrete

Property	Concrete w/Minibars	Regular concrete	%Difference (Increase)
Compressive strength (MPa)	63.18 ± 3.35 (CV: 5.3%)	59.66 ± 1.98 (CV: 3.32%)	+5.91%
Flexural strength (MPa)	6.28 ± 0.50 (CV: 7.96%)	3.06 ± 0.05 (CV: 1.63%)	+105.23%
Elastic Modulus (GPa)	47.36 ± 2.83 (CV: 5.97%)	33.53 ± 0.39 (CV: 1.16%)	+41.23%

For longitudinal reinforcement, 6 mm diameter steel and BFRP bars were used.

3. Experimental program

This study examines the ultimate load capacity, failure modes, cracking behavior, and deflection of reinforced concrete beams. Five beams (80 × 120 × 1100 mm) were tested: two with steel reinforcement (STL-1, STL-2), two with BFRP bars and regular concrete (BFP-1, BFP-2), and one with BFRP bars and basalt minibar concrete (BFMB3.5).

All beams were tested under two-point bending, starting from a 0 kN preload and increasing in 2 kN steps using a hydraulic cylinder controlled by a PZA machine. Midspan deflection was measured with Megatron-Munchen inductive sensors, and crack patterns were documented through image analysis. Data on load capacity, deflection, and cracking were recorded.

4. Results

The following table 2 summarizes the test results. It includes load of initial crack, maximum deflection, ultimate load bearing capacity and failure modes of the specimens.

TABLE 2. Test results

Beam notations	b (mm)	D (mm)	No. ϕ diameter (mm)	(kN)	(kN)	Max. Deflection (mm)	Failure mode
STL-1	80	120	4 ϕ 6	8	20	4.76	Flexural
STL-2	80	120	4 ϕ 6	10	21.8	4.65	Flexural
BFP-1	80	120	4 ϕ 6	2	26.3	16.71	Flexural



Beam notations	b (mm)	D (mm)	No. ϕ diameter (mm)	(kN)	(kN)	Max. Deflection (mm)	Failure mode
BFP-2	80	120	4 $\phi 6$	2	30.5	21.50	Flexural
BFMB3.5	80	120	4 $\phi 6$	8	34	9.08	FRP rupture

where, b = width, D = depth, P_{cr} = Load where crack initiated, P = maximum load

5. Conclusion

The study observed that BFRP bar-reinforced concrete beams exhibited a 35.88% higher ultimate load capacity compared to steel-reinforced beams. When basalt minibars were added, the BFRP-reinforced beams achieved a 62.67% increase over steel-reinforced beams and a 19.7% increase over BFRP beams with regular concrete. Additionally, the inclusion of basalt minibars reduced the maximum deflection by 47.5% compared to BFRP-reinforced beams without minibars. While early crack formation was observed in beams with BFRP bars alone, the addition of basalt minibars effectively delayed crack initiation.

References

1. Adam, M. A., Said, M., Salah, A., & Elsheikh, A. (2023). Experimental and analytical study of high-performance concrete beams reinforced with Basalt FRP bars. *Structures*, 55, 510–530. <https://doi.org/10.1016/j.istruc.2023.06.061>
2. Kudyakov, K. L., Plevkov, V. S., & Nevskii, A. V. (2015). Strength and deformability of concrete beams reinforced by non-metallic fiber and composite rebar. *IOP Conference Series: Materials Science and Engineering*, 71, 012030. <https://doi.org/10.1088/1757-899X/71/1/012030>
3. Kosior-Kazberuk, M., & Krassowska, J. (2019). Analysis of deflection and cracking of concrete beams with non-metallic reinforcement. *System Safety: Human-Technical Facility-Environment*, 1, 782–789.
4. Urbanski, M., Lapko, A., & Garbacz, A. (2013). Investigation on concrete beams reinforced with basalt rebars as an effective alternative of conventional R/C structures. *Procedia Engineering*, 57, 1183–1191. <https://doi.org/10.1016/j.proeng.2013.04.149>
5. Krassowska, J., & Ramírez, C. P. (2022). Flexural capacity of concrete beams with basalt fiber-reinforced polymer bars and stirrups. *Materials*, 15, 8270. <https://doi.org/10.3390/ma15228270>



Accelerated CO₂ curing of alkali-activated pervious paving blocks with seashell aggregates

Ágata González-Caro¹, Antonio Manuel Merino-Lechuga²,
José Ramón Jiménez², José María Fernández-Rodríguez¹

¹Inorganic Chemistry Area. University of Cordoba, Spain q32gocaa@uco.es, um1feroj@uco.es

²Construction Engineering Area. University of Cordoba, Spain ammlechuga@uco.es, jrjimenez@uco.es

Keywords: coal mining tailings; alkali-activated materials; CO₂ curing; seashell sand.

1. Introduction

The construction sector heavily depends on ordinary Portland cement (OPC), whose production exceeds 4 Gt annually and contributes significantly to global CO₂ emissions. To mitigate this impact, alkali-activated materials (AAMs) such as fly ash (FA) and coal mining tailings (CMT) have been investigated as sustainable alternatives. At the same time, the rapid growth of shellfish farming generates large volumes of shell waste, which pose environmental concerns but can be valorized as aggregates in concrete. The present study explores the production of pervious paving blocks using FA and CMT binders, with 50% and 100% replacement of natural sand by *Acanthocardia tuberculata* seashells and evaluates the effects of accelerated CO₂ curing on strength, durability, and permeability.

2. Materials and methods

FA was collected from the Sines power plant and CMT from the Pozo San José mine in Spain, both processed to suitable particle sizes and densities for use as binders. *Acanthocardia tuberculata* seashells were sourced from the canning industry and ground to sand-sized particles. The alkali activator consisted of sodium silicate solution combined with NaOH pellets, with borax and a water-reducing admixture (WRA). A preliminary study identified a 50%FA-50%CMT blend as the optimal binder, with a water-to-binder ratio of 0.3 and a SiO₂/Na₂O ratio of 0.75. Based on this, two experimental mixes were prepared: one with 50% substitution of natural sand by seashell sand and another with 100% replacement. *Table 1* details the composition of each mix produced.

TABLE 1. Mix composition of blocks with varying sand replacement ratios (kg/m³)

Materials	0%SS	50%SS	100%SS
FA	120.0	120.0	120.0
CMT	120.0	120.0	120.0
Water	18.7	18.7	18.7
WRA	2.4	2.4	2.4
Borax	9.6	9.6	9.6
Natural sand	500.0	250.0	–
Sand-gravel	900.0	900.0	900.0
Gravel	800.0	800.0	800.0
Seashell aggregate	–	259.5	519.1
NaOH	28.3	28.3	28.3
Na ₂ SiO ₃ solution	81.8	81.8	81.8

3. Results and discussion

Mechanical results (Fig. 1) show that carbonation significantly enhanced the performance of all block mixtures. After 7 days of CO₂ exposure, splitting tensile strength increase by 45% in the reference blocks (0%SS), 48% in the 50%SS replacement, and up to 60% when using natural sand in 100%SS. Similarly, compressive strength increased by 24%, 30%, and 27%, respectively. These improvements are attributed to the formation of carbonates and gel N-A-S-H within the pore structure, which promote densification and better inter-particle bonding.

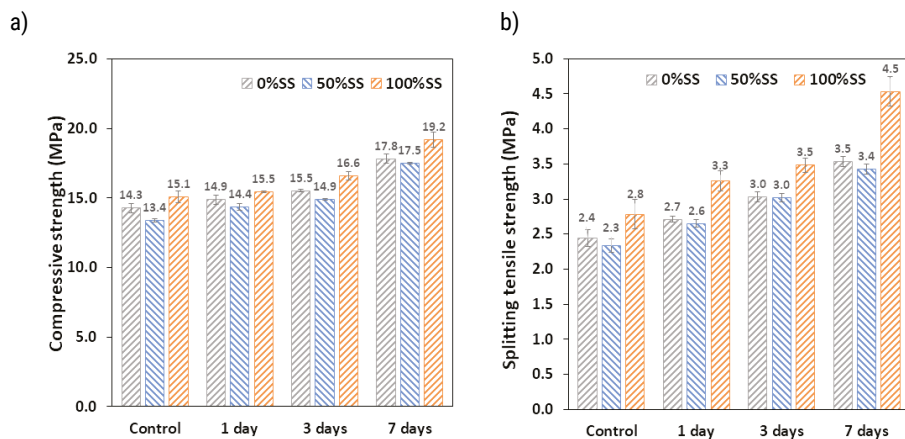


FIG. 1. a) Compressive and b) splitting tensile strengths results of non-carbonated (control) and blocks carbonated for different periods

Durability indicators also improved. Abrasion resistance, measured by mass loss, decreased from around 13% in non-carbonated samples to about 6% after 7 days of CO₂ curing.

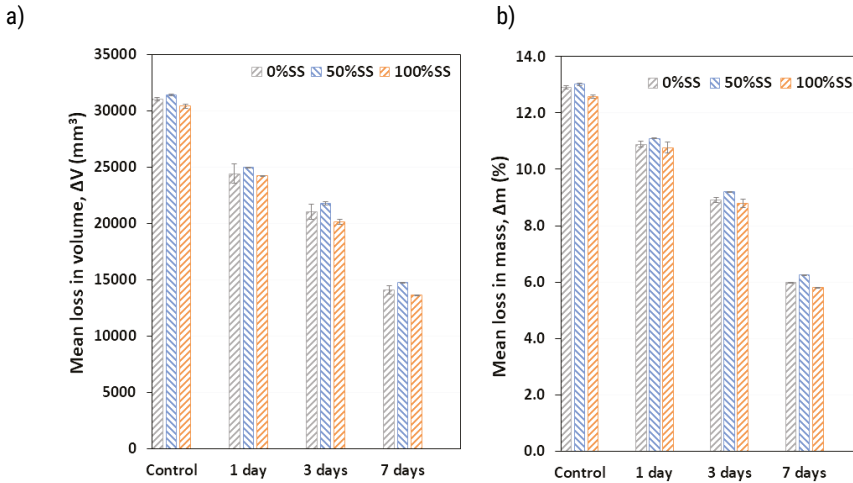


FIG. 2. Abrasion resistance results of carbonated and non-carbonated blocks showing a) the mean loss in mass after 16 cycles and b) the mean loss in specimen volume ΔV

4. Conclusions

Coal mining tailings still require refinement before they can be effectively used as binders in the production of alkali-activated concrete. However, when mixed with fly ash, this precursor demonstrates satisfactory performance for use in precast non-structural pervious blocks. The results confirm that accelerated carbonation not only enhances mechanical strength but also improves durability parameters. On the other hand, the use of shell aggregates has proven to be a sustainable alternative to natural sand.

Acknowledgments

Partial support from the Research Groups FQM-391 (<https://www.uco.es/matapli/>) and TEP-227 (<https://www.uco.es/ingconst/>) at the University of Córdoba (Spain).



Influence of pore structure on mechanical and thermal performance of cementitious composites

Marzena Kurpińska

Gdańsk University of Technology, Poland, marzena.kurpinska@pg.edu.pl

Keywords: cementitious composites, porosity, thermal performance, mechanical properties

1. Introduction

Mechanical and durability characteristics of cementitious composites are strongly governed by microstructural features, in particular total porosity and pore size distribution [1]. Previous research has mainly focused on the role of pore structure in frost resistance, while comprehensive studies linking porosity to mechanical and thermal properties remain limited [2], [3].

To address this gap, an experimental program was conducted on 12 mixtures with varying water-to-cement ratios and different proportions of natural and lightweight aggregates (0%, 50%, 100%), including sintered fly ash and foamed glass. A image-based method was applied to evaluate porosity and pore distribution, enabling direct correlation with water transport in the capillary zone, thermal conductivity, elastic modulus, and compressive strength. The aim of this study is to demonstrate how porosity characteristics can be used to predict and tailor the performance of cementitious composites.

2. Materials and methods

Cement CEM III/A 42.5N was used. Natural aggregate was used: sand (0–4 mm), gravel (2–8 mm), lightweight aggregate: granulated foamed glass (GA) (0–4 mm) and sintered fly ash aggregate (AA) (2–8 mm). A polycarboxylate-based superplasticizer (PCE) was added at dosages ranging from 0.55% to 1.0% of the binder mass to ensure proper workability and water-to-cement ratio: 0.40, 0.45, 0.50, and 0.55. Detailed mixture proportions are presented in Table 1.

TABLE 1. The detailed mix proportions

Mix No.	W/C	Cement (kg)	Water (kg)	Sand 0–4 mm (kg)	CA 2–8 mm (kg)	GA0–4 mm (kg)	AA 2–8 mm (kg)	Adm. PCE (%c.c.)
1	0.4	400	160	942	942	–	–	1
2	0.45	400	180	916	916	–	–	0,85
3	0.5	400	200	889	889	–	–	0,7
4	0.55	400	220	863	863	–	–	0,55
5	0.4	400	160	–	942	196	–	1
6	0.45	400	180	–	916	190	–	0,85
7	0.5	400	200	–	889	185	–	0,7
8	0.55	400	220	–	863	179	–	0,55
9	0.4	400	160	–	–	196	480	1
10	0.45	400	180	–	–	190	466	0,85
11	0.5	400	200	–	–	185	453	0,7
12	0.55	400	220	–	–	179	439	0,55

Composite mixtures were prepared using standard mixing procedures. Samples were made for testing. After 28 days of curing, compressive strength tests were conducted according to EN 12390-3, while testing of modulus of elasticity was conducted according to EN 12390-13, and thermal conductivity tests were performed according to EN 12664. All tests were performed in triplicate, and the average values were reported. The structure was analyzed using a digital microscope equipped with a specialized optical head. Porosity, pore structure and pore distribution were evaluated using image analysis. This method allowed quantification of pore size distribution and spatial arrangement, enabling correlation with water transport in the capillary zone, thermal conductivity, elastic modulus, and compressive strength.

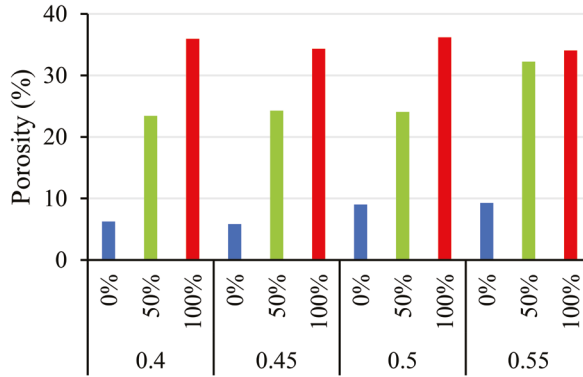
3. Results

The incorporation of foamed glass aggregate (GA) increased total porosity, particularly the fraction of closed pores, which improved thermal insulation by reducing effective heat transfer through the composites. Mixtures with a higher share of pores below 300 μm showed limited capillary water transport, indicating the importance of pore size distribution in durability-related behavior.

Compressive strength after 28 days ranged up to 40 MPa, depending on w/c ratio and aggregate type, with 50% replacement by GA providing the best balance between

density reduction and strength. Elastic modulus values decreased with increasing porosity, from 42 GPa for natural aggregate mixtures to 7–9 GPa for full lightweight aggregate replacement, confirming the strong link between pore structure and stiffness.

a)



b)

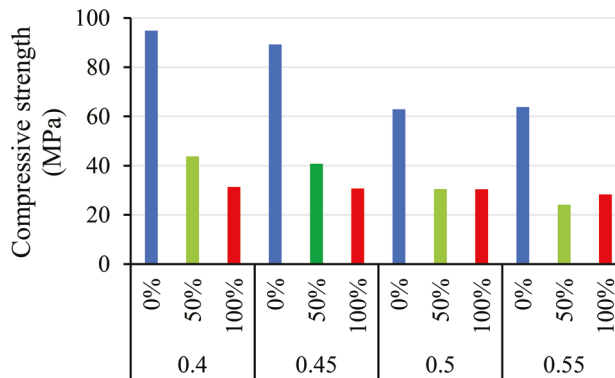


FIG. 1. Properties of cement composites

4. Conclusion

Image analysis confirmed that pore size distribution, particularly the fraction of pores smaller than $300\ \mu\text{m}$, significantly influences the reduction of capillary water transport. A higher content of closed pores enhanced thermal insulation while simultaneously reducing the stiffness of the composites. The results demonstrate that both the w/c ratio and the amount of lightweight aggregate govern the microstructure, and consequently thermal conductivity, modulus of elasticity and compressive strength.



References

1. Neville, A. M. (2000). *Właściwości betonu*. Stowarzyszenie Producentów Cementu.
2. Domagała, L. (2014). *Konstrukcyjne lekkie betony kruszywowe*. Wydawnictwo Politechniki Krakowskiej.
3. Hearn, N., Hooton, R. D., & Nokken, M. R. (2006). Pore structure, permeability, and penetration resistance characteristics of concrete. *ASTM Special Technical Publication*, 169, 238–252.



Accelerated carbonation curing of alkali-activated pervious paving blocks

*Antonio Manuel Merino-Lechuga¹, Ágata González Caro²,
José María Fernández-Rodríguez², José Ramón Jiménez¹*

¹*Construction Engineering Faculty. University of Cordoba, Spain,
ammlechuga@uco.es, jrjimenez@uco.es*

²*Inorganic Chemistry Faculty. University of Cordoba, Spain,
q32gocaa@uco.es, um1feroj@uco.es*

Keywords: alkali-activated materials, accelerated carbonation curing, pervious paving blocks

1. Introduction

The construction industry is one of the main contributors to global CO₂ emissions due to the extensive use of ordinary Portland cement (OPC), which can release up to 1 tonne of CO₂ per tonne produced [1]. Alkali-activated materials (AAM) derived from industrial by-products, such as fly ash and slag, have emerged as low-carbon alternatives that align with circular economy principles [2].

Accelerated carbonation curing (ACC) has gained attention as a method to improve the performance of AAM while capturing CO₂ within the material matrix [3]. Its effectiveness depends largely on the chemical composition and reactivity of the precursor, particularly its CaO content.

Pervious concrete is widely used in sustainable urban drainage systems but typically presents limitations in strength and long-term durability [4]. This study explores the application of ACC to alkali-activated pervious paving blocks to enhance mechanical and physical properties while contributing to carbon mitigation. Mechanical performance was evaluated according to EN 1338, and water absorption, dry density and porosity were measured following UNE 83980:2014. Infiltration capacity was assessed using an adaptation of ASTM C1701/C1701M-09.

2. Materials and methods

Fly ash from a Portuguese power plant was used as precursor, combined with natural limestone aggregates (sand, fine gravel, coarse gravel). An alkaline activator based on sodium silicate and sodium hydroxide was employed, with borax as a set retarder. Blocks (200 × 100 × 60 mm³) were produced and cured in three stages: (i) thermal curing at 70°C for 24 h, (ii) dry curing at 20 °C and 65% RH, and (iii) accelerated carbonation at 5% CO₂, 23°C, and 60% RH for up to 7 days. Performance was assessed

following EN 1338 and UNE 83980 standards, including compressive and tensile strength, abrasion, porosity, water absorption, and infiltration tests.

TABLE 1. Mix formulation (kg/m³)

Materials	FA	Water	Borax	NS	FG	CG	NaOH	Na ₂ SiO ₃ solution
Content	240	18.7	9.6	500	900	800	28.3	81.1

3. Results and discussion

Accelerated carbonation curing significantly enhanced the performance of the paving blocks. After 7 days of CO₂ curing, compressive strength increased by over 30% (from 27.4 MPa to 36.6 MPa), while splitting tensile strength improved by nearly 60% (from 3.9 MPa to 6.3 MPa). Abrasion resistance was also improved, with mass loss reduced from 8.2% in control specimens to 5.6% in carbonated ones.

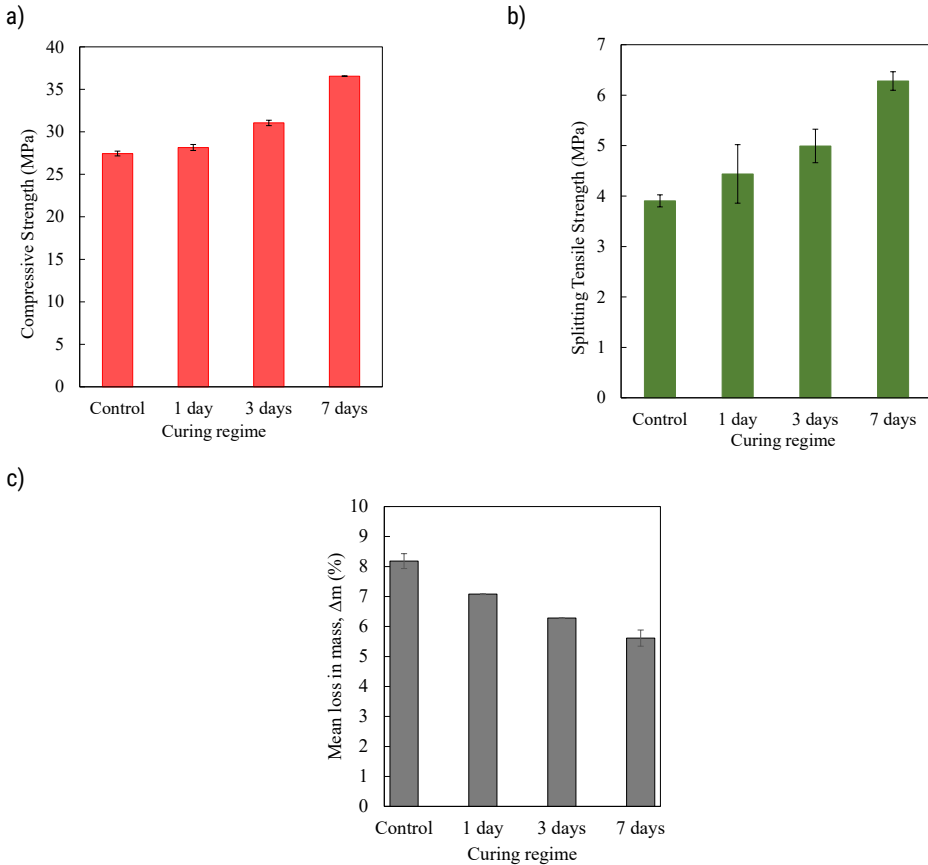


FIG. 1. Compressive (a), splitting tensile (b) strength and average loss in mass results of the non-carbonated (control) and carbonated blocks at different CO₂ curing ages



After 7 days of CO₂ curing, dry bulk density rose from 2.15 to 2.20 g/cm³ (+2.3%), while water absorption decreased from 6.5% to 6.3% (≈4%) and porosity from 14.0% to 12.9% (≈8.4%), confirming the densification effect of carbonation.

4. Conclusions

This study demonstrates the feasibility of manufacturing alkali-activated pervious paving blocks cured by accelerated carbonation. The process improved mechanical strength, abrasion resistance, density, and reduced porosity and absorption. The results confirm the potential of ACC as a sustainable technology for precast pervious elements, combining CO₂ sequestration with enhanced performance.

Acknowledgments

Partial support from the Research Groups FQM-391 (<https://www.uco.es/matapli/>) and TEP-227 (<https://www.uco.es/ingconst/>) at the University of Córdoba (Spain).

References

1. Higuchi, T., Morioka, M., Yoshioka, I., & Yokozeki, K. (2014). Development of a new ecological concrete with CO₂ emissions below zero. *Construction and Building Materials*, 67, 338–343.
2. Palomo, A., Grutzeck, M. W., & Blanco, M. T. (1999). Alkali-activated fly ashes: A cement for the future. *Cement and Concrete Research*, 29(8), 1323–1329.
3. Lamaa, G., Duarte, A. P. C., Silva, R. V., & de Brito, J. (2023). Carbonation of alkali-activated materials: A review. *Materials*, 16, 3086.
4. Aoul, T., Noguchi, M., Shafiq, M. T., Attoye, D. E., Anwar, F. H., El-Hassan, H., Hamouda, M., Hinge, G., & Hung Mo, K. (2022). Meta-analysis of the performance of pervious concrete with cement and aggregate replacements. *Buildings*, 12, 461.



Effect of calcium nitrate and fly ash on the mechanical properties of grout for two-stage concrete

*Farzam Omidi Moaf¹, Marzena Kurpinska¹, Hakim S. Abdelgader²,
Mikolaj Miskiewicz¹, Barbara Sadowska-Buraczewska³*

¹Gdansk University of Technology, Poland, farzam.omidi.moaf@pg.edu.pl,
marzena.kurpinska@pb.edu.pl, mikolaj.miskiewicz@pg.edu.pl

²Universito of Tripoli, Libiya, h.abdelgader@uot.edu.ly

³Bialystok University of Technology, Poland, barbara.sadowska@pb.edu.pl

Keywords: two-stage concrete, calcium nitrate, fly ash, cement reduction

1. Introduction

Two-stage concrete, also known as preplaced aggregate concrete (PAC), is a construction method where coarse aggregates are first packed into the formwork, and then a flowable grout is injected to fill the voids between the aggregates [1]. This technique offers benefits such as reduced shrinkage, better control of coarse aggregate distribution, and improved mechanical properties, making it especially valuable for specialized applications like underwater or repair works [2].

In the construction industry, the drive toward sustainability has led to innovations in reducing cement content, a major contributor to CO₂ emissions [3]. This study focuses on the development of grout mixtures for two-stage concrete by partially replacing cement with fly ash and incorporating calcium nitrate (Ca(NO₃)₂) as an additive.

Notably, the sand used in all mixes is 100% recycled sand sourced from demolition waste, further enhancing the environmental benefits. The objective is to assess how calcium nitrate affects the mechanical performance – particularly compressive and flexural strength – of grout when used alongside fly ash.

2. Materials and methods

A total of eight grout mix designs were developed for use in two-stage concrete. All mixes used 100% recycled sand obtained from processed demolition waste as the fine aggregate, supporting the sustainability goals of the study. The binders included ordinary Portland cement (OPC) partially replaced with fly ash at varying percentages, aiming to reduce the overall cement content and lower the environmental footprint.



Calcium nitrate was added at dosages ranging from 0% to 5% by binder weight to evaluate its effect on early-age strength. Water-to-binder (w/b) ratios were kept constant across the mixes to ensure comparability. The detailed mix proportions, including quantities of cement, fly ash, calcium nitrate, water, and recycled sand, are provided in Table 1.

The fresh grout mixtures were prepared using standard mixing procedures and cast into molds for mechanical testing. After 7 days of curing, compressive strength tests were conducted according to EN 12390-3, while flexural strength was evaluated using EN 12390-5 standards. All tests were performed in triplicate, and the average values were reported.

TABLE 1. The detailed mix proportions

Mix No.	F/C	Cement (kg)	Fly Ash (kg)	Ca(NO ₃) ₂ (gr)	Ca(NO ₃) ₂ (%)	Water (kg)	Sand (kg)
1	15%	2.040	0.360	72.00	3%	1.104	2.496
2	25%	1.800	0.600	72.00	3%	1.104	2.321
3	35%	1.560	0.840	72.00	3%	1.104	2.216
4	25%	1.800	0.600	96.00	4%	1.080	2.264
5	15%	2.040	0.360	96.00	4%	1.080	2.369
6	25%	1.800	0.600	120.00	5%	1.056	2.220
7	25%	1.800	0.600	0.00	0%	1.176	2.438
8	15%	2.040	0.360	0.00	0%	1.176	2.543

3. Results and discussions

The compressive strength results ranged from 20.43 MPa to 33.81 MPa, while flexural strength varied between 4.32 MPa and 5.70 MPa at 7 days. Mixes with 3–4% calcium nitrate showed improved strengths compared to the reference mix without calcium nitrate, indicating its beneficial effect on early-age strength development. However, excessive calcium nitrate (5%) did not significantly enhance performance, suggesting an optimal dosage threshold. The results also confirmed that partial cement replacement with fly ash is feasible without compromising mechanical properties, aligning with sustainability goals.

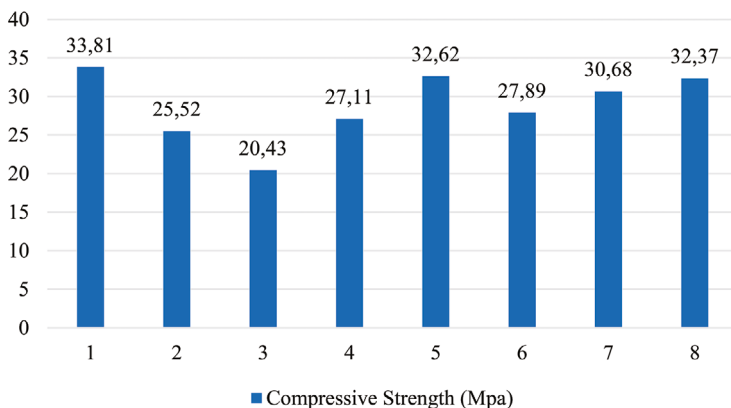


FIG. 1. Compressive strength (MPa) of grout mixes at 7 days

4. Conclusion

The study demonstrates that using calcium nitrate at optimal dosages (around 3–4%) in combination with fly ash effectively reduces cement demand while maintaining or improving early-age mechanical performance in grout for two-stage concrete. These findings support the development of more sustainable grout formulations for structural applications.

References

1. Moaf, F. O., Rajabi, A. M., Abdelgader, H. S., Kurpińska, M., Murali, G., & Miśkiewicz, M. (2024). Triaxial compression and shear strength characteristics of two-stage concrete: An experimental study. *Scientific Reports*, 14(1), 29396.
2. Rajabi, A. M., & Moaf, F. O. (2017). Simple empirical formula to estimate the main geomechanical parameters of preplaced aggregate concrete and conventional concrete. *Construction and Building Materials*, 146, 485–492.
3. Suh, J. I., Yum, W. S., Song, H., Park, H. G., & Oh, J. E. (2019). Influence of calcium nitrate and sodium nitrate on strength development and properties in quicklime (CaO)-activated Class F fly ash system. *Materials and Structures*, 52, 1–13.



Innovative formulation and evaluation of bio-based self-healing capsules (biocach) for enhanced concretes sustainability and durability. Capsule formulation, stability (pH-value of 7.77), and preliminary compressive strength of capsule-modified concrete

Isaac O. Agbamu^{1,2}, Marcin Wysokowski²,
Teofil Jesionowski³, Mieczysław Kuczma⁴

¹Poznan University of Technology, Institute of Building Engineering, Poland,
isaac.agbamu@doctorate.put.poznan.pl

²Poznan University of Technology, Institute of Chemical Technology and Engineering, Poland,
marcin.wysokowski@put.poznan.pl

³Poznan University of Technology, Institute of Chemical Technology and Engineering, Poland,
teofil.jesionowski@put.poznan.pl

⁴Poznan University of Technology, Institute of Building Engineering, Poland,
mieczyslaw.kuczma@put.poznan.pl

Keywords: bio-based materials (biopolymers), chitin, self-healing concrete, sustainability

1. Introduction

Micro-cracking reduces the service life of reinforced concrete by increasing the speed of chloride intrusion and steel corrosion. Recent bio-based strategies incorporate curing agents that will release CaCO_3 when cracks form, but the majority of them utilize synthetic polymers [1, 2]. Chitin – a renewable polysaccharide in abundance, found in marine waste – is a low-carbon option with biocompatibility. Calcium-alginate-chitin (*Bio – CACH*) capsules $\sim 5.5 \times 3$ mm are fabricated and the effect on the mechanical strength is assessed. The capsule formulation (w/w) contains sodium alginate, water, Triton-X 1%, chitin (Fig. 1), and sunflower oil that is dripped in a CaCl_2 solution at pH 7.77 (Fig. 4) as per ISO 10523 (Table 1). These capsules are used in concrete with the help of a portable mixer with the aim to increase the strength and increase the working life of reinforced concrete buildings, concrete specified and manufactured to EN 206 [3] were homogenised and CEM I 42.5R, water-to-binder ratio 0.50 and sand / aggregate were used. Eurocode 2 (EN 1992-1-1) micro-cracking reduces durability through the promotion of chloride ingress and reinforcement corrosion and therefore reduces the design working life in Eurocode 0 (EN 1990). Chitin sea waste polysaccharide is a renewable source of low-carbon alternative. The application

of biodegradable, completely bio-based capsules correspond to the goals of sustainability as it helps to reuse the biomass of waste (chitin) and reduces the use of synthetic materials.

Aqueous phase (wt.%): sodium alginate + water + TritonX (nonionic surfactant) 1.0 + chitin + oil 12.0

TABLE 1. Physical properties of Bio – CACH capsules (n = 50)

Property	Mean ± SD	Test method
Equivalent diameter (mm)	~5.5 ± 0.3	Optical Microscopes
Aspect ratio (–)	1.8 ± 0.1	Scanning Electron Microscopes SEM
pH of dispersion (–)	7.77	ISO 10523

Testing programme

- Compressive strength ascertained to EN 12390 3 [4] (Fig. 2 setup).
- Strength calculated as:

$$f_c = P_{max} \quad (1)$$

where f_c is compressive strength (MPa), P_{max} is peak load (N) and A is loaded area (mm²). Eurocode 2 definitions and notations are followed [5].

1.1. Sustainability considerations and planned healing and durability metrics (ongoing)

Pre cracking of prism/beam and wet-dry conditions; measurement of crack closure, water permeability and the recovery of strength in accordance with RILEM TC 221-SHC collection and literature on microbial precipitation. *Bio – CACH* (Fig. 3) enhances the sustainability profile by (i) utilising shellfish waste to valorise chitin [1]; (ii) using algae waste to make alginate [2]; and (iii) aiming at reduced maintenance through autonomous repair of cracks that can reduce life-cycle emissions by extending life span.

1.2. Eurocode-compliant strength

Compression strength of ~30 MPa was used as reference and *Bio – CACH* had a compression strength of ~28 MPa. The ~2 MPa decrease is relatively small and in line with capsule-based concretes. The next steps (in progress) refer to EN congruent durability test following: pre cracking of beams/prisms, wet dry test, quantification of crack closure, and transport test to vindicate service life improvement of Eurocode congruent designs (EN 1990, EN 1992 1 1).



FIG. 1. Chitin feedstock used in capsule formulation (biowaste valorisation and sustainability)



FIG. 2. Compressive strength test on a 100 mm cube (EN 123903)



FIG. 3. BioCACH capsules after synthesis and storage (hydrated bulk)



FIG. 4. pH meter



Acknowledgments

The authors gratefully acknowledge Grant, 0412 | SBAD |0081

References

1. Rinaudo, M. (2006). Chitin and chitosan: Properties and applications. *Progress in Polymer Science*, 31(7), 603–632. <https://doi.org/10.1016/j.progpolymsci.2006.06.001>
2. Lee, K. Y., & Mooney, D. J. (2012). Alginate: Properties and biomedical applications. *Progress in Polymer Science*, 37, 106–126. <https://doi.org/10.1016/J.PROGPOLYMSCI.2011.06.003>
3. CEN. (2021). *Concrete – Specification, performance, production and conformity*.
4. CEN. (2019). EN 12390-3:2019 *Testing hardened concrete – Part 3: Compressive strength of test specimens*. <https://standards.iteh.ai/catalog/standards/cen/7eb738ef-44af-436c-ab8e-e6561571302c/en-12390-3-2019>
5. CEN. (2014). EN 1992-1-1:2004/A1:2014 *Eurocode 2 – Design of concrete structures – Part 1-1: General rules and rules for buildings*. <https://standards.iteh.ai/catalog/standards/cen/cd143039-e932-4be9-bfc1-d8b88beea6e4/en-1992-1-1-2004-a1-2014>



Finite element analysis of steel-concrete composite beams with web openings

Bilal Ahmed¹, Jan Kubica¹, Mohamad Ahmad²

¹*Silesian University of Technology, Poland, bilal.ahmed@polsl.pl, jan.kubica@polsl.pl*

²*Cervenka Consulting, Czech Republic, eng.mhd.a@gmail.com*

Keywords: composite beam, web opening, finite element analysis, shear bearing capacity

1. Introduction

In modern structural engineering, steel-concrete composite beams are vital, combining steel's tensile strength with concrete's compressive capacity. Web openings are often added to these beams to allow utilities such as HVAC ducts and electrical conduits to pass through, serving practical needs but potentially significantly affecting their structural performance. These composite beams integrate steel's tensile strength with concrete slabs' compressive strength through shear connectors, leveraging the strengths of both materials. This leads to members with enhanced load-bearing capacity, stiffness, and ductility. Thanks to their efficiency and cost advantages, including improved bearing capacity, stiffness, seismic performance, fire resistance, and durability [1–3], such systems are widely used in modern construction. They are especially common in long-span and high-rise buildings to reduce height and costs [4–7].

The goal of this study is to identify critical factors affecting performance and to develop strategies to enhance both the strength and ductility of composite beams with web openings through nonlinear finite element analysis, focusing on the effects of concrete flange thickness, reinforcement ratios, and opening sizes on structural behavior.

2. Properties and specimen details

A finite element analysis with ATENA Science was performed to examine the stress behavior of steel-concrete composite beams with web openings. In total, 10 specimens labeled CB1-CB10 were modeled; CB1, the control specimen, had no openings. The other nine beams featured different opening configurations. The study focused on variables such as the thickness of the concrete flange plate, the reinforcement ratio,

and the opening sizes. All specimens were designed to ensure full shear connection. Figures 1 show the geometric details.

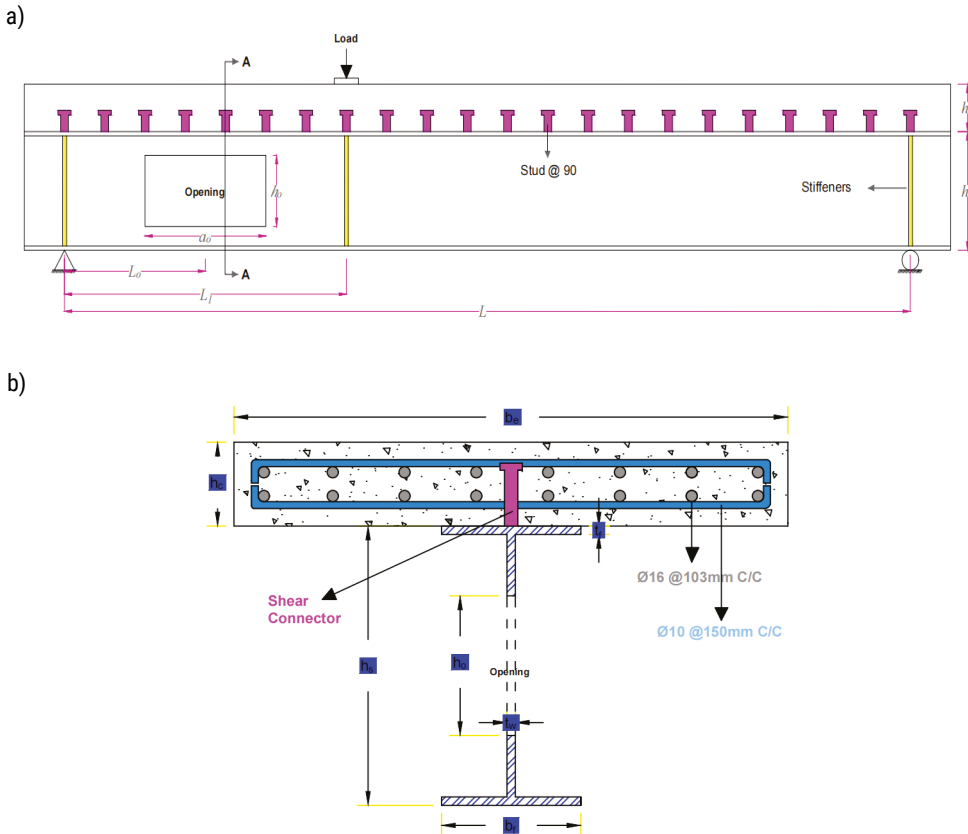


FIG. 1. a) Geometrical sizes of the specimen; b) Cross-section of the specimen

3. Finite element analysis model

A three-dimensional nonlinear finite-element model was created using ATENA Science to simulate the combined steel–concrete behavior in composite beams with web openings. This model employs different element types for concrete, reinforcement, steel profiles, and shear connectors, each chosen to model cracking, yielding, and interface slip accurately. Exploiting symmetry, only half of the beam section was modeled. Mesh refinement was applied locally around openings to capture high stress gradients without excessively increasing the global element count. Rigid bearing plates (stiffeners) were placed at load and support points to prevent local convergence issues, as shown in Figure 2. The analysis employed force-controlled loading, a displacement-based

convergence criterion, von Mises yield checks for steel, and the Newton–Raphson nonlinear solver in ATENA.

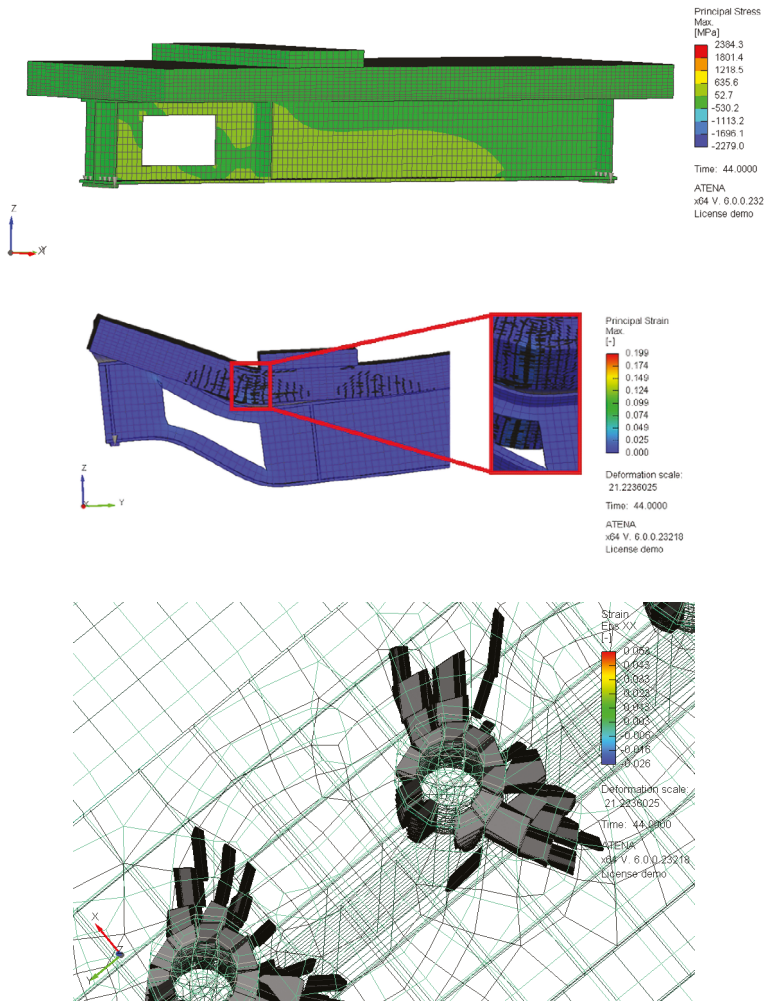


FIG. 2. A typical finite element model simulation

4. Conclusion

Introducing web openings in steel-concrete composite beams significantly reduces their load-bearing capacity and stiffness. Moreover, these modifications negatively impact the beams' deformation ability. Finite element analyses using ATENA Science on nine composite beam specimens with web openings show that the concrete slab above the opening supports between 40% and 69% of the total sectional shear force. This highlights the concrete slab's important role in resisting vertical shear in beams



with web openings. Increasing the thickness of the concrete slab effectively enhances the load-bearing capacity of composite beams with web openings. This improvement is due to the increased shear resistance of the thicker slab. However, this change does not significantly affect the beams' deformation capacity. Increasing the reinforcement ratio within the concrete slab results in modest improvements in both load-bearing capacity and stiffness of the composite beam, but the most significant benefit is an increase in the beam's deformation capacity.

This comprehensive analysis, facilitated by ATENA Science, offers valuable insights into the structural behavior of steel-concrete composite beams with web openings, highlighting the key factors that influence their performance.

References

1. Brozzetti, J. (2000). Design development of steel-concrete composite bridges in France. *Journal of Constructional Steel Research*, 55(1–3), 229–243.
2. Queiroz, F. D., Vellasco, P. C. G. S., & Nethercot, D. A. (2007). Finite element modelling of composite beams with full and partial shear connection. *Journal of Constructional Steel Research*, 63(4), 505–521.
3. Du, H., Hu, X., Meng, Y., Han, G., & Guo, K. (2020). Study on composite beams with pre-fabricated steel bar truss concrete slabs and demountable shear connectors. *Engineering Structures*, 210, 110419.
4. Ferreira, F. P. V., Martins, C. H., & De Nardin, S. (2020). Advances in composite beams with web openings and composite cellular beams. *Journal of Constructional Steel Research*, 172, 106182.
5. Shanmugam, N. E., Darehshouri, S. F., & Osman, S. A. (2014). Experimental study on composite plate girders with web opening. *Proceedings of the Institution of Civil Engineers – Structures and Buildings*, 167(12), 704–717.
6. Chen, T., Gu, X., & Li, H. (2011). Behavior of steel-concrete composite cantilever beams with web openings under negative moment. *International Journal of Steel Structures*, 11, 39–49.
7. Ju, Y. K., Kim, S. D., & Kim, D. H. (2003). Experimental study on the shear and the seismic capacities within panel zone for asymmetric steel composite beam with web openings. *International Journal of Steel Structures*, 3(1), 29–37.



Development of an elastic and waterproof cement mortar incorporating polymeric aggregate: An innovative and sustainable solution for screed application

Carolina Piña Ramírez¹, Alejandra Vidales Barriguete², Sonia Navarrete Ocaña³

¹*Departamento de Construcciones Arquitectónicas y su Control, Escuela Técnica Superior de Edificación, Universidad Politécnica de Madrid, 28040 Madrid, Spain, carolina.pina@upm.es*

²*Departamento de Tecnología de la Edificación, Escuela Técnica Superior de Edificación, Universidad Politécnica de Madrid, 28040 Madrid, Spain, alejandra.vidales@upm.es*

³*Escuela Técnica Superior de Edificación, Universidad Politécnica de Madrid, 28040 Madrid, Spain, sonia.navarreteocan@alumnos.upm.es*

Keywords: Polymeric Aggregate, Cement Mortar, Waterproofing, Sustainable Construction

1. Introduction

This work introduces a new type of cement mortar incorporating recycled polymer aggregate, offering improved impermeability, elasticity, and lightness. The use of recycled polymer from electrical cable waste helps address the growing demand for sustainable construction materials while reducing environmental impact. The polymeric aggregate replaces part of the traditional sand, enhancing the mortar's properties without compromising its structural viability [1].

This mortar is especially suited for floor screeds and the creation of slopes in flat roofs, where lightweight and moisture resistance are crucial [2]. The inclusion of recycled materials not only reduces waste but also aligns with the principles of the circular economy, contributing to more sustainable construction practices [3]. The research focuses on balancing mechanical performance and environmental benefits, aiming to create a material that meets current standards and promotes eco-friendly construction [4].

2. Materials and methods

The mortar of this invention consists of Portland cement CEM II/B-L 32.5 N, potable water from the Canal de Isabel II, standardized river sand (sieve ≤ 4 mm), and polymer aggregate in flake form with a maximum size of 3 mm, derived from the recycling of electrical cables (mostly polyethylene, polypropylene, and PVC).

The mass ratio is 1:3:0.7 (cement:total aggregate:water). The percentage of polymer aggregate varies between 25% and 55% of the total aggregate volume, with 35% being the optimal value. The manufacturing process follows the steps outlined in UNE-EN 1015-2 for preparing specimens: initial mixing of cement and polymer waste (15–20 s), addition of water (30 s at low speed), incorporation of sand (60 s), and pouring into molds in two stages. The specimens cure for 28 days in a humid chamber at 20°C and 95% relative humidity before testing (Figure 1).



FIG. 1. Sustainable mortar mixing process. Standardized mold (40x40x160 cm) placed in a humid chamber

3. Results and discussion

The mortar with polymer aggregate exhibits an apparent density ranging from 1.91 to 1.565 g/cm³ (a 10–27% decrease compared to conventional mortar), with Shore D hardness between 60 and 73. Its flexural strength varies from 4.3 to 3.1 MPa and compressive strength from 12.5 to 6.7 MPa, in compliance with UNE-EN 998-1. The static Young's modulus decreases by up to 72%, indicating greater elasticity (from 2,566 MPa to 1,300 MPa). Capillary absorption decreases by 44–72% (as low as 0.13 Kg/m²·min^{0.5}), and the entrained air content increases by up to 14%, improving waterproofing and reducing cracking.

4. Conclusions

The addition of recycled polymer waste significantly improves the mortar's performance in terms of moisture resistance and reduces the material's stiffness, making it more elastic. The reductions in density and water absorption favor its use



in applications such as floor screeds and roofs, where lightness and waterproofing are required. Despite a partial loss in mechanical strength, the formulations meet the regulatory requirements, validating their immediate industrial application. This mortar represents a sustainable and technically feasible solution within the construction industry.

References

1. García, R., & Sánchez, M. (2024). Sustainable cement mortar with recycled plastics enabled by polymer coating. *Journal of Cleaner Production*, 345, 131–142. <https://doi.org/10.1016/j.jclepro.2022.131>
2. López, J., & Martínez, P. (2023). Environmental sustainable cement mortars based on polyethylene terephthalate (PET) aggregates. *Materials Science and Engineering: A*, 812, 141–150. <https://doi.org/10.1016/j.msea.2022.141>
3. Ramírez, C. P., del Río Merino, M., Arrebola, C. V., Barriguete, A. V., & Kosior-Kazberuk, M. (2019). Analysis of the mechanical behaviour of the cement mortars with additives of mineral wool fibres from recycling of CDW. *Construction and Building Materials*, 210, 56–62. <https://doi.org/10.1016/j.conbuildmat.2019.03.062>
4. Wang, Y., & Zhang, L. (2024). Durability of mortars made with recycled plastic aggregates. *Journal of Materials in Civil Engineering*, 36(4), 04022056. [https://doi.org/10.1061/\(ASCE\)MT.1943-5533.0003566](https://doi.org/10.1061/(ASCE)MT.1943-5533.0003566)



Bond-slip behavior between concrete with pozzolanic additives and BFRP and GFRP bars

*Julita Krassowska¹, Filip Chyliński²,
Marta Kosior-Kazberuk¹, Dai Wang³, Dawei Shu³*

¹*Bialystok University of Technology, Poland, j.krassowska@pb.edu.pl, m.kosior@pb.edu.pl*

²*Building Research Institute, Poland, f.chylinski@itb.pl*

³*Tianjin Chengjian University, China, wgd@tcu.edu.cn, 963175765@qq.com*

Keywords: bond-slip, basalt fiber-reinforced polymer, basalt fibers, basalt fiber-reinforced polymer stirrups, flexural capacity

1. Introduction

Within the European Union steel consumption fell by 4.5% in two years, while energy and fuel costs raised construction prices by over 13% annually [1]. FRP bars thus represent a more sustainable alternative to steel. Bond between reinforcement and concrete is key for durability, influenced by bar surface, concrete quality, and environment. Strong adhesion improves load transfer and limits cracking, while poor bond reduces capacity. Studies show larger GFRP bars lose up to 16% strength [2], sand coatings improve bond [3], and higher temperature weakens it [4]. Stronger concrete enhances adhesion [5], while recycled aggregates reduce it [6]. Complex methods (fibers, nanomaterials) can improve bond, but simpler and greener modification uses pozzolanic additives like metakaolin and zeolite. These reduce cement use and CO₂ emissions while refining microstructure and increasing durability [7].

This study examines how metakaolin and zeolite affect the bond of basalt and glass FRP bars versus steel, aiming to optimize concrete mix design for improved bond strength and sustainability.

1.1. Experimental program

Two types of concrete were used: ordinary cement concrete and concrete with 10% cement replaced by metakaolin or zeolite. The study, conducted in nine series (Figure 1), analyzed how these additives affect the bond of steel, basalt, and glass bars with concrete.

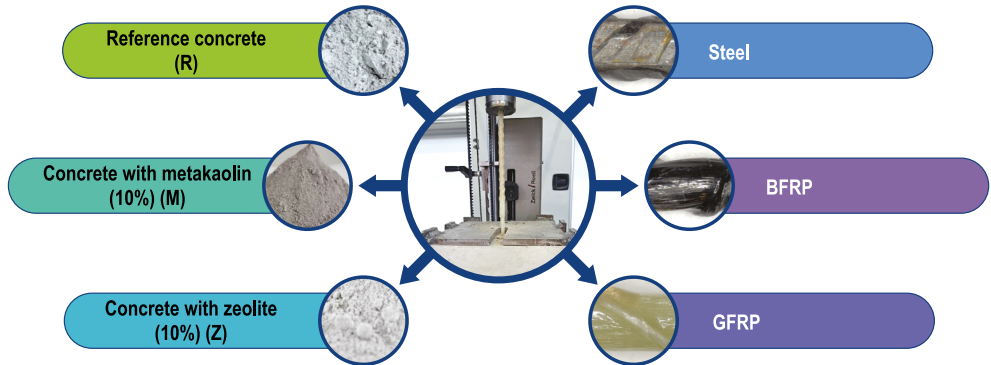


FIG. 1. The research program (type of concrete: R – reference, M – metakaolin, Z – zeolite; type of bars: steel, BFRP – basalt fibers reinforced bars, GFRP – glass fibers reinforced bars)

1.2. Test procedure

The bond test followed EN 10080:2005, Annex C [8], using 200 mm concrete cubes with a bonded length of $5d$ from the free edge. Loading was applied at a rate below 20 kN/min, and displacement was measured on both loaded and free bar ends with LVDT sensors accurate to 0.01 mm. The average bond stress was calculated based on the applied load, bar perimeter, and bonded length, while slip was corrected for FRP.

2. Results

Table 1 presents the average force values applied to the samples during the bar-to-concrete adhesion tests at specific slip levels, along with the corresponding bond stress values τ_{dm} and the observed failure modes. Four main failure modes were observed: FRP pull-out (P), concrete splitting (S), FRP rupture (R), and steel yielding (Y). In pull-out failure, bars were gradually extracted without breaking, showing surface damage and worn ribs. Splitting failure occurred mainly in GFRP and BFRP samples when circumferential tension caused longitudinal cracks in concrete. FRP rupture was sudden and brittle due to limited plasticity, while steel bars exhibited yielding followed by ductile fracture after reaching tensile strength.

TABLE 1. Results of tensile stress measurements in the bar

Bars	Average value of force applied to the sample [kN] at slip				Adhesive stresses τ_{dm} for slip				Failure mode*
	$F_{0,05}$	$F_{0,1}$	F_1	F_{max}	$\tau_{0,01}$	$\tau_{0,1}$	τ_1	τ_{max}	
	kN	kN	kN	kN	MPa	MPa	MPa	MPa	–
R-steel	0,04	0,36	2,69	31,71	0,04	0,34	2,52	29,70	Y

Bars	Average value of force applied to the sample [kN] at slip				Adhesive stresses τ_{dm} for slip				Failure mode*
R-BFRP	0,06	0,64	5,07	29,80	0,07	0,75	5,93	34,84	S,P
R-GFRP	0,04	0,33	2,40	36,67	0,03	0,31	2,26	31,41	S,P
M-steel	0,03	0,11	3,49	34,69	0,02	0,09	2,73	27,16	Y
M-BFRP	0,04	0,47	4,44	38,99	0,04	0,46	4,34	38,12	R,P
M-GFRP	0,04	0,42	4,85	38,99	0,04	0,40	4,40	34,59	P
Z-steel	0,06	0,64	5,34	34,73	0,05	0,53	4,38	27,19	Y
Z-BFRP	0,08	0,35	1,23	38,56	0,08	0,36	1,26	37,70	P
Z-GFRP	0,02	0,10	2,23	49,65	0,02	0,08	1,84	39,16	P,R

* – Rebar Pull-out Failure (P); Concrete Splitting Failure (S); FRP bar rapture (R); Steel bars yielding (Y)

Acknowledgments

The work was carried out at the Białystok University of Technology under financing from the Ministry of Science and Higher Education of the Republic of Poland; project number WZ/WB-III/6/2023.

References

1. Europejska Federacja Przemysłu Budowlanego (FIEC). (2022). *Construction activity in Europe: Trends and challenges*.
2. Ebrahimi, F., Eslami, A., & Pilakoutas, K. (2024). Bond behaviour of staggered/non-staggered lap-spliced GFRP bars in concrete. *Structures*, 64, 106546. <https://doi.org/10.1016/j.istruc.2024.106546>
3. Solyom, S., & Balázs, G. L. (2020). Bond of FRP bars with different surface characteristics. *Construction and Building Materials*, 264, 119839. <https://doi.org/10.1016/j.conbuildmat.2020.119839>
4. Amin, M. N., Iqbal, M., Althoey, F., Khan, K., Faraz, M. I., Qadir, M. G., Alabdullah, A. A., & Ajwad, A. (2022). Investigating the bond strength of FRP rebars in concrete under high temperature using gene-expression programming model. *Polymers*, 14(15), 2992–2992. <https://doi.org/10.3390/polym14152992>
5. Hu, X., Xue, W., & Jiang, (2024). J. Bond-slip behavior of lapped sand-coated deformed GFRP rebars in UHPC under double-row splice test. *Cement and Concrete Composites*, 154, 105746. <https://doi.org/10.1016/j.cemconcomp.2024.105746>
6. Liang, J., Liu, J., Fan, L., Ren, R., Li, W., & Yang, W.-R. (2021). Bond behavior of FRP bars in CR concrete. *Computers and Concrete*, 28(2), 107–114. <https://doi.org/10.12989/cac.2021.28.2.107>
7. Ambroise, J., Maximilien, S., & Pera, J. (1994). Properties of metakaolin blended cements. *Advanced Cement Based Materials*, 1(4), 161–168. [https://doi.org/10.1016/1065-7355\(94\)90007-8](https://doi.org/10.1016/1065-7355(94)90007-8)
8. EN 10080-2005 *Steel for the reinforcement of concrete* (2007).



Investigation of concrete beams reinforced with GFRP or steel bars: An experimental approach

Janusz Rogowski, Damian Szczech, Jakub Zajac, Renata Kotynia

*Lodz University of Technology, Poland, janusz.rogowski@p.lodz.pl,
damian.szczech@p.lodz.pl, jakub.zajac@p.lodz.pl, renata.kotynia@p.lodz.pl*

Keywords: shear, GFRP, beams, failure mode

1. Introduction

The complex stress state resulting from combined action of shear force and bending moment is inherently difficult to characterize, as shear transfer involves the interaction of concrete, transverse reinforcement, and, indirectly, longitudinal reinforcement. Assessing the shear capacity of beams with transverse reinforcement becomes even more complex when the reinforcement is made of Glass Fiber Reinforced Polymer (GFRP), which, unlike steel, is an anisotropic material. Several parameters may affect shear strength, including the longitudinal reinforcement ratio, transverse reinforcement ratio, stirrup diameter, and stirrup spacing. Most previous studies have focused on beams made of normal-strength concrete [2]. Comparisons between normal-strength concrete (<50 MPa) and high-strength concrete (>50 MPa) indicate that shear capacity increases with higher concrete compressive strength [1]. The present study investigates beams with either GFRP or steel reinforcement, cast from C50/60 concrete, with varying levels of transverse reinforcement.

2. Experimental program

Four simply supported T-section beams were tested under three-point bending setup. The beams had a span of 1800 mm and the following cross-sectional dimensions: $b_{\text{eff}} = 650$ mm, $b_w = 250$ mm, $h_f = 80$ mm, $h_{\text{tot}} = 400$ mm. The shear span-to-depth ratio was set to 3.15, in order to eliminate arching effects. The applied load was positioned 1050 mm from the support, and only the left shear span was considered in the investigation.

The longitudinal reinforcement consisted of five 25 mm diameter bars ($\rho_l = 2.91\%$), while the transverse reinforcement consisted of 8 mm closed stirrups spaced at 200 mm and 250 mm. Both longitudinal and transverse reinforcements were made

of two types of materials: GFRP bars (tensile strength >1000 MPa, elastic modulus >60 GPa) and steel bars of class B500. All beams were cast with ready-mixed concrete of class C50/60.

TABLE 1. Details of specimens

Element	Type of reinforcement	Flexural reinforcement ratio ρ_l [%]	Shear reinforcement ratio ρ_s [%]	Stirrups spacing s_s [mm]
TG-525-8-200	GFRP	2,91	0,20	200
TG-525-8-250	GFRP	2,91	0,16	250
TS-525-8-200	Steel	2,91	0,20	200
TS-525-8-250	Steel	2,91	0,16	250

Test setup included LVDTs arranged along the beam length for deflection measurement, in triangular rosettes at mid-depth for shear deformations and in both compression and tension zones to record concrete strains. Strain gauges were mounted to the longitudinal reinforcement and GFRP stirrups. Additionally, displacement and strain data in the analyzed zone were obtained using a 3D digital image correlation system (ARAMIS).

3. Test results

According to the test element design, shear failure developed solely in the left support region, whereas the right side showed no such failure. The initial damage appeared as nearly vertical flexural cracks. After the onset of shear cracking, cracks developed from mid-depth of the beam towards the support, extending into both the tensile reinforcement zone and the upper compressive zone. With increasing load, the critical shear crack cut the flange and propagated to the loading point, leading to failure. The position of the critical crack, defined by the distance from the support, as well as its inclination, varied depending on the reinforcement type and the transverse reinforcement ratio.

The behaviour of the beam under load is shown in Fig. 1. Tensile concrete strain measurements and observations of the beams indicated that the first flexural cracks appeared at similar load levels in all beams. A higher transverse reinforcement ratio, achieved by reducing stirrup spacing, resulted in increased stiffness (it was confirmed by smaller deflections). However, in GFRP-reinforced beams, this did not lead to higher shear capacity, most likely due to local effects in the beam TG-525-8-200. Beams reinforced with steel demonstrated greater load-bearing capacity compared to those reinforced with GFRP.

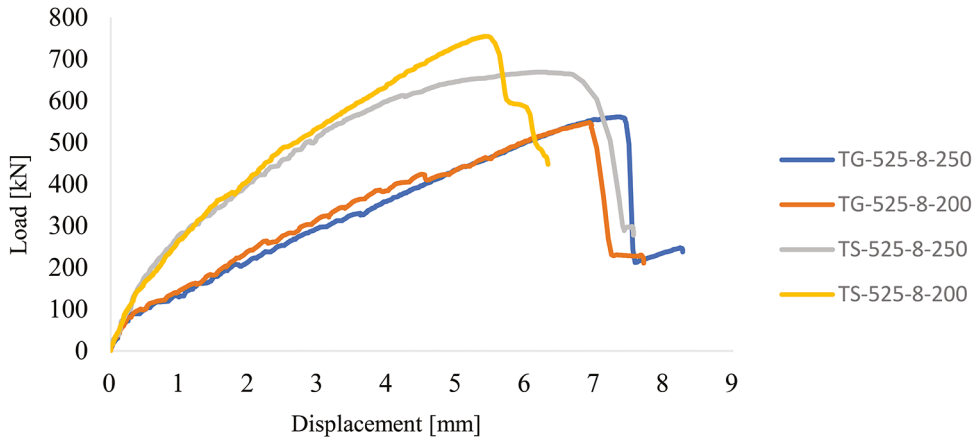


FIG. 1. Load-displacement curves for tested beams

Funding

This research work was funded by the National Science Centre, Poland under the OPUS call in the Weave programme no 2023/51/I/ST11/00069 under the title “Multi-fidelity modelling of shear concrete strength based on experiments, simulation and probabilistic approaches (MMOSS)”.

References

1. El-Sayed, A. K., El-Salakawy, E. F., & Benmokrane, B. (2006). Shear capacity of high-strength concrete beams reinforced with FRP bars. *ACI Structural Journal*, 103, 383–389.
2. Szczech, D., & Kotynia, R. (2021). Effect of shear reinforcement ratio on the shear capacity of GFRP reinforced concrete beams. *Archives of Civil Engineering*, 67, 425–437.



Predicting pre-failure behaviour of GFRP lighting poles

Filip Broniewicz

Bialystok University of Technology, Poland, filip.broniewicz@pb.edu.pl

Keywords: composite poles, FEM analysis, experimental investigation, flexural behaviour

1. Introduction

The primary objective of the study is to develop and experimentally validate a finite element model (FEM) of glass fibre-reinforced polymer (GFRP) lighting poles. A correct numerical formulation must reproduce the nonlinear response up to the failure phase and accurately resolve the stress state in the vicinity of the unreinforced inspection opening under the applied loading. To support model development and validation, eleven full-scale GFRP lighting poles were tested, and complementary material characterization of the composite laminate was performed to determine the pole's properties.

2. Development of the fem model

Numerical models were developed in ANSYS Structural based on material characterization and pole-scale experimental data. A shell idealization was adopted; pole shafts were represented as truncated cones with a 200×75 mm inspection opening located approximately 1.0 m above the base, positioned on the compressive side under the applied load, and without local reinforcement. The poles consisted of a glass-fibre laminate in a polyester resin matrix, and the material data used for the constitutive definition were obtained from dedicated material tests. The increased stiffness of the 0–1 m segment (measured from the base), attributable to a steel flange at the base, was captured by locally increasing the laminate thickness; the steel flange itself was not modelled explicitly. SHELL181 elements [1] were used for thin laminated shells. SHELL181 is a four-node element with six degrees of freedom per node (UX, UY, UZ, ROTX, ROTY, ROTZ). The laminate was modelled at the ply level in ACP Pre-Post with a layup comprising bidirectional woven plies and chopped strand mat plies, enabling stress and failure checks at the lamina scale using the maximum stress criterion. The material response was treated as transversely isotropic (in-plane isotropic with distinct through-thickness properties) [2]. Through-thickness integration points were set to three per layer in the section definition for the 4 mm laminate; a sensitivity check with five points per layer was considered in regions of elevated bending gradients

near the inspection opening. Boundary conditions reproduced the test arrangement: the base of the shaft was fully fixed (all translations and rotations constrained). The pole was oriented horizontally in the experiment with an auxiliary support near the tip to suppress gravity-induced bending; gravity was omitted in the numerical model. Meshing used a global element size of 30 mm with graded refinement toward the inspection opening, reducing to 1 mm along the opening perimeter.

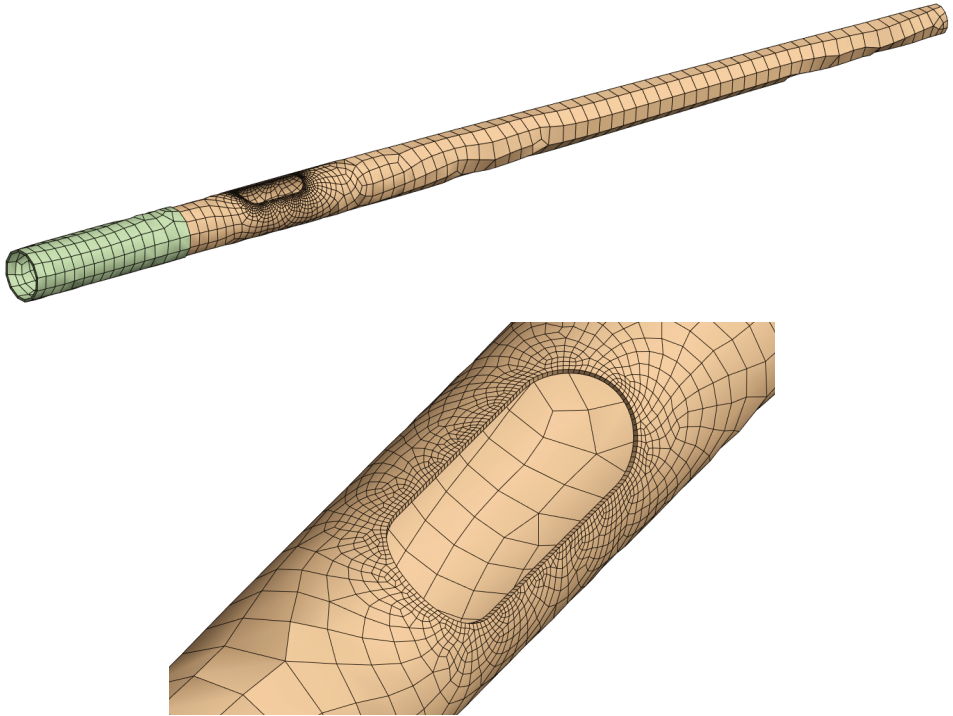


FIG. 1. FE model of the 3-meter-long pole

The analyses employed the Reissner–Mindlin first-order shear deformation shell formulation [3], appropriate for moderately thick composite shells, to capture transverse-shear effects in the laminate. Through-thickness integration was defined as three points per ply in the section, with a sensitivity check using five points per ply in regions of elevated bending gradients near the inspection opening. Statistical procedures were applied to the displacement-at-peak metric derived from the F - Δ curves.



3. Validation of the numerical model

Validation proceeded in two stages addressing global response and local behaviour. Globally, finite element predictions were benchmarked against full-scale load displacement ($F-\Delta$) curves, using the displacement at peak load as the primary validation metric. Locally, numerical strains/stresses sampled at the strain-gauge positions around the inspection opening were compared with strain-gauge measurements to appraise model fidelity in the anticipated (and actual) failure region. Normality was assessed with the Shapiro-Wilk test; for data satisfying normality, an F-test for homoscedasticity was followed by Student's t-test, otherwise the Mann-Whitney U-test was applied. Differences were considered not significant when the resulting p-value exceeded the significance level $\alpha = 0.05$. Statistical procedures were applied to the displacement-at-peak metric derived from the $F-\Delta$ curves.

4. Conclusions

In the vast majority of comparisons, p-values for the displacement-at-peak metric and for local response around the inspection opening exceeded the significance threshold $\alpha = 0.05$, indicating no statistically detectable differences between experimental measurements and finite-element predictions for the tested poles. Consistent outcomes across the prescribed statistical workflow [4] (Shapiro-Wilk, Student's t-tests and Mann-Whitney tests) support the fact that the model reproduces both the global load-displacement behaviour and the local response with sufficient accuracy.

References

1. Lin, Z. M. (1995). *Analysis of pole-type structures of fibre reinforced plastics by finite element method*. University of Manitoba.
2. Sandberg, M., Yuksel, O., Comminal, R. B., Sonne, M. R., Jabbari, M., Larsen, M., Salling, F. B., Baran, I., Spangenberg, J., & Hattel, J. H. (2020). Numerical modeling of the mechanics of pultrusion. In V. V. Silberschmidt (Ed.), *Mechanics of materials in modern manufacturing methods and processing techniques* (pp. 173–195). Elsevier. <https://doi.org/10.1016/B978-0-12-818232-1.00006-0>
3. Rakowski, J., & Wielentejczyk, P. (2022). Dynamics of Reissner-Mindlin plate strips by FEM. *Vibrations in Physical Systems*, 20, 250–251.
4. STATISTICA v. 13.0. <https://statistica.software.informer.com/13.0> (accessed: October 8, 2025).



Shear and bending capacities of concrete beams with composite reinforcement

Rafał Kostro, Marta Kosior-Kazberuk, Julita Krassowska

Białystok University of Technology, Poland, rafal.kostro@sd.pb.edu.pl

Keywords: concrete beam, composite reinforcement, basalt microbars, bending and shear capacity

1. Introduction

Composite, non-metallic reinforcement is becoming increasingly popular in construction, both as fibers or microbars, and as longitudinal external and internal reinforcement. One of the main arguments for its use is that it is more environmentally friendly compared to steel reinforcement, primarily due to significantly lower CO₂ emissions generated during the manufacturing process. Additionally, composite reinforcement offers superior durability performance owing to its inherent corrosion resistance. This characteristic makes it particularly suitable for use in structural elements exposed to aggressive environmental conditions. Typical applications include foundations – especially foundation slabs – as well as marine infrastructure and nuclear power plants.

Composite reinforcement is also characterized by nearly twice the tensile strength of conventional steel bars, while having a mass that is two to three times lower. This advantageous strength-to-weight ratio, along with good cohesion to the concrete, enables the design of structural elements with bending and shear capacities comparable to those of traditional reinforced concrete, without compromising the level of structural safety. Moreover, the incorporation of dispersed reinforcement – such as fibers or microbars – into the concrete matrix contributes to a significant reduction in the number of cracks and crack widths. This limits the penetration of aggressive environmental agents into deeper parts of the structural element, enhancing its long-term durability and service life.

These aspects show that further tests on the behaviour of concrete beams reinforced with composite materials are needed in order to define new design methods and develop more comprehensive guidelines for such structural elements. This is particularly important given that no standardized algorithm has been established for the design of Fiber Reinforced Concrete (FRC) with composite longitudinal reinforcement and composite stirrups.

An experimental research program was carried out. Mechanical properties of concretes with Basalt Fiber Reinforced Concrete (BFRC) were determined. Shear and bending capacities of BFRC beams with composite longitudinal and transverse reinforcement were analysed.



An experimental study was conducted to evaluate the influence of basalt microbar content on the properties of concrete. Three concrete mixes with varying amounts of dispersed reinforcement were tested: M15 – containing 1.5 kg of microbars per 1 m³ of concrete, M25 – 2.5 kg, and M35 – 3.5 kg respectively.

Based on the obtained results, a slight increase in the compressive strength of concrete was observed with increasing content of dispersed reinforcement, compared to the reference concrete. Tensile strength was also evaluated using two different test methods: flexural tensile strength test and splitting tensile strength test. In both tests, a significant improvement in tensile performance was noted as a result of using basalt microbars. The longitudinal modulus of elasticity of concrete was also determined. Tests showed that the addition of dispersed reinforcement caused an increase in the elastic modulus. In particular, for the concrete containing 3.5 kg of microbars, the modulus of elasticity corresponded to concrete one class grade higher than the reference concrete without microbars. Fracture mechanics parameters were also investigated, and the results indicated a considerable enhancement in the mechanical behaviour of the concrete due to the addition of basalt microbars. A more detailed analysis of the mechanical properties of the concretes can be found in [1].

The study analyzed the results of tests on composite reinforced beams, which are reported in the literature [5–7]. Results were compared with design capacities determined in accordance with design standards [2, 3]. The aim of the calculations was to determine the shear capacity, bending capacity, and deflections of beams reinforced with non-metallic bars, with or without the addition of dispersed reinforcement, and with or without transverse shear reinforcement (stirrups). The obtained results were compared with experimental data by calculating capacity reserves.

The ratio of theoretical to experimental capacity was evaluated for all beam types, taking into account the material of longitudinal reinforcement, the presence of dispersed reinforcement and its quantity in the volume of concrete, and the presence of stirrups. Beam deflections were also compared with calculated values obtained for similarly steel reinforced beams.

Based on the material tests, it was found that the addition of dispersed reinforcement to concrete improves its mechanical properties as well as its fracture mechanics parameters. Better material properties lead to increased shear and bending capacities of the beams and a reduction in beam deflections. Beams made of concrete with dispersed reinforcement also showed fewer cracks and reduced crack widths. Properly designed composite reinforced concrete beams achieve shear and bending capacities comparable to steel reinforced beams. The results of the analysis may support the potential optimization of the way of reinforcing concrete beams using non-metallic bars and non-metallic dispersed reinforcement.



References

1. Kostro, R., Kosior-Kazberuk, M., Krassowska, J., Protchenko, K., & Belay, A. (2024). Selected mechanical properties of basalt microbars reinforced concrete. *Materiały Budowlane*, 1(7), 8–14.
2. Recommendation TC 89-FMT RILEM, *Materials and Structures, Determination of fracture parameters (K_{Ic} and $CTOD_c$) of plain concrete using three-point bend test* 23, 1990.
3. ACI Committee. (2015). *ACI 440.1R-15: Guide for the design and construction on structural concrete reinforced with FRP bars*, 440.
4. CEN/TC 250/SC 2 N 1874 *Eurocode 2 – Design of concrete structures, latest draft prEN 1992-1-1*, ver. 2021-01.
5. Al-Hamrani, A., & Alnahhal, W. (2021). Shear behavior of basalt frc beams reinforced with basalt FRP bars and glass FRP stirrups: Experimental and analytical investigations. *Engineering Structures*, 242, 112612.
6. AlHamaydeh, M., Markou, G., Bakas, N., & Manolis, P. (2022). AI-based shear capacity of FRP-reinforced concrete deep beams without stirrups. *Engineering Structures*, 264, 114441.
7. El Refai, A., Alnahhal, W., Al-Hamrani, A., & Hamed, S. (2022). Shear performance of basalt fiber-reinforced concrete beams reinforced with BFRP bars. *Composite Structures*, 288, 115443.



Investigation of concrete beams reinforced with GFRP bars: finite element modelling

Jakub Zajac, Damian Szczech, Janusz Rogowski, Renata Kotynia

Lodz University of Technology, Poland, jakub.zajac@p.lodz.pl, damian.szczech@p.lodz.pl, janusz.rogowski@p.lodz.pl, renata.kotynia@p.lodz.pl

Keywords: shear, GFRP, beams, failure mode, FEM

1. Introduction

Numerical modelling can be used to verify and interpret experimental observations, providing insights into the structural response. When applied and correlated across a series of experimental data, the models enable systematic analysis of shear force distribution and the influence of varying transverse and longitudinal reinforcement configurations. This approach also allows extending the analyses to additional values of parameters beyond those examined experimentally [1]. The present paper focuses on the modelling of beams with Glass Fiber Reinforced Polymer (GFRP) transverse reinforcement, build on results for beams without stirrups presented at the SPACE conference. This work is part of the MMOSS project, whose objectives and experimental program were introduced at the 69th Krynica Conference, that was based on previous works [2]. In the context of MMOSS, modelling plays a crucial role in supporting probabilistic assessment of structural behaviour, allowing more robust evaluation of uncertainties and enhancing the reliability of the conclusions of experimental campaigns. This paper complements another submission to the conference that addresses exclusively the experimental investigation of the beams.

2. Model configuration and parameters

Three simply supported T-section beams were tested under a three-point bending setup, with a span of 1800 mm and cross-sectional dimensions: $b_{\text{eff}} = 650$ mm, $b_w = 250$ mm, $h_f = 80$ mm, $h_{\text{tot}} = 400$ mm. The load was applied at a distance of 1050 mm from the support. Longitudinal reinforcement comprised five 25 mm bars ($\rho_l = 2.91\%$) while transverse reinforcement consisted of 8 mm closed stirrups spaced at 200 mm and 250 mm. Both reinforcement types were made of GFRP (tensile strength >1000 MPa, elastic modulus >60 GPa), the remaining reinforcement was made as steel (class B500A). All beams were cast with ready-mixed C50/60 concrete; the measured cube compressive strength was relatively low, averaging 60 MPa (table. 1).

TABLE 1. Details of specimens

Element	Type of reinforcement	Flexural reinforcement ratio ρ_f , %	Shear reinforcement ratio ρ_s , %	Stirrups spacing s_s , mm	Concrete compressive strength $f_{cm, cube}$, MPa
TG-525-8/250-30	GFRP	2.91	0.16	250	47.7
TG-525-8/250-50	GFRP	2.91	0.16	250	60.0
TG-525-8/200-50	GFRP	2.91	0.20	200	60.0

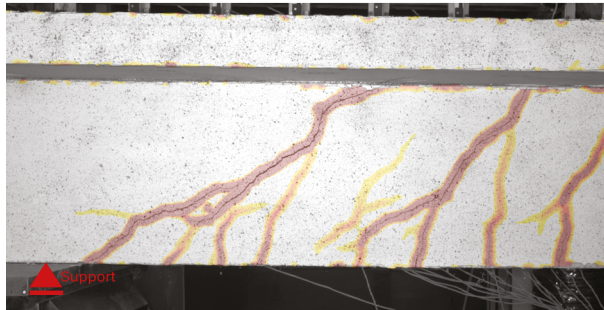
The material parameters of concrete and steel, together with the bond–slip relationship for steel reinforcement, were adopted according to the provisions of Model Code 2010. Required parameters, particularly the bond behaviour of GFRP reinforcement, were supplemented based on previous analyses and experimental studies. The numerical models were developed in ATENA 2025, incorporating nonlinear material properties as well as the specific characteristics of GFRP reinforcement. The models presented for the C50/60 concrete series were not fully calibrated; except for the concrete parameters, they were based on the previously calibrated model TG-525-8/250-30, for which nearly perfect convergence was obtained between the predicted and experimental maximum load as well as the crack pattern development.

3. Finite element models results

High correlation with the experimental crack patterns was achieved in all models, while the reference model TG-525-8/250-30 represent the maximum load with full accuracy. For beams made of higher-strength concrete, however, the failure load was lower, reaching 90% for a stirrup spacing of 200 mm and 83% for a spacing of 250 mm. A comparison of the crack patterns of the beams based on Aramis DIC system and Atena software FEM analysis is presented in Fig. 1.

Tensile concrete strain measurements and observations of the beams indicated that the first flexural cracks appeared at similar load levels in all beams. The analyses demonstrate that the developed numerical models effectively capture the cracking behaviour of beams with GFRP transverse reinforcement, providing insights into the influence of reinforcement configuration and concrete strength on structural response. Slight deviations in failure load for higher-strength concrete highlight areas for refinement in material calibration. The study establishes a validated basis for the extension of parametric and probabilistic analyses within the MMOSS project, supporting future investigations of safety factors, reliability, and performance prediction for reinforced concrete structures.

a)



b)

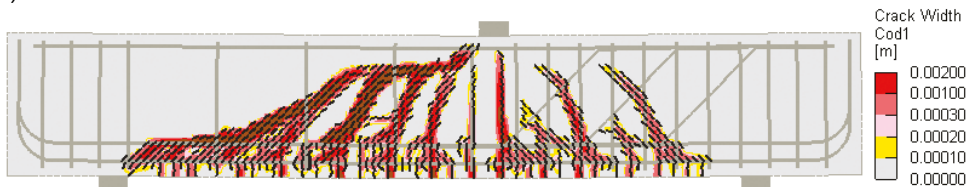


FIG. 1. Crack pattern comparison: a) TG525-8/250-50 experiment DIC view ($F = 450$ kN); b) FEM model ($F = 451.2$ kN)

Funding

This research work was funded by the National Science Centre, Poland under the OPUS call in the Weave programme no 2023/51/I/ST11/00069 under the title “Multi-fidelity modelling of shear concrete strength based on experiments, simulation and probabilistic approaches (MMOSS)”.

References

1. Novák, D., & Lehký, D. (2006). ANN inverse analysis based on stochastic small-sample training set simulation. *Engineering Applications of Artificial Intelligence*, 19(7), 731–740.
2. Szczech, D., & Kotynia, R. (2021). Effect of shear reinforcement ratio on the shear capacity of GFRP reinforced concrete beams. *Archives of Civil Engineering*, 67, 425–437.



Experimental investigation of the bond behaviour of GFRP reinforcing bars in low-clinker concrete

*Paul Heber¹, Oliver Sikorski², Alexander Schumann³,
Paul-Martin Großkopf⁴, Birgit Beckmann¹, Steffen Marx¹*

¹TUD Dresden University of Technology, Germany, paul.heber@tu-dresden.de,
birgit.beckmann@tu-dresden.de, steffen.marx@tu-dresden.de

²Implenia Civil Engineering GmbH, Germany, oliver.sikorski@implenia.com

³CARBOCON GMBH, Germany, schumann@carbocon-gmbh.de

⁴Kleihues Betonbauteile GmbH & Co. KG, Germany, m.grosskopf@kleihues-beton.de

Keywords: eco-concrete, GFRP, non-metallic reinforcement, bond behaviour

1. Introduction

Eco-concretes (ECs), i.e., concrete mixes with low clinker content, contribute to a reduction in CO₂ emissions in construction, which is critical for mitigating global warming. The lower alkalinity of ECs necessitates corrosion-resistant reinforcements such as glass fibre-reinforced plastic (GFRP). In this study, pull-out (PO) and beam-end (BE) tests were performed on GFRP rebars embedded in EC to determine the general bond behaviour and the influence of bond length and concrete cover.

2. Materials

2.1. Concrete

The eco-concrete (EC) mixture with reduced clinker content used in this study is given in Table 1.

TABLE 1. Concrete mixture composition of the developed eco-concrete

Aggregate 0/2 [kg/m ³]	Aggregate 2/8 [kg/m ³]	Aggregate 8/16 [kg/m ³]	Limestone powder [kg/m ³]	CEM III/A 52,5 N SR/NA [kg/m ³]	Water [kg/m ³]	Superplasticiser (PCE) [kg/m ³]
678	486	775	60	280	126	2.52



2.2. GFRP reinforcing bars

The GFRP rebars used (see Fig. 1) are produced by solidian GmbH and had diameters of 8 mm ($\varnothing 8$) and 10 mm ($\varnothing 10$) and are composed of unidirectional glass fibres in an epoxy (EP) matrix. The surface profiling consists of likewise EP-impregnated fibre strands wrapped helically around the rebar core. The mechanical properties of the rebars are given in their datasheet [1].

3. Test setup

3.1. Pull-out test

Two series of pull-out tests were conducted: series $\varnothing 8$ -PO (diameter 8 mm; 6 specimens) and series $\varnothing 10$ -PO (diameter 10 mm; 5 specimens), with each a bond length of five times the respective rebar diameter. The tests, which are based on the RILEM RC 6 test [2], were conducted in accordance with [3], in a strain-controlled way (loading rate 1.0 mm/min).

3.2. Beam-end-test

The beam-end tests were conducted in accordance with [3]. Three series with each six specimens, all with a concrete cover of 20 mm were tested strain-controlled at 1.0 mm/min. The rebars had bond lengths of 5 times ($\varnothing 10$ -BE-5), 20 times ($\varnothing 10$ -BE-20) and 40 times ($\varnothing 10$ -BE-40) the rebar diameter.

4. Experimental results

The tests were conducted at concrete cube compressive strengths of 63.8 N/mm² ($\varnothing 8$ -PO), 60.5 N/mm² ($\varnothing 10$ -PO) and 44.7 N/mm² (BE series). All specimens failed in valid manner due to shearing and tearing of the profiling. However, series $\varnothing 10$ -BE-40 failed also due to partial or complete rebar tensile failure. The bond stress-slip curves are depicted in Fig. 1.

In the PO comparison, series $\varnothing 8$ -PO showed stiffer bond behaviour and a higher maximal bond strength than $\varnothing 10$ -PO, due to the difference in bond length and rebar diameter. This reduction in bond stiffness and bond strength is, however, higher in series $\varnothing 10$ -BE-5 compared to series $\varnothing 10$ -PO, showing a mitigating influence of the lower concrete cover. With increase in bond length ($\varnothing 10$ -BE-20 and $\varnothing 10$ -BE-40) the bond strength decreased further, whereas the bond stiffness increased. The onset of tensile failure in series $\varnothing 10$ -BE-40 showed a nearly sufficient anchoring length of the rebars.

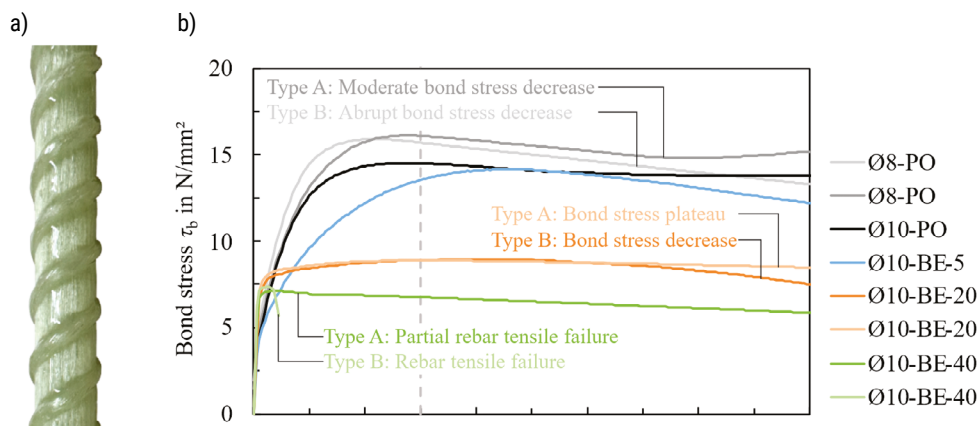


FIG. 1. (a) Tested GFRP rebar (Photo: Paul Heber); (b) Average bond stress-slip relationships of PO and BE tests

5. Conclusions

This study investigated the bond behaviour of GFRP rebars in eco-concrete. With increasing rebar diameter and bond length the bond strength decreased, while bond stiffness varied. The required anchoring length of the rebars was found to be at approximately 40 times the rebar diameter.

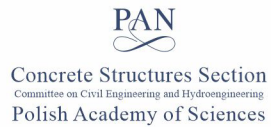
Funding

This research is funded by the Federal Ministry for Economic Affairs and Energy (grant number 03LB2085, based on a decision by the German Bundestag, as part of the Lightweight Construction Technology Transfer Program (Technologietransfer-Programm Leichtbau, TTP LB).

References

1. Solidian GmbH. (2023). *Technical product data sheet – solidian REBAR Dxx-RRE*. <https://www.solidian-kelteks.com/de/downloads>.
2. International Union of Testing and Research Laboratories for Materials and Structures. (1994). *RILEM Technical Recommendations for the testing and use of construction materials* (1st ed.). CRC Press. <https://doi.org/10.1201/9781482271362>
3. Deutscher Ausschuss für Stahlbeton. (2024). *DAfStb-Richtlinie – Betonbauteile mit nicht-metallischer Bewehrung*.

CONFERENCE ORGANIZED BY



SPONSOR



STRATEGIC PARTNER



EVENT PARTNER



HONORARY PATRONAGE



Patronat Marszałka
Województwa Podlaskiego



Honorowy Patronat
Prezydenta
Miasta Białegostoku

INTERNATIONAL PATRONAGE



POLISH PATRONAGE



MEDIA PATRONAGE

